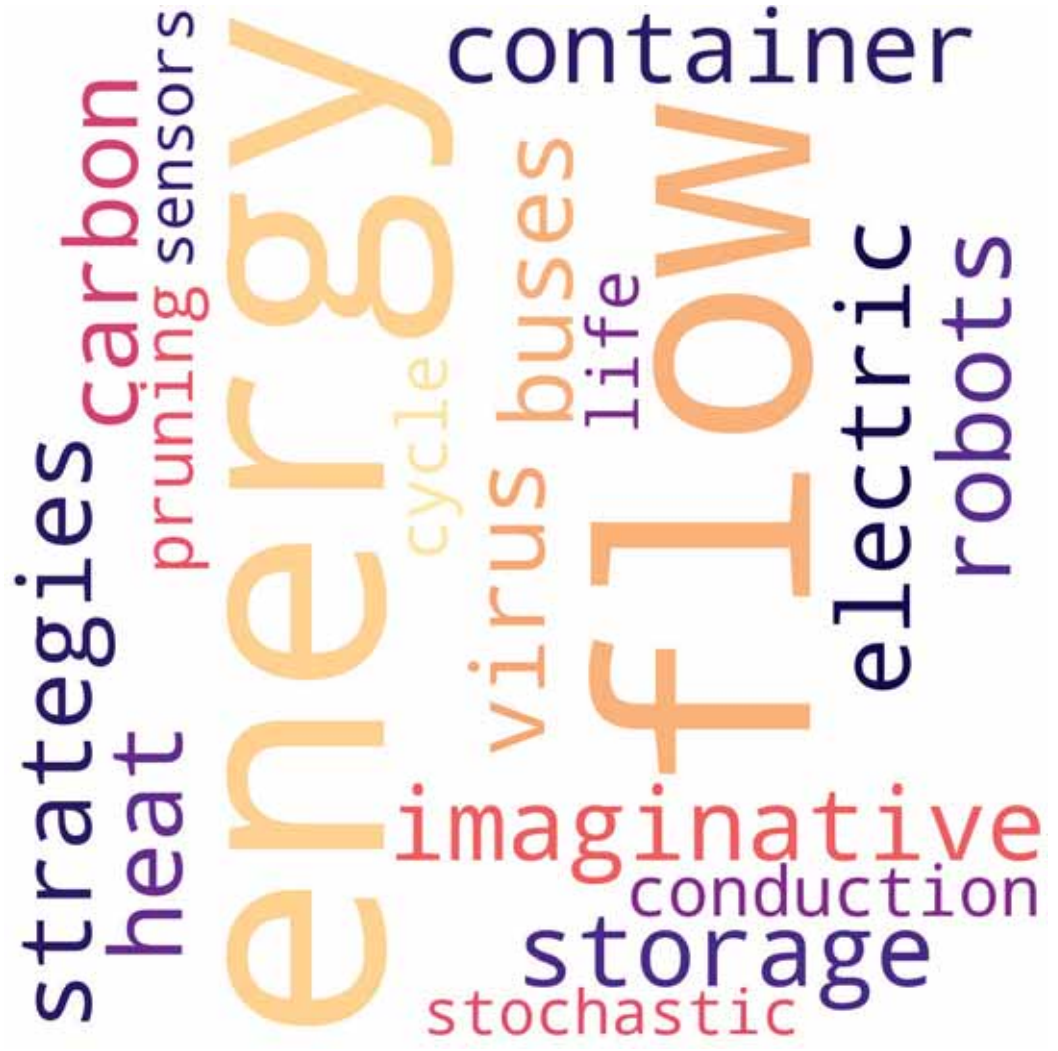


# SNE SIMULATION NOTES EUROPE



Journal on Developments and Trends in Modelling and Simulation

EUROSIM Scientific Membership Journal

Vol. 35 No.1, March 2025

ISSN Online 2306-0271

DOI 10.11128/sne.35.1.1072

ISSN Print 2305-9974



## SNE - Aims and Scope

**Simulation Notes Europe (SNE)** provides an international, high-quality forum for presentation of new ideas and approaches in simulation - from modelling to experiment analysis, from implementation to verification, from validation to identification, from numerics to visualisation ([www.sne-journal.org](http://www.sne-journal.org)).

**SNE** seeks to serve scientists, researchers, developers and users of the simulation process across a variety of theoretical and applied fields in pursuit of novel ideas in simulation. **SNE** follows the recent developments and trends of modelling and simulation in new and/or joining areas, as complex systems and big data. **SNE** puts special emphasis on the overall view in simulation, and on comparative investigations, as benchmarks and comparisons in methodology and application. For this purpose, **SNE** documents the **ARGESIM Benchmarks** on *Modelling Approaches and Simulation Implementations* with publication of definitions, solutions and discussions. **SNE** welcomes also contributions in education in/for/with simulation.

**SNE** is the scientific membership journal of **EUROSIM**, the *Federation of European Simulation Societies and Simulation Groups* ([www.eurosim.info](http://www.eurosim.info)), also providing Postconference publication for events of the member societies. **SNE**, primarily an electronic journal **e-SNE** (ISSN 2306-0271), follows an open access strategy, with free download in basic version (B/W, low resolution graphics). Members of most **EUROSIM** societies are entitled to download **e-SNE** in an elaborate full version (colour, high resolution graphics), and to access additional sources of benchmark publications, model sources, etc. (via group login of the society), **print-SNE** (ISSN 2305-9974) is available for specific groups of **EUROSIM** societies.

**SNE** is published by **ARGESIM** ([www.argesim.org](http://www.argesim.org)) on mandate of **EUROSIM** and **ASIM** ([www.asim-gi.org](http://www.asim-gi.org)), the German simulation society. **SNE** is DOI indexed with prefix 10.11128.

**Author's Info.** Individual submissions of scientific papers are welcome, as well as post-conference publications of contributions from conferences of **EUROSIM** societies. **SNE** welcomes special issues, either dedicated to special areas and/or new developments, or on occasion of events as conferences and workshops with special emphasis.

Authors are invited to submit contributions which have not been published and have not being considered for publication elsewhere to the **SNE** Editorial Office.

**SNE** distinguishes different types of contributions (*Notes*), i.e.

- **TN** Technical Note, 6–10 p.
- **SN** Short Note, max. 5 p.
- **SW** Software Note, 4–6 p.
- **BN** Benchmark Note, 2–10 p.
- **ON** Overview Note – only upon invitation, up to 14 p.
- **EN** Education Note, 6–8 p.
- **PN** Project Note 6–8 p.
- **STN** Student Note, 4–6 p., on supervisor's recommendation
- **EBN** Educational Benchmark Note, 4–10 p.

Further info and templates (doc, tex) at **SNE**'s website, or from the Editor-in-Chief

[www.sne-journal.org](http://www.sne-journal.org)

[office@sne-journal.org](mailto:office@sne-journal.org), [eic@sne-journal.org](mailto:eic@sne-journal.org)

## SNE Editorial Board

**SNE - Simulation Notes Europe** is advised and supervised by an international scientific editorial board. This board is taking care on peer reviewing of submission to **SNE** (and extended for special issues and Postconference Publication):

- Felix Breitenecker, [Felix.Breitenecker@tuwien.ac.at](mailto:Felix.Breitenecker@tuwien.ac.at)  
TU Wien, Math. Modelling, Austria, Editor-in-chief
- David Al-Dabass, [david.al-dabass@ntu.ac.uk](mailto:david.al-dabass@ntu.ac.uk),  
Nottingham Trent University, UK
- Maja Atanasijevic-Kunc, [maja.atanasijevic@fe.uni-lj.si](mailto:maja.atanasijevic@fe.uni-lj.si)  
Univ. of Ljubljana, Lab. Modelling & Control, Slovenia
- Aleš Belič, [ales.belic@sandoz.com](mailto:ales.belic@sandoz.com), Sandoz
- Peter Breedveld, [P.C.Breedveld@el.utwente.nl](mailto:P.C.Breedveld@el.utwente.nl)  
University of Twente, Netherlands
- Agostino Bruzzone, [agostino@itim.unige.it](mailto:agostino@itim.unige.it)  
Universita degli Studi di Genova, Italy
- Vlatko Čerić, [vceric@efzg.hr](mailto:vceric@efzg.hr), Univ. Zagreb, Croatia
- Russell Cheng, [rhc@maths.soton.ac.uk](mailto:rhc@maths.soton.ac.uk)  
University of Southampton, UK
- Roberto Cianci, [cianci@dime.unige.it](mailto:cianci@dime.unige.it),  
Math. Eng. and Simulation, Univ. Genova, Italy
- Eric Dahlquist, [erik.dahlquist@mdh.se](mailto:erik.dahlquist@mdh.se), Mälardalen Univ., Sweden
- Umüt Durak, [umut.durak@dlr.de](mailto:umut.durak@dlr.de)  
German Aerospace Center (DLR) Braunschweig, Germany
- Horst Ecker, [Horst.Ecker@tuwien.ac.at](mailto:Horst.Ecker@tuwien.ac.at)  
TU Wien, Inst. f. Mechanics, Austria
- Vadim Engelson, [vadime@mathcore.com](mailto:vadime@mathcore.com)  
MathCore Engineering, Linköping, Sweden
- Peter Groumpos, [groumpos@ece.upatras.gr](mailto:groumpos@ece.upatras.gr), Univ. of Patras, Greece
- Edmond Hajrizi, [ehajrizi@ubt-uni.net](mailto:ehajrizi@ubt-uni.net)  
University for Business and Technology, Pristina, Kosovo
- Glenn Jenkins, [GLJenkins@cardiffmet.ac.uk](mailto:GLJenkins@cardiffmet.ac.uk)  
Cardiff Metropolitan Univ., UK
- Emilio Jiménez, [emilio.jimenez@unirioja.es](mailto:emilio.jimenez@unirioja.es)  
University of La Rioja, Spain
- Peter Junglas, [peter@peter-junglas.de](mailto:peter@peter-junglas.de)  
Univ. PHTW Vechta, Mechatronics, Germany
- Esko Juuso, [esko.juuso@oulu.fi](mailto:esko.juuso@oulu.fi)  
Univ. Oulu, Dept. Process/Environmental Eng., Finland
- Kaj Juslin, [kaj.juslin@enbuscon.com](mailto:kaj.juslin@enbuscon.com), Enbuscon Ltd, Finland
- Claudia Krull, [claudia@isg.cs.ovgu.de](mailto:claudia@isg.cs.ovgu.de), Univ. Magdeburg, Germany
- Andreas Körner, [andreas.koerner@tuwien.ac.at](mailto:andreas.koerner@tuwien.ac.at)  
TU Wien, Math. E-Learning Dept., Vienna, Austria
- Francesco Longo, [f.longo@unicat.it](mailto:f.longo@unicat.it)  
Univ. of Calabria, Mechanical Department, Italy
- Yuri Merkurjev, [merkur@itl.rtu.lv](mailto:merkur@itl.rtu.lv), Riga Technical Univ.
- David Murray-Smith, [d.murray-smith@elec.gla.ac.uk](mailto:d.murray-smith@elec.gla.ac.uk)  
University of Glasgow, Fac. Electrical Engineering, UK
- Gaspar Music, [gasper.music@fe.uni-lj.si](mailto:gasper.music@fe.uni-lj.si)  
Univ. of Ljubljana, Fac. Electrical Engineering, Slovenia
- Thorsten Pawletta, [thorsten.pawletta@hs-wismar.de](mailto:thorsten.pawletta@hs-wismar.de)  
Univ. Wismar, Dept. Comp. Engineering, Wismar, Germany
- Niki Popper, [niki.popper@dwh.at](mailto:niki.popper@dwh.at), dwh Simulation Services, Austria
- Kozeta Sevrani, [kozeta.sevrani@unitir.edu.al](mailto:kozeta.sevrani@unitir.edu.al)  
Univ. Tirana, Inst.f. Statistics, Albania
- Yuri Senichenkov, [sneyb@dcn.infos.ru](mailto:sneyb@dcn.infos.ru)  
St. Petersburg Technical University, Russia
- Michal Štepanovský, [stepami9@fit.cvut.cz](mailto:stepami9@fit.cvut.cz)  
Technical Univ. Prague, Czech Republic
- Oliver Ullrich, [oliver.ullrich@iais.fraunhofer.de](mailto:oliver.ullrich@iais.fraunhofer.de)  
Fraunhofer IAIS, Germany
- Siegfried Wassertheurer, [Siegfried.Wassertheurer@ait.ac.at](mailto:Siegfried.Wassertheurer@ait.ac.at)  
AIT Austrian Inst. of Technology, Vienna, Austria
- Sigrid Wenzel, [S.Wenzel@uni-kassel.de](mailto:S.Wenzel@uni-kassel.de)  
Univ. Kassel, Inst. f. Production Technique, Germany
- Grégory Zacharewicz, [gregory.zacharewicz@mines-ales.fr](mailto:gregory.zacharewicz@mines-ales.fr)  
IMT École des Mines d'Alès, France

## Editorial

*Dear Readers*, This first issue of SNE Volume 35, 2025, SNE 35(1), shows the very broad area of modelling and simulation with conference post-publications from ASIM Symposium Simulation Technique2024 in Munich: from energy flow to imaginative robots, from carbon storage to container strategies, from west Nile virus to electric buses, from heat conduction to pruning, etc.

And we come along with a novelty: SNE is licensed under Creative Commons Licence: 'SNE - Simulation Notes Europe © 2025 by ARGESIM Vienna - ASIM/GI - EUROSIM is licensed under CC BY 4.0'. This CC BY license legally covers the regulations for the previous ARGESIM/ASIM/EUROSIM copyright, with main regulation 'credit must be given to the creator' in case of re-use of the paper (from CC BY 4.0). So the basic version of SNE and all SNE contributions are published with open access. For members of the societies we still additionally provide a member version (prev. 'restricted access', now 'member access') with advanced features (colour, high-res, and in case of conference post-publications with references to slides, etc.)

And furthermore, for postconference publications in SNE we clarify the differences to the conference publication by the attributes 'revised' (typos, improved formatting), 'improved' (typos, improved formatting, minor reformulations), extended (typos, improved formatting, reformulations and extensions); in case of not-English conference publications the attribute 'English version' is added. I would like to thank all authors for their contributions, and many thanks to the SNE Editorial Office for layout, typesetting, electronic publishing, license update, and much more. And have a look at the info on EUROSIM-related simulation events this year: ASIM Conference in Dresden, I3M conference in Morocco, SIMS- EUROSIM conference in Stavanger, and WinterSim in Seattle.

Felix Breitenecker, SNE Editor-in-Chief, [eric@sne-journal.org](mailto:eric@sne-journal.org); [felix.breitenecker@tuwien.ac.at](mailto:felix.breitenecker@tuwien.ac.at)

### Contents SNE 35(1)

e-SNE 35(1), DOI 10.11128/sne.35.1.1072

[www.sne-journal.org/sne-volumes/volume-35](http://www.sne-journal.org/sne-volumes/volume-35)

SNE Basic e-Version with Open Access, CC BY 4.0

SNE Full e-Version for Members of publication-active EUROSIM Societies: ASIM, CEA-SMSG, CSSS, DBSS, KA-SIM, LIOPHANT, NSSM, PTSK, SIMS, SLOSIM, UKSIM

print-SNE for members on demand (printer INTU TU Wien)

Modeling Material and Energy Flow in an Eco-industrial Park using Discrete Event Simulation. S. Xie, T. Zhang, T. Uhlig, O. Rose, B. Vollack .....	1
A Meta-model for Comparing Carbon Capture Storage and Utilisation Technologies using Life Cycle Analysis J. Benz, K. Blank, S. Hötzel, J. Just, C. Lau, F. Schicks, N. von der Ahe, J. Wittmann .....	9
Mathematical Analysis of a Compartment Model. A. Niotis, K. Chudej .....	17
Mathematical Model for Spatial and Temporal Risk Analysis of West Nile Virus Transmission in Bavaria, Germany. O. C. Mbaoma, S. M. Thomas, C. Beierkuhnlein .....	25
Simulation-Based Analysis of Storage Strategies for an Inland Container Terminal. M. Mowe, J. Manemann, L. Jurgeleit, M. Kiefer, U. Clausen .....	31
Simulation and Control of 2-Dimensional Anisotropic Heat Conduction. S. Scholz, C. Bonenberger, N. Scheiter, L. Berger .....	35
Comparing Different Pruning Strategies for the Evaluation Task of Virtual Stochastic Sensors. D. Bodnár, C. Krull	41
Development of a Simulation Model for Predicting Energy Consumption of Battery-Electric Buses. A. Konzept, A. Hitz, B. Reick .....	49
Data-adaptive Dynamic Simulation via Structured Dynamic Mode Decomposition. C. Bonenberger, S. Scholz, N. Scheiter .....	55

Towards Imaginative Robots: A Generative Pipeline for Simulated Environments.

C. May, L. Suchy, J. Franke, S. Reitelshöfer ..... 61

Obituary Thomas Schriber ..... ii

EUROSIM Societies & ARGESIM/SNE Short Info .. N1 – N4

Conferences EUROSIM / ASIM ..... Covers

### SNE Contact & Info

SNE Online ISSN 2306-0271, SNE Print ISSN 2305-9974

→ [www.sne-journal.org](http://www.sne-journal.org)

✉ [office@sne-journal.org](mailto:office@sne-journal.org), [eric@sne-journal.org](mailto:eric@sne-journal.org)

#### ✉ SNE Editorial Office

Felix Breitenecker (Organisation, Author Mentoring)  
Irmgard Husinsky (Web, Electronic Publishing),  
ARGESIM/Math. Modelling & Simulation Group,  
Inst. of Analysis and Scientific Computing, TU Wien  
Wiedner Hauptstrasse 8-10, 1040 Vienna, Austria

WEB: → [www.sne-journal.org](http://www.sne-journal.org), DOI prefix 10.11128/sne

Scope: Developments and trends in modelling and simulation in various areas and in application and theory;

comparative studies and benchmarks (documentation of ARGESIM Benchmarks on modelling approaches and simulation implementations); modelling and simulation in and for education, simulation-based e-learning; society information and membership information for EUROSIM members (Federation of European Simulation Societies and Groups).

Editor-in-Chief: Felix Breitenecker, TU Wien, Math. Modelling Group

✉ [Felix.Breitenecker@tuwien.ac.at](mailto:Felix.Breitenecker@tuwien.ac.at), ✉ [eric@sne-journal.org](mailto:eric@sne-journal.org)

Print SNE: INTU (TU Wien), Wiedner Hauptstrasse 8-10, 1040, Vienna, Austria – [www.intu.at](http://www.intu.at)

ARGESIM Publisher: ARBEITSGEMEINSCHAFT SIMULATION NEWS  
c/o Math. Modelling and Simulation Group, TU Wien / 101,  
Wiedner Hauptstrasse 8-10, 1040 Vienna, Austria;  
[www.argesim.org](http://www.argesim.org), ✉ [info@argesim.org](mailto:info@argesim.org) on behalf of  
ASIM [www.asim-gi.org](http://www.asim-gi.org) and EUROSIM → [www.eurosims.info](http://www.eurosims.info)

© 2025 SNE is licensed under CC BY 4.0 by ARGESIM Vienna - ASIM/GI - EUROSIM

## Thomas Schriber

On December 31, 2024, Thomas Schriber, well-known simulationist passed away. Our modelling and simulation community has lost a pioneer in discrete modelling and simulation.



### Obituary from Ann Arbor Observer (short.)

Thomas Jude Schriber passed away peacefully on December 31, 2024, at the age of 89 in his beloved “Little Ann Arbor Town,” surrounded by his immediate family.

In the hundreds of condolences received, the words used most often to describe Tom are kind, thoughtful, generous, and gentle. He was warm and jovial and consistently put other people first. His legacy lives on through his loving family, academic contributions, the countless students he inspired, and the warmth he brought to all who knew him.

Born on October 28, 1935, in Flint, Michigan, Tom was raised in East Tawas and Rogers City. A pioneering figure in business information technology and simulation science, he dedicated his life to education and innovation. Tom’s academic journey began at his beloved Notre Dame, where he graduated Magna Cum Laude with a BS in Chemical Engineering in 1957. He then earned his MSE in 1958, MA in 1959, and PhD in Chemical Engineering in 1964 from the University of Michigan.

Tom’s teaching career started at Eastern Michigan University in 1963 as Assistant Professor and Director of its Academic Computer Center. In 1966, he joined the Business School at the University of Michigan, where he spent five decades shaping minds and advancing simulation science. Rising through the ranks, he became Assistant Professor in 1966, Associate Professor in 1969, and Professor of Business Information Technology in 1972. His expertise took him around the world as a Visiting Scholar at Stanford University, the Swiss Federal Technical University, and the National University of Singapore.

Tom’s research focused on discrete-event simulation, a methodology for building computer-based systems models and conducting experiments to understand system behaviour. His work included modeling language design, model verification and validation, system visualization through animation, statistical design of experiments, and output analysis. He made significant contributions to the logical foundations of simulation software, variance-reduction techniques, and applications in manufacturing and transportation systems.

Recognized for his excellence by INFORMS with both the Simulation Society’s Distinguished Service Award and its Lifetime Professional Achievement Award, Tom was also known for his kindness, infectious laugh, and ability to host a great cocktail party. He never missed sending an email for birthdays, anniversaries, weddings, or funerals, showing his deep care for personal connections.

Tom’s passion for teaching was unmatched. At his final Thanksgiving dinner, when asked about his perfect day, he answered without hesitation that it would be giving back-to-back lectures followed by office hours.

He continued teaching at the University of Michigan Ross School of Business until age 80, touching thousands of students’ lives during his 50-year tenure.

Known for his methodical approach to decision-making (sometimes to a fault), Tom would often delay purchasing new technology, knowing something better would soon come to market. This led to his charming habit of using older models until they became obsolete. His family fondly remembered his careful deliberation over restaurant menus, reading them aloud to patient waiters while searching for the perfect choice.

Source:

<https://annarborobserver.com/thomas-jude-schriber/>

### Thomas Schriber – ASIM and SNE

Thomas Schriber also visited Magdeburg University, Institute for Simulation. On one of these occasions he came in contact with ASIM, initiated by Prof. Peter Lorenz, ASIM Honorary Member – and he became ASIM member in 1993. In ASIM, he has stimulated work on discrete event simulation, and underlined the importance of teaching, for students, but also for simulation professionals. He was also publishing in SNE. So, he has authored in 1996 the SNE-ARGESIM benchmark ‘Canal-and-Lock System, which stimulated many SNE publication.

ASIM and SNE have lost a pioneer in modelling and simulation, and an enthusiastic teacher in this area.

### Thomas Schriber – Personal Remark

Via Magdeburg and ASIM Thomas Schriber also got contact with our Modelling and Simulation Group at TU Wien. We could arrange at TU Wien courses on discrete-event modelling using with GPSS/H given by him. And in 1995, he was Invited Speaker at our EUROSIM 1995 Congress, organised by ARGESIM and ASIM at TU Vienna – the picture below shows him with his wife on occasion of the welcome reception.

Thomas Schriber stimulated also my work and teaching in discrete modelling and simulation, and related publications in simulation. And in my library, there still stands not only the classic edition of his ‘Simulation with GPSS’ with yellow cover, but also the Russian edition, with red cover. Thomas Schriber was a beacon for me – personally and in profession.

Felix Breitenecker, EiC SNE



# Modeling Material and Energy Flow in an Eco-industrial Park using Discrete Event Simulation

Shufang Xie<sup>1\*</sup>, Tao Zhang<sup>1</sup>, Tobias Uhlig<sup>1</sup>, Oliver Rose<sup>1</sup>, Björn Vollack<sup>2</sup>

<sup>1</sup>Institute for Computer Science, University of Bundeswehr Munich, Werner-Heisenberg-Weg 39,  
85579 Neubiberg, Germany; \*[shufang.xie@unibw.de](mailto:shufang.xie@unibw.de)

<sup>2</sup>Chair of Logistics Engineering, TUD Dresden University of Technology, Dresden, Germany

SNE 35(1), 2025, 1-8, DOI: 10.11128/sne.35.tn.10721  
Selected ASIM SST 2024 Postconf. Publication: 2024-12-10  
Received Revised: 2025-02-17; Accepted: 2025-02-25  
SNE - Simulation Notes Europe, ARGESIM Publisher Vienna  
ISSN Print 2305-9974, Online 2306-0271, [www.sne-journal.org](http://www.sne-journal.org)

**Abstract.** In recent times, a specific number of eco-industrial parks have emerged as a viable solution to address the escalating environmental challenges. Within these industrial parks, factories engage in mutual interaction through the flow of materials and energy. By modeling the material and energy flow within an eco-industrial park, we gain a comprehensive understanding of how resources circulate. This understanding not only provides strategic insights but also enables the identification of optimization opportunities, fostering more efficient resource utilization, waste reduction, and significant cost savings. Therefore, this research focuses on modeling the material and energy flow in the park using the discrete event simulation technique. We will provide a detailed explanation of our modeling approach, outlining how we employ this method to optimize resource usage, reduce waste, and minimize the environmental impact of industrial activities within the park. As part of our research, we have also developed a simple virtual eco-industrial park example to validate and demonstrate the effectiveness of our modeling approach. This practical illustration will serve to showcase the real-world applicability and benefits of our research in creating more sustainable and efficient eco-industrial parks.

## Introduction

In response to the increasing global environmental concerns, eco-industrial park (EIP) has emerged as a proactive and sustainable solution.

EIPs are communities of manufacturing and service businesses collaborating to enhance environmental and economic performance through effective management of resources like energy, water, and materials. This collaborative approach seeks collective benefits greater than individual optimizations [1]. The concept of EIPs has recently captured significant interest from both industry and academic research communities, much of the focus has been on the planning and design stages, with limited attention to operational parks [2-5]. Boix et al. provide a comprehensive literature review on the optimization methods applied to the design of EIP [6]. As of 2011, there were over 20,000 operational industrial parks globally [7], offering substantial opportunities for material, energy, and waste savings. However, research on operational parks has been limited, often targeting specific environmental issues rather than providing comprehensive analyses for optimization. For instance, one study utilized a Monte Carlo model to simulate wastewater treatments in an industrial park in China, focusing on reducing pollution [8].

This paper aims to bridge this gap by employing modeling and simulation techniques to thoroughly investigate an operational industrial park. By employing modeling techniques, we can comprehensively analyze the intricate interactions and processes within the park. The central activity in an EIP revolves around the physical exchange of materials, energy, and services. Efficiently managing the flow of energy and materials is a cornerstone of any industrial park's operations. Prior to efficient management, the analysis and modeling of material and energy flow are essential. Consequently, this article places its primary focus on the simulation and modeling of energy and material flow within existing industrial parks, employing discrete event simulation method (DES).

Widely utilized in modeling, DES enables the study of systems that are discrete, dynamic, and stochastic [9]. It facilitates the simulation and understanding of how materials and energy traverse the system, providing valuable insights into resource management, waste reduction, and energy efficiency. A detailed explanation of our modeling approach will be provided, and a simple hypothetical park will be used to demonstrate the effectiveness of our modeling techniques.

The paper is structured as follows: a brief conceptual model is described in Section 1 while a more detailed formal model of material and energy flow are addressed in Section 2 and 3 respectively. The implementation and application of the simulation model are introduced in Section 4. The paper is concluded in the last section.

## 1 Conceptual Model of Material and Energy Flow in EIP

### 1.1 Eco-industrial Park

In EIPs, common components typically include the factory infrastructure, material flow systems, and energy flow systems. These components are essential for the functioning of the park and its sustainable operations. Figure 1 illustrates a simplified EIP where multiple factories coexist. Suppliers from outside the EIP provide raw materials, and customers from outside the EIP consume the final products manufactured within the park. Instead of solely relying on externally purchased raw materials, the factories within the EIP promote resource synergy by using outputs from neighboring factories as valuable raw materials.

Moreover, in pursuit of sustainable waste management, the EIP adopts waste-to-energy (WTE) technology instead of depositing waste in landfills.

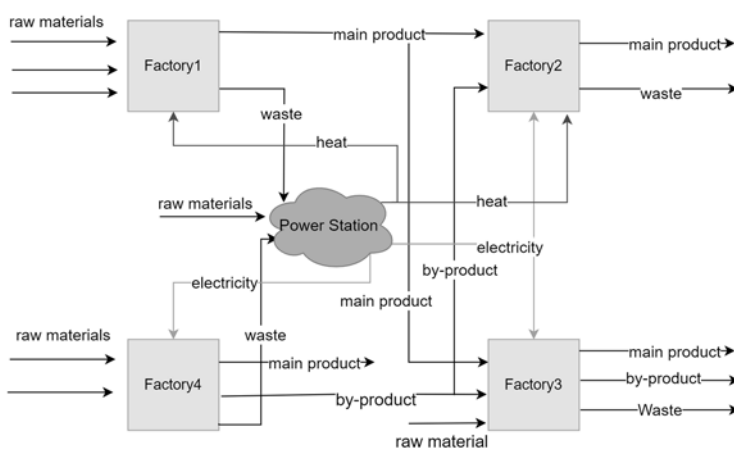


Figure 1: An EIP example.

Moreover, in pursuit of sustainable waste management, the EIP adopts waste-to-energy (WTE) technology instead of depositing waste in landfills.

This process recovers energy from waste sources in the form of heat, electricity, or transport fuels [10], complemented by a dedicated power plant within the park. This integrated approach minimizes environmental impact and provides a valuable energy source for the park's factories, promoting eco-friendly solutions and reducing reliance on external energy sources. Notably, in many cases, WTE plants are combined heat and power (CHP) producers [11]. In addition to WTE initiatives, the EIP enhances energy efficiency by incorporating CHP plants, known for simultaneously producing electricity and useful heat from a single fuel source. Unlike traditional power plants, CHP plants capture and utilize waste heat for heating and cooling applications, optimizing energy utilization.

### 1.2 Material and Energy flow in an EIP

From the perspective of each factory, materials can be categorized into two aspects: input materials and output materials. Input materials encompass not only the raw materials acquired from external suppliers but also the innovative utilization of by-products and waste generated within one factory, fostering a symbiotic relationship with another.

On the output side, factories yield main products that form the core of their operations, accompanied by valuable by-products and, inevitably, waste materials. In an industrial park, energy operates in two essential forms: electricity and heat. These dual components play a crucial role in powering various processes and activities within the industrial complex.

Material and energy flow refers to the movement, transfer, or transition of materials and energy within a system or process. In the context of Industrial Park, the material flow contains the exchange of materials between factories and within a single factory. Between factories, material flow could be materials transition from the output storage of one factory to the input storage of another. Within a factory, materials move from the input storage to the machines for processing. Once processed, the resulting output materials are routed to the output storage area, awaiting delivery to their respective customers.

When considering energy flow within the context of an industrial park, two distinct types can be identified. The first type involves energy carried along with material flow. For instance, when an output material possesses a higher temperature and another factory within the park requires specific temperature conditions for its inputs. The second type of energy flow pertains to the energy generated by the power plant within the park. The energy produced by CHP is consumed by the various factories and members operating within the industrial park. It plays a crucial role in supporting the energy needs of the park's internal processes and activities.

Material and energy flow control refers to the management, regulation, and optimization of the movement of materials and energy within EIP. Material and energy flow control encompasses decision-making at various stages of material and energy flow, addressing questions of what, where, when, and how materials and energy move within a system.

Typical decision-making aspects in material and energy flow control include:

- material and energy dispatching
- supplier selection
- alternative material choice
- inventory management.

These decisions are critical in optimizing the efficiency, sustainability, and cost-effectiveness of material and energy utilization within industrial processes.

## 2 Formal Model of Material Flows

### 2.1 Factory

Factories or industrial facilities are common elements within EIPs, and they can be integrated into an input-output model. Input-output modelling, having the advantage of tracing all primary inputs, wastes, by-products, and main product flows of a production unit, is an appropriate tool for designing industrial symbiosis networks [12].

**Input and Output.** To ensure the production of high-quality products that meet user requirements, factories often rely on specific production recipes [12]. These recipes are represented by input ratios, which indicate the quantity of raw materials needed to produce one unit of the main product. However, due to uncertainties in the production process or variations in raw material quality, these input ratios can exhibit stochastic behavior.

Additionally, factories may have multiple options for each input. Equation (1) illustrates a scenario where a factory has three inputs, and for the first input, there are two alternative materials to choose from. The input ratio is denoted as 'r'.

$$\text{InputAmount} = \text{productAmount} \times [[r_{1a}, r_{1b}][r_{2a}][r_{3a}, r_{3b}, r_{3c}]] \quad (1)$$

Throughout the production process, input materials undergo a transformation, resulting in the generation of the main product, by-products, and waste materials. The output from each factory can be mathematically represented using the formula (2):

$$\text{outputAmount} = \text{productAmount} \times [1 \ w_1 \ w_2 \ w_3]^T \quad (2)$$

where the vector 'w' represents the output ratios. These ratios specify the quantities of by-products or waste materials produced in conjunction with one unit of the primary product. Given the intricate nature of the production process, it is important to recognize that numerous uncertain factors come into play. Furthermore, occasional, random changes in output ratios may occur because of advancements in production technology.

**Inventory and production process.** Input and output materials are typically stored within the factory's warehouse, with each type of material having its dedicated inventory. Inventory management involves defining safety levels ( $L_s$ ) and target levels ( $L_t$ ) for each type of material. The purpose of these levels is twofold:

- 1) To prevent production disruptions caused by a shortage of raw materials, the factory initiates the purchase of raw materials when the current inventory level ( $I$ ) reaches the safety level ( $L_s$ ), with the aim of restoring it to the target level ( $L_t$ ).
- 2) To prevent overproduction, if the inventory of the primary product reaches the target level ( $L_t$ ), production within the factory is halted. Additionally, if the quantity of waste exceeds the available inventory capacity, any excess material is disposed of in a landfill.

In our production setup, each factory has a maximum production capacity denoted as  $C_m$ , representing the highest achievable monthly or yearly production volume. Factories typically operate at a target capacity level, denoted as  $C_t$ , where  $C_t$  is less than or equal to  $C_m$ . The actual capacity, denoted as  $C$ , may vary due to factors such as machine breakdowns, worker absences, and other operational fluctuations.

Specifically, the actual capacity can change as follows:  $C = C + \Delta$ , where  $\Delta$  represents either a capacity loss or gain. Production planning follows a level strategy, assuming customer demands ( $d$ ) equal to the target capacity ( $d = C_t$ ). A production plan specifies the quantity of products to be completed on a weekly or monthly basis, which then generates a material requirement plan divided into daily or shift-based schedules. These schedules are transmitted to the shop floor as manufacturing orders. The shop floor accepts and schedules items within the manufacturing orders for processing. Individual machines are consolidated into a single machine, and the processing time ( $p$ ) for one item is calculated as  $p = 1/C$ . If raw materials for a particular item are insufficient, the item enters a queue following the "first in, first out" (FIFO) rule, ensuring items are processed in the order they arrived.

### 2.2 Material Flow

Material flows are governed by specific protocols that dictate when and how materials are moved within the system. Each type of material adheres to its own set of rules and procedures. This section outlines three types of material flow protocols: pushing, purchasing, and ordering. Purchasing and ordering fall under pulling protocols, involving requesting materials as needed, while pushing protocols supply materials without direct requests.

Before detailing material flow protocols, let's introduce the batch concept, which is widely employed by manufacturers to optimize production. In our model, batches take various forms. Production batches, defined in the production planning system, are subdivided into smaller process batches (manufacturing orders) on shop floors, each containing multiple jobs. Suppliers deliver products in delivery batches, while customers order in order/purchase batches, typically multiples of the delivery batch.

**Pushing.** In this protocol, the produced material is directly delivered to customers as soon as a delivery batch is assembled, as depicted in Figure 2. When one process batch is produced in one factory, the output inventories of this factory will be updated. Push events happen regularly in the factory to check if the amount of output inventories is enough to form a delivery batch. If sufficient material is available, it's transported to the chosen customer. However, if no customers can accept the delivery batch due to capacity constraints, and the supplier's output inventory reaches its limit, excess material may be discarded if it's considered waste.

### Purchasing and Ordering.

Both purchasing and ordering are fundamental pulling protocols utilized in different manufacturing contexts. Purchasing is typically employed in make-to-stock factories, where materials are stored in warehouses until customers make purchases.

On the other hand, ordering is prevalent in make-to-order factories, where customers initiate orders that suppliers then produce and deliver.

In both protocols, regular events are triggered based on inventory levels. When the inventory reaches a safety level, actions are taken to restore it to the target level. Supplier selection policies are often employed to optimize decision-making when multiple suppliers are available.

The order details are then transmitted to the selected supplier's planning system, and the production process begins. Ultimately, orders may be split into process batches, and delivery occurs once the required quantity is fully produced.

The choice of protocol depends on the type of materials involved. For instance, waste materials are typically not subject to purchase, and by-products cannot be ordered.

The applicable protocols between external suppliers, customers, and factories are outlined in Table 1 below.

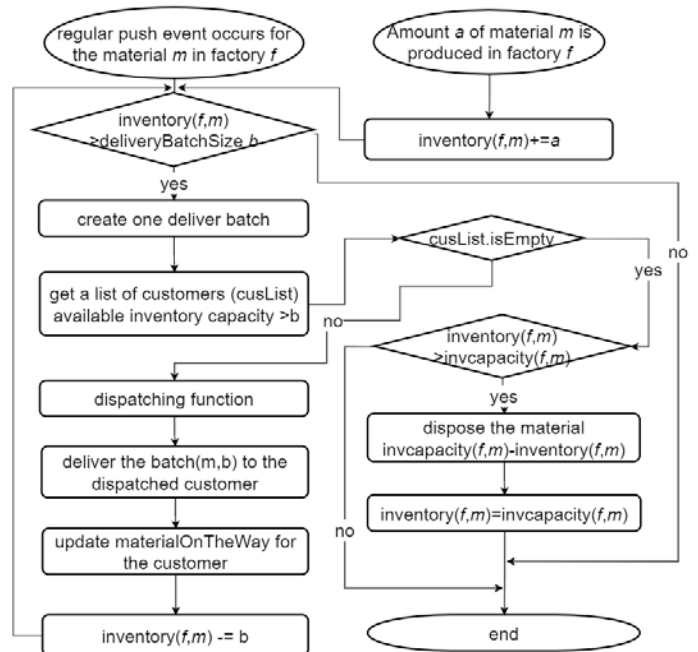


Figure 2: Pushing protocol of material flows.

Material	From	To	Protocols
Products	Supplier	Factory	Purchasing
Products	Factory	Customer	Purchasing /Ordering
By-products	Factory	Customer	Purchasing
Waste	Factory	Disposal	pushing
Products	Factory	Factory	Purchasing /Ordering /Pushing
By-products	Factory	Factory	Purchasing /Pushing
Waste	Factory	Factory	Pushing

**Table 1:** Possible protocols between suppliers, factories, and customers.

### 3 Formal Model of Energy Flow in an EIP

In our study, we focus on energy flow which concerns the consumption of energy generated by the CHP system by the factories located within the park. It illustrates how the energy produced by the CHP system is efficiently utilized by the diverse factories operating within the park. This energy flow serves as the central and indispensable component of the park's overall energy dynamics. In the following section, we will provide an in-depth explanation of our approach to modeling this specific energy flow which can be broken down into three fundamental components: power station, power consumption, and power scheduling. We will elaborate on our approach from the perspective of each of these components.

#### 3.1 Power Station

The CHP power station element is modeled within a formal factory framework, distinguished primarily by its output type. Unlike traditional factories producing physical materials, the power station generates both heat and electricity. Its main input material comprises waste materials generated by other factories within the park. In instances where these waste materials are insufficient, the model seamlessly integrates external raw materials like coal to maintain uninterrupted operations. Additionally, our model includes parameters to configure the total number of available power generators, and the capacity allocated to each individual generator within the power station.

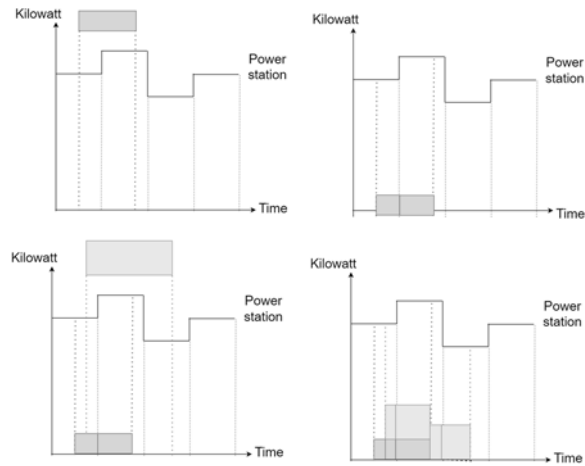


**Figure 3:** Area cutting algorithm.

#### 3.2 Power Consumption

Each factory's power requirement is closely tied to its production needs and is represented as a tuple (factory, start time, end time, requested power). This structured format signifies that within the specified time frame, the factory requires a specific supply of power, as quantified by the requested power value. In our study, power consumption is managed through the application of an area cutting algorithm, as depicted in Figure 3.

This algorithm operates by representing each power request as a rectangular area on a graph. The length of the rectangle corresponds to the duration of the power request, which is calculated based on its start and end times. Meanwhile, the width of the rectangle represents the amount of power requested. Concurrently, the power production of the station is graphically depicted as an upper black line over discrete time periods.

Upon initiation of a power request, the algorithm compares its time frame with the periods of power production at the station. This comparison determines whether the request falls within a single period or spans across multiple periods. To enhance accuracy, the periods of power production are further divided into smaller segments based on the start and end times of the request. For each power request, the algorithm updates the remaining power for the relevant segments from the start time to the end time of the request. This ensures precise tracking of power utilization during specific time intervals.

Subsequent power requests undergo a similar process, where their time frames are compared with refined station periods from previous requests, and remaining power is updated accordingly.

### 3.3 Power Scheduling

To optimize energy utilization, the implementation of power scheduling is a key strategy. This strategic approach encompasses determining the quantity of power to be generated and strategically coordinating how individuals or organizations utilize this power.

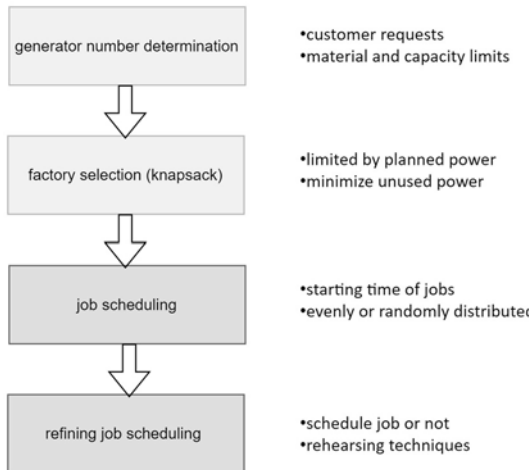


Figure 4: Energy scheduling strategy.

Our initial energy management strategy, as depicted in Figure 4, comprises several steps. Firstly, the number of generators to be activated is determined. Factories develop production plans over a specified time frame, typically a week or a month, while simultaneously creating power usage plans. These plans are transmitted to the center controller, which then calculates energy requests based on them, aggregating all requirements. The center controller formulates a power production plan, considering energy requests and the power station's capacity, including input material constraints and generator availability. This plan specifies how many generators should be activated for the upcoming period.

Next, we select users in a way that minimizes unused power, similar to solving a knapsack problem with a limit on planned power. Following factory selection, we proceed to schedule jobs, determining the start time for each. This decision can be made by either evenly distributing the starting times or assigning them randomly throughout the planned period. The final step in this energy scheduling plan focuses on improving the schedule derived from earlier steps, a rehearsing technique is used here.

A virtual power station is set up to check and improve the existing schedule. In this phase, jobs that are already scheduled request power according to the initial schedule. If there isn't enough power available to meet a job's power requirements, that specific job is excluded from the pre-determined scheduling.

## 4 Implementation and Application

In this section, we have used a virtual and simplified industrial park as an illustrative example to demonstrate our modeling approach. We made this choice due to our constraints in obtaining data from a specific real-world industrial park. We utilized simulation software, specifically AnyLogic, to create this example, which is depicted in Figure 5.

In this example, Factories 1 and 5 serve as primary manufacturing facilities within the EIP, while the upstream two factories act as suppliers of raw materials to support the main factories. Factories 3 and 4 are responsible for managing the waste generated by the main factories. All waste from these factories is directed to a central power station within the park, which generates energy to support the park's members.

To provide context for this example, several assumptions were made: Material flows between factories follow a 'push' protocol. When multiple input sources are available, materials from upstream factories take precedence over those from external suppliers. Factories acquire materials from external suppliers through a purchasing process rather than traditional ordering. The target inventory level equals the inventory capacity. The safety inventory level is maintained at a quantity equivalent to a 30-day supply of throughputs.

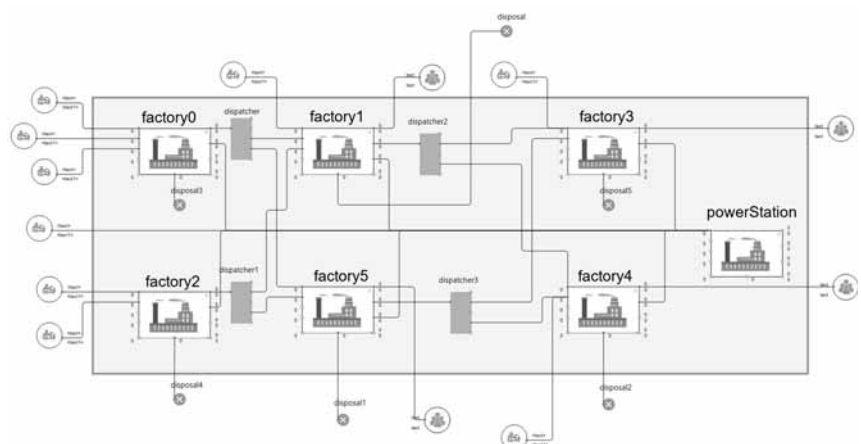


Figure 5: Instance of an EIP Created Using AnyLogic.

It's worth noting that while the power station utilizes recycled waste to generate energy, its output may not always meet the energy needs of all park members.

### 4.1 Experiment of Material Flow

The experiment on material flow aimed to establish an efficient dispatching policy for scenarios where a single material is shared among multiple customer factories, common in industrial symbiosis networks.

The application employed various dispatching policies:

- (1) Random dispatching.
- (2) Directing materials to factories with the highest available inventory.
- (3) Allocating materials based on the ratio of available inventory to capacity.
- (4) Assigning materials to factories maximizing main product output.
- (5) Allocating materials to minimize main product output.
- (6-9) Allocation based on maximum requirements lookahead up to three planning periods.

The KPIs used to evaluate the different policies are divided into three categories: total waste disposal, total sales, and external requirements, which denote economic and environmental objectives. "Total waste disposal" refers to waste disposal across all factories within the park. Specifically, "Total Sale 1" represents the main product amounts that can be sold by factories 1 and 5, while "Total Sale 2" represents the main product outputs of factories 3 and 4. "External requirements" refer to the number of raw materials purchased by factories 1, 3, and 4 from external suppliers. The simulation results of these evaluations are presented in Figure 6.

The simulation results emphasize the effectiveness of scenario 6, "maximal requirement lookahead 0," in minimizing waste disposal. Prioritizing factories with high demand for waste material reduces excess disposal. Conversely, scenario 2, the "available inventory-based rule," leads to higher waste disposal due to surplus allocation to plants with substantial available inventory. Regarding "total sales 1" and "total sales 2," scenario 3, the "available inventory ratio-based rule," proves most effective. This suggests that downstream factories can meet input material requirements, reducing production stoppages, enhancing throughput, and increasing sales. Scenario 4 performs worst for the total external requirement KPI.

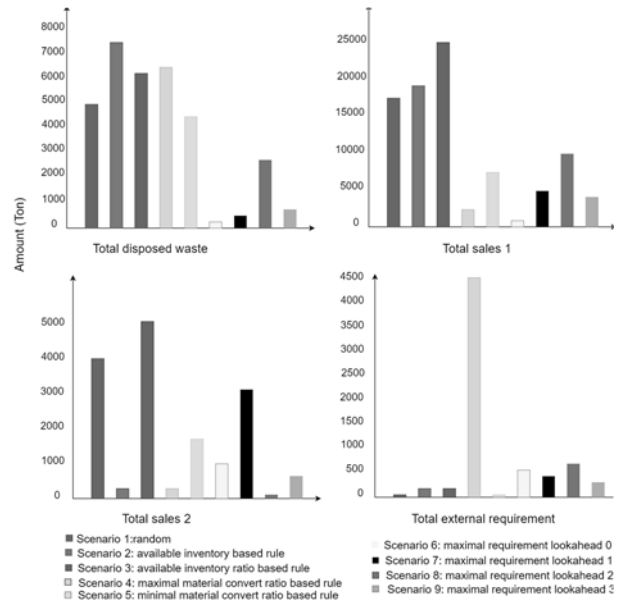


Figure 6: Experiment results of the material flow control.

This is likely due to consistently directing waste materials to the factory with the highest material transformation ratio, forcing other factories to purchase external materials for production. Overall, the simulation provides valuable insights into how different policies impact waste disposal and sales performance.

### 4.2 Experiment of Energy Flow

In this experiment, the simulation duration spans 10 weeks, with each planning period structured as a one-week timeframe, totaling 10 planning periods. The objective was to optimize energy utilization in each planning period. Table 2 presents the outcomes of the experiment for each planning period. It includes details such as the selected factories, indicating which factories were chosen to utilize the energy produced by the internal power station during the respective period.

Plan period	Selected factories	Scheduled jobs ratio	Energy utilization
1	0,1,4,5	0.81	0.66
2	1,3,5	0.72	0.62
3	0,1,2,5	0.77	0.69
4	2,5	0.69	0.68
5	0,1,2,4,5,	0.78	0.75
6	2,4,5	0.59	0.65
7	2,4	0.80	0.67
8	1,2,5	0.66	0.63
9	0,1,2,3,4,5,	0.82	0.79
10	3,5	0.77	0.79

Table 2: Experiment results in each period.

The scheduled jobs ratio represents the proportion of scheduled jobs compared to the total planned jobs across all factories. Additionally, the energy utilization ratio denotes the percentage of energy consumed by the scheduled jobs relative to the total energy generated by the power station.

## 5 Conclusion

In response to escalating environmental concerns, EIPs have emerged as innovative and sustainable solutions for industrial development. Given this context, effective management becomes imperative for these industrial parks. To pave the way for such management, a comprehensive understanding of the dynamic interactions and processes within EIPs is crucial. Material and energy flows are the primary representations of interactions among factories. Consequently, this paper employs discrete event simulation techniques to model the intricate material and energy flows within the park, providing a detailed account of our model's construction.

Through our modeling efforts, we aim to optimize the allocation and distribution of resources within these parks, with a specific emphasis on waste reduction and the maximization of energy utilization. The outcomes of our study can provide practical guidance for eco-industrial park management and policy development, ultimately contributing to a more sustainable and environmentally responsible industrial landscape.

While our primary emphasis remains on existing operational parks, it is worth noting that our modeling approach can also be adapted to the planning phase of industrial parks, providing a means to evaluate the advantages of establishing industrial symbiosis.

Despite our comprehensive approach, it's important to note that, in this study, our management efforts are limited to a simple energy schedule. A more refined strategy is required. Therefore, our future research will specifically concentrate on energy scheduling, aiming to develop strategies that optimize energy utilization through production scheduling.

**Publication Remark.** This contribution is the revised version of the conference version published in *Tagungsband Langbeiträge ASIM SST 2024*, ARGESIM Report AR 47, ISBN ebook: 978-3-903347-65-6, p 27-34, DOI: 10.11128/arep.47.a4718

## References

- [1] Chertow MR. Industrial Symbiosis: Literature and Taxonomy. *Annu. Rev. Energy. Environ.* 2000; 25 (1), pp. 313–337. DOI 10.1146/annurev.energy.25.1.313
- [2] Afshari H, Farel R, Peng Q. Challenges of value creation in Eco-Industrial Parks (EIPs): A stakeholder perspective for optimizing energy exchanges. *Resources, Conservation and Recycling.* 2018; 139, pp. 315–325. DOI 10.1016/j.resconrec.2018.09.002
- [3] Kuznetsova E, Zio E, Farel R. A methodological framework for Eco-Industrial Park design and optimization. *Journal of Cleaner Production.* 2016; 126, pp. 308–324. DOI 10.1016/j.jclepro.2016.03.025
- [4] Leong YT, Lee JY, Tan RR, Foo JJ, Chew I, Leng M. Multi-objective optimization for resource network synthesis in eco-industrial parks using an integrated analytic hierarchy process. *Journal of Cleaner Production.* 2017; 143, pp. 1268–1283. DOI 10.1016/j.jclepro.2016.11.147
- [5] Nuhu SK, Manan ZA, Wan Alwi SR, Md Reba MN. Integrated modelling approach for an eco-industrial park site selection. *Journal of Cleaner Production.* 2022; 368, p. 133141. DOI 10.1016/j.jclepro.2022.133141
- [6] Boix M, Montastruc, Azzaro-Pantel C, Domenech S. Optimization methods applied to the design of eco-industrial parks: a literature review. *Journal of Cleaner Production.* 2015; 87, pp. 303–317. DOI 10.1016/j.jclepro.2014.09.032
- [7] Sakr D, Baas L, El-Haggag S, Huisingh D. Critical success and limiting factors for eco-industrial parks: global trends and Egyptian context. *Journal of Cleaner Production.* 2011; 19 (11), pp. 1158–1169. DOI 10.1016/j.jclepro.2011.01.001
- [8] Long S, Zhao L, Liu H, Li J, Zhou X, Liu Y. A Monte Carlo-based integrated model to optimize the cost and pollution reduction in wastewater treatment processes in a typical comprehensive industrial park in China. *The Science of the total environment.* 2019; 647, pp. 1–10. DOI 10.1016/j.scitotenv.2018.07.358
- [9] Fishman GS. *Discrete-event simulation: modeling, programming, and analysis.* New York: Springer; 2001. Vol. 537.
- [10] Cucchiella F, D'Adamo I, Gastaldi M. Sustainable waste management: Waste to energy plant as an alternative to landfill. *Energy Conversion and Management.* 2017; 131, pp. 18–31. DOI 10.1016/j.enconman.2016.11.012
- [11] Touš M, Pavlas M, Putna O, Stehlík P, Crha L. Combined heat and power production planning in a waste-to-energy plant on a short-term basis. *Energy.* 2015; 90, pp. 137–147. DOI 10.1016/j.energy.2015.05.077
- [12] Yazan DM, Fraccascia L. Sustainable operations of industrial symbiosis: an enterprise input-output model integrated by agent-based simulation. *International Journal of Production Research.* 2020; 58 (2), pp. 392–414. DOI 10.1080/00207543.2019.1590660

# A Meta-model for Comparing Carbon Capture Storage and Utilisation Technologies using Life Cycle Analysis

J. Benz, K. Blank, S. Hötzel, J. Just, C. Lau, F. Schicks, N. von der Ahe,  
J. Wittmann

HTW Berlin - Univ. of Applied Sciences, Wilhelminenhofstraße 75A, 12459 Berlin; [Jochen.Wittmann@htw-berlin.de](mailto:Jochen.Wittmann@htw-berlin.de)

SNE 35(1), 2025, 9-16, DOI: 10.11128/sne.35.tn.10722  
Selected ASIM SST 2024 Postconf. Publication: 2024-12-10  
Received Revised: 2025-02-16; Accepted: 2025-02-25  
SNE - Simulation Notes Europe, ARGESIM Publisher Vienna  
ISSN Print 2305-9974, Online 2306-0271, [www.sne-journal.org](http://www.sne-journal.org)

**Abstract.** This research paper comprehensively reviews current carbon capture and storage (CCS) and carbon capture and utilization (CCU) technologies with the aim of developing a metamodel to make the different approaches comparable. Furthermore, the study examines the different pathways of the technologies in a life cycle analysis (LCA) concerning their efficiency in terms of carbon footprint. The analysis shows that some processes are highly energy-intensive, underlining the need for renewable electricity to minimize CO<sub>2</sub> emissions. However, the study also points out several challenges, including in-complete data and unknown variables that hinder the implementation and evaluation of these technologies. In addition, the criticisms and limitations associated with CCS and CCU stress the need for further research and development in this critical area.

## Introduction

The Paris Agreement [United Nations, 2015] is a crucial milestone in global efforts to mitigate climate change and underlines the urgent need for nations to work together to tackle greenhouse gas emissions. Carbon Capture and Storage (CCS), the process of trapping and storing Carbon dioxide (CO<sub>2</sub>) emissions, and Carbon Capture and Utilization (CCU), the transformation of CO<sub>2</sub> into valuable products, are crucial technologies for meeting the agreement's ambitious targets. In CO<sub>2</sub>-intensive industries like the cement industry, capturing and mineralizing 1t of Carbon dioxide equivalents (CO<sub>2</sub>-Eq) could avoid over 1t of CO<sub>2</sub>-Eq emissions by substitution of conventional production Ostovari et al. [2020]. However, the pressing issue is how effectively these technologies can fulfill current commitments and drive progress.

Understanding the opportunities and limitations of these technologies is essential to assess their potential to achieve the goals set out in the Paris Agreement. While there is extensive research on the individual aspects of these technologies, there still is a notable gap in synthesizing this knowledge into a co-herent framework. Therefore, our aim is twofold: to consolidate the existing research into a comprehensive overview by developing an over-all meta-model and to assess the collective potential of CCS and CCU to meet global emission reduction targets in terms of their carbon footprint, evaluated by a Life Cycle Assessment (LCA). In addition, our analysis will highlight existing data gaps and areas that require further investigation, thereby contributing to the ongoing discourse on climate change mitigation strategies.

## 1 Meta-Model

A model is required to execute a LCA calculating the environmental impact of technologies and processes. LCAs of carbon mineralization face the challenge of modeling many different processes and materials simply and comparably. For this reason, we developed a simplified meta-model. The model should consider the complexity of the various processes and feedstocks involved in carbon mineralization.

### Problems creating a meta-model

Carbon mineralization involves various processes depending on the technology and feedstock used. These processes include CO<sub>2</sub> capture, the reaction of CO<sub>2</sub> with mineral materials, the transport of materials and products, the pretreatment of feedstocks, the further processing of products, and the utilization of electric energy, heat, and water.

Modeling these processes in a single comprehensive LCA model can be highly complex and resource-intensive.

Some of the specific modeling issues we encountered during this study are:

**Technology pathways:** various technologies and approaches to carbon mineralization can differ greatly in their processes, materials, and environmental impacts. Modeling this diversity requires the development of a flexible model that can accommodate the different technologies without becoming too detailed.

**Feedstock diversity:** Feedstocks for carbon mineralization can vary widely and include natural minerals (like olivine or serpentine), waste products (like steel slag, ashes, etc.), and CO<sub>2</sub> from various sources. Each feedstock has different properties and requires different processes and conditions to optimally capture CO<sub>2</sub>. The model must analyze the varying environmental impacts resulting from the different resources and energy amounts required by each feedstock.

**Interactions between processes:** The various carbon mineralization processes interact in complex ways that influence the system's overall performance and environmental impact. These interactions must be integrated and simplified into the model to enable a holistic assessment.

#### Requirements for the meta-model

We developed a simplified meta-model to analyze the complexity of different carbon mineralization technologies and ensured comparability between different technologies and feedstocks. This meta-model should be an abstract model that simplifies the structure and behavior of the complex system by identifying the most critical factors and relationships. We intended the meta-model to have the following characteristics:

**Simplification:** The developed meta-model should reduce the complexity of carbon mineralization by eliminating unnecessary details and boundary effects. The goal was to abstract the different processes of the various pathways at a superordinate level and to summarize sub-processes.

**Comparability:** The meta-model should enable the comparability between different technologies and feedstocks by using consistent processes and a common functional unit as an assessment reference to quantify the relevant environmental impacts.

**Parameterization:** It should be possible to parameterize the meta-model to enable the variation of relevant variables such as energy consumption, input quantities, and outputs. In this way, the user can execute various scenarios and sensitivity analyses to investigate the effects of changes to the input parameters.

#### Development of the simplified meta-model

A detailed literature review has been elaborated, but cannot be included in this paper for reasons of space. Based on this review we analyzed various existing LCAs of CCS/CCU processes concerning the technologies, feedstocks, and process steps described. The relevant processes were determined based on these LCAs and the described models. The goal was to identify the intersections between the different models and determine generally applicable processes for the various pathways. The identified processes for the meta-model are feedstock supply, CO<sub>2</sub> capture, pre-treatment, carbonation, and post-processing. With the help of these processes, we derived an initial model that serves as the basis for the LCA analysis which is shown in Figure 1. Carbonation itself and the necessary pretreatment are the main processes at the center, accompanied by feedstock supply and CO<sub>2</sub>-supply-processes on the input side and the post-processing on the output side. A possible utilization of end-products is not covered by the proposed meta-model because no meaningful generalising model assumption can be made at this point due to the large number of usage options. The next step was to implement this model in the LCA-software Umberto [ifu, 2024] to carry out the LCA for various carbon mineralization pathways.

## 2 Life Cycle Assessment

LCA is a method used to comprehensively analyze a product's or technology's environmental impact over its life cycle. The ISO 14040 and ISO 14044 [ISO, 2020a,b] standardize and describe the procedure and structure of an LCA. Despite being standardized, LCAs in the field of carbon mineralization are challenging to compare, as critical factors such as the functional unit, system boundaries, and individual processes can be selected differently. For this reason, a guideline for implementing LCAs for carbon capture was used as a basis for this study [Müller et al., 2020].

**Goal and scope** The main objective of this LCA is to quantify and compare the environmental impact of different carbon mineralization processes with the developed meta-model. Therefore, testing the meta-model with actual data is another study objective. The assessment concentrates on the carbon foot-print caused by the different technologies.

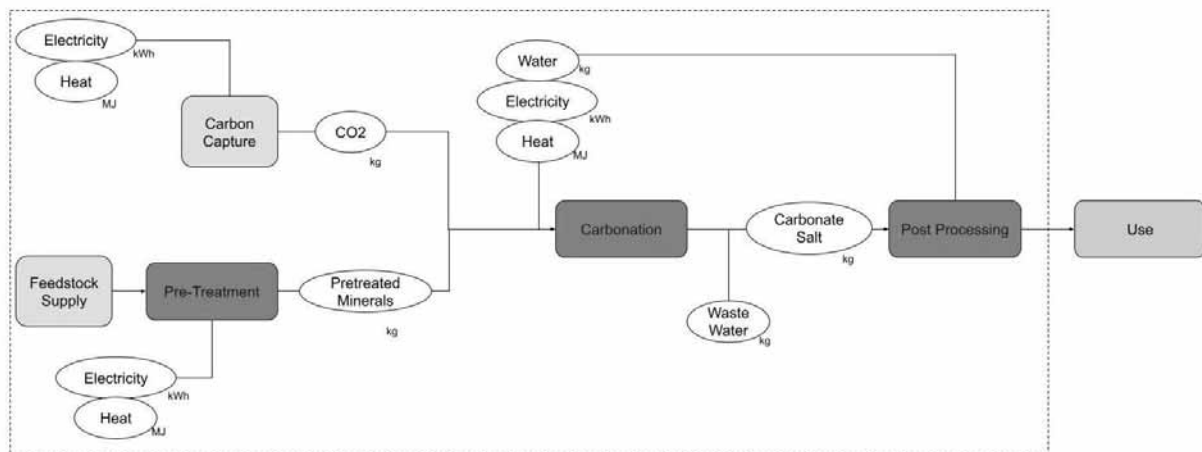


Figure 1: Developed meta-model for LCA.

Such a comparison helps drive the development and implementation of environmentally friendly carbon capture technologies and, thus, significantly contribute to reducing global CO<sub>2</sub> emission. Carbon mineralization is an approach for per-manently storing carbon by reacting and binding carbon dioxide in a stable mineral form [Stokreef et al., 2022]. For this reason, we defined the functional unit in this study as 1t of CO<sub>2</sub> bound by a carbonization process. This choice provides a direct and comparable bench-mark for assessing different carbon capture technologies and processes. With this definition of the functional unit, we can cross-check the CO<sub>2</sub> emissions from all activities during the mineralization. If the emissions are less than 1t of CO<sub>2</sub> eq per tonne of bound CO<sub>2</sub>, we can state that the emissions are net-negative, i.e., the process removes CO<sub>2</sub> from the atmosphere.

The system boundaries of this LCA were defined to consider the direct environmental impacts of the carbonization processes. It was decided not to include the use of potential end products that could result from carbonization processes in this analysis. This focus allows a more accurate assessment of the carbonization technologies' environmental impacts without being distracted by variable application contexts, use scenarios and substitutions. The CO<sub>2</sub> supply was included in the system boundary, as the process of CO<sub>2</sub> supply can require a huge amount of energy and is, therefore, a decisive factor in determining the environmental impact of carbon mineralization.

The following two types of CO<sub>2</sub> sources were considered in this study: direct air capture and point sources (such as industrial facilities like power plants and factories).

Umberto was used to implement the developed meta-model and calculate the environmental impact. In Umberto, the relevant process parameters and resource inputs were mapped in the model (see supplementary files). Figure 2 shows the implemented Umberto model. To simplify the modeling in Umberto, we made the following assumptions:

- Identical transport (60km by lorry) for the feedstocks was assumed in all pathways
- Electricity generation based on the German electricity mix
- For comparison, label certified electricity from Switzerland with renewable energies
- Heat from natural gas
- Non-existent extraction of olivine and serpentine in Umberto was replaced by a comparable process of limestone extraction

## 2.1 Life cycle inventory and data situation

We had to obtain reliable data for different carbon mineralization pathways for the analyses on the developed meta-model. Own measurements or actual data from a company were not available. For this reason, we analyzed the data from LCAs found in the literature review to identify relevant data.

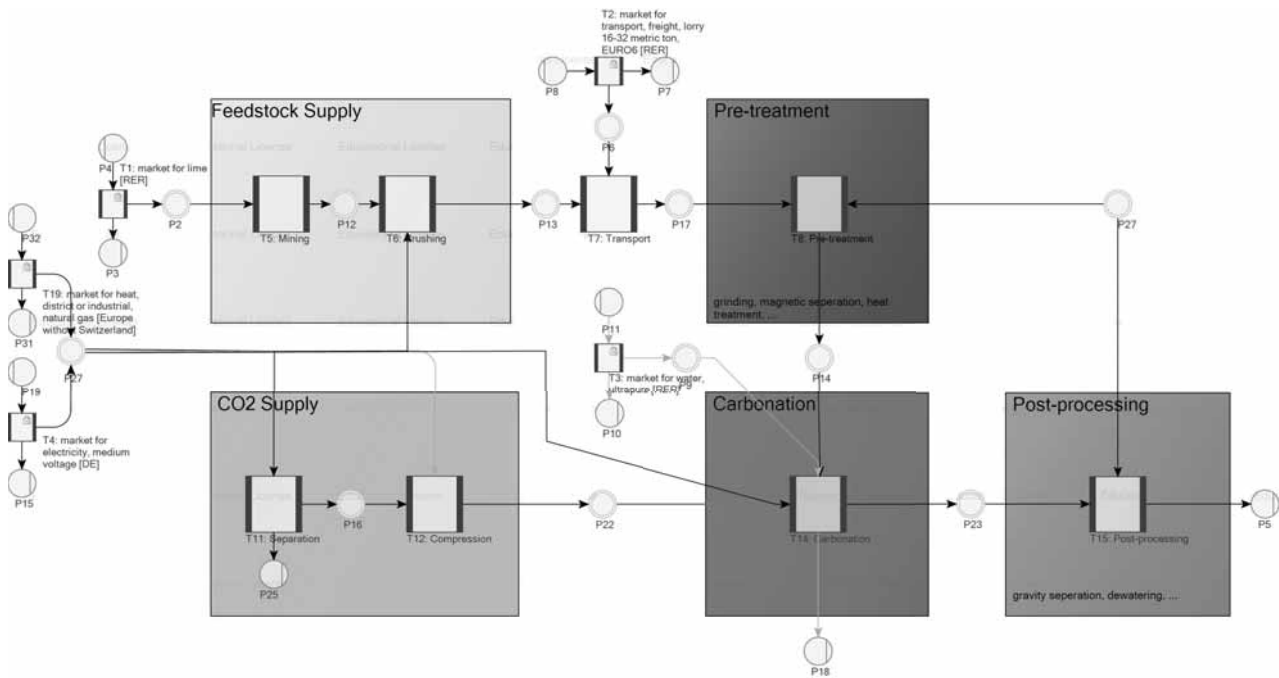


Figure 2: Developed model for LCA in Umberto.

This data research results in a collection of data presented in several tables, sorted according to the processes described in the meta-model (see supplementary files).

For further investigation, we found data on various technology pathways (direct and indirect). It was also important to consider data for different feedstocks, as different feedstocks used to have a considerable influence on the mass balances of inputs and outputs. Data was found for olivine, serpentine, and various waste materials such as steel slack [Bargiacchi et al., 2020, Digulla and Bringezu, 2023, Müller et al., 2020, Narahariseti et al., 2017, Ostovari et al., 2020, Sanna et al., 2012, 2014, William Oconnor et al., 2005]. In addition to the data collected, various libraries and markets were used in Umberto to enable realistic modeling of the energy requirements [ecoinvent, 2023]:

- market for transport, freight, lorry 16-32 metric ton, EURO6 [RER]
- market for lime [RER]
- market for electricity, medium voltage [DE]
- market for electricity, medium voltage, label-certified [CH]
- market for heat, district or industrial, natural gas [Europe without Switzerland]

- market for water, ultrapure [RER] (only for serpen-tine )
- market for blast furnace slag [GLO] (rotary packed bed pathway)

During the data research, we identified several issues and challenges:

**Up-to-date data:** Up-to-date data is essential to correctly map technological developments and trends to obtain meaningful results in the LCA. Our data research revealed that in some cases, only older data (for example William Oconnor et al. [2005]) is available for individual processes and that this data formed the basis for various other LCAs found in the literature review [compare Ostovari et al., 2020, Narahariseti et al., 2017, Kremer et al., 2022]. We must critically question whether this data is still meaningful today and reflects the current state of the art.

**Accessibility of the data:** In our data research, we have encountered problems with restricted access to specific datasets or data not being published in full. Reasons for this could be data protection, commercial interests, or other legal and administrative reasons. Due to the limited data available, we could not guarantee completeness across all carbon mineralization pathways in our LCA. We could only map and analyze the processes and technologies for which data was available.

**Accuracy:** The accuracy of the data is crucial, as incorrect or inaccurate information can lead to false conclusions. That applies, in particular, to data on the inputs and outputs of the individual processes and on energy consumption. As we have not measured any data, we have to rely on third-party information for the data we use. Note that some of the data come from experiments under laboratory conditions [Wang and Maroto-Valer, 2011, Bodéan et al., 2014, Fabian et al., 2010, Romão et al., 2012]. For this reason, we can only make limited statements about our results for industrial and scaled applications where other conditions may exist.

**Consistency:** Data consistency is a critical factor in comparing different studies, technologies, and locations. As already described, there is the problem that sometimes only limited data can be retrieved, or data is only available for individual processes. For this reason, we combined our data from different sources. This results in a loss of consistency, as data generated under different conditions and for different purposes is correlated and summarized.

## 2.2 Life cycle impact assessment

The created meta-model enables the modeling of different CCS methods but builds on a limited data situation. In order to obtain meaningful results with the meta-model, we attempted to perform the impact analyses with data that was as coherent as possible. For this reason, this impact assessment focused on modeling the five pathways described in Ostovari et al. [2020]. We implemented the meta-model with the modeling software Umberto LCA+.

Carbonation occurs in the direct pathway with a continuously stirred tank reactor (CSTR) without any intermediate steps. The pre-treatment and carbonation conditions depend on the feedstock. Data for olivine and serpentine were available in the study. Olivine is mined and prepared by grinding and milling in the pre-treatment stage. In the subsequent carbonization, the pulverized olivine reacts with water and CO<sub>2</sub> from the CO<sub>2</sub> supply. After that, the results undergo further processing in the post-processing stage. The procedure with serpentine is the same except for the pre-treatment stage. Magnetic separation isolates the iron, and heat treatment is required. The pathway OlivineCSTR100 is based on the study by Eikeland et al. [2015]. The pathway SerpentineCSTR115 described in Ostovari et al. [2020] referenced results from William Oconnor et al. [2005].

These sources also investigate the direct process using a rotary-packed bed reactor (RPB). This RPB often uses steel slack as a feedstock. Steel slack is a waste product in various industries, requiring no additional extraction process. After grinding, it can react with CO<sub>2</sub>. The RPB process offers several advantages, including using off-gas containing 15-20% CO<sub>2</sub> instead of pure CO<sub>2</sub>. Furthermore, the waste product steel slack is utilized as feedstock, resulting in possible cost and energy savings [Ostovari et al., 2020, Pan et al., 2015].

In addition to these direct concepts, Ostovari et al. [2020] describe two indirect pathways examined in this study using the meta-model. These are the Nottingham pathway and the AA pathway. Serpentine is usually the feedstock for both of these pathways. Pre-treatment and post-processing in the AA pathway correspond to the direct concepts, while it takes intermediate steps in the carbonation. The serpentine reacts with ammonium sulfate in a solid-solid reaction, and the actual reaction with CO<sub>2</sub> follows afterward [Romão et al., 2012]. In the Nottingham pathway, the actual carbonation also takes place in two steps: first, an aqueous extraction and then an aqueous carbonation. In the Nottingham process, the feedstock supply and the pre-treatment stage are identical to the direct processes, as serpentine is also used as feedstock here. One exception is heat treatment during pre-treatment, which is unnecessary for the Nottingham Pathway. During the carbonation, the serpentine initially reacts with ammonium bisulfate in an aqueous reaction to generate a magnesium-rich solution that reacts with CO<sub>2</sub> in the second stage and binds the CO<sub>2</sub>. The described Nottingham Pathway in Ostovari et al. [2020] is based on Wang and Maroto-Valer [2011].

With the modeling, we aimed to analyze which process is responsible for how much of the CO<sub>2</sub> emissions. The model was calculated once with the German electricity mix and heat from natural gas and once with a green electricity mix. Due to the data availability, which usually only contains energy consumption for a single process, we analyzed only CO<sub>2</sub> equivalence. However, this does not mean that other influences are irrelevant; instead, there is insufficient data to provide further information on other aspects.

Figure 3 shows the results for the German electricity mix. The CO<sub>2</sub> equivalence is positive in two methods, implying that the process produces more CO<sub>2</sub> than is stored. In the Rotary packed bed pathway, the CO<sub>2</sub> equivalence for the feedstock supply is negative, as it uses a blast furnace slag here.

Umberto LCA+ rewards further use of this waste product with a negative CO<sub>2</sub> equivalence. For the Nottingham Pathway and Rotary packed bed pathway, no energy is required for the CO<sub>2</sub> supply, as emissions from point sources, such as industrial facilities, are used here.

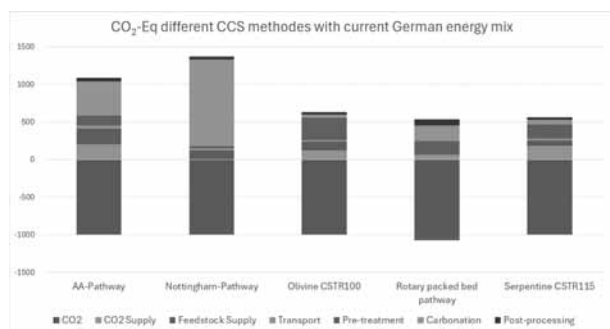


**Figure 3:** CO<sub>2</sub>-eq for different mineralization pathways with German energy mix.

We then calculated all five models using green electricity. Due to the lack of a sustainable heat source in the Ecoinvent database, we also used green electricity as the heat source in these models. The results can be seen in Figure 4. All energy-intensive processes now have a significantly better CO<sub>2</sub> equivalence, and all methods store more CO<sub>2</sub> than they emit. On the other hand, the feedstock supply and transport processes still generate almost the same amount of CO<sub>2</sub> and are therefore responsible for a large proportion of CO<sub>2</sub> emissions.

The latter happens because we include the pre-chains in these steps using data from Ecoinvent. We assume current rock extraction and transport conditions, not future conditions, that could decarbonize these steps.

In all models, CO<sub>2</sub> is permanently bound in rock, i.e., long-term storage. We did not investigate other methods like producing e-fuels, which are burnt later in their lifecycle, emitting CO<sub>2</sub> again.

### 2.3 Life cycle interpretation

The results from diagrams 3 and 4 show that the energy-intensive processes are responsible for the CO<sub>2</sub>-eq in particular. Using renewable electricity can avoid a large proportion of the CO<sub>2</sub> emissions caused by the storage of CO<sub>2</sub>. Until this is the case, CCS only makes limited sense. The Nottingham pathway is particularly striking, as this process emits significantly more CO<sub>2</sub> than is stored under the current German electricity mix.

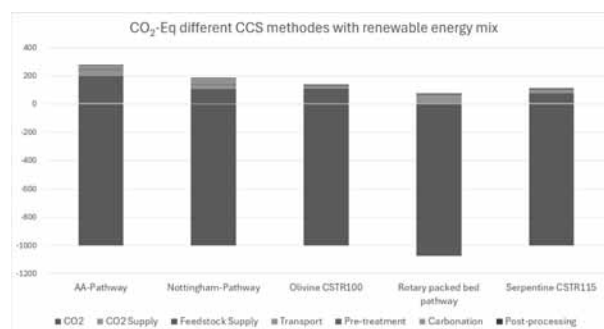


**Figure 4:** CO<sub>2</sub>-eq for different mineralization pathways with renewable energy mix.

That leads to the conclusion that CCS only makes sense if the electricity mix is entirely renewable.

It is worth noting that there is an issue with the data situation. For various process steps, data from different sources, including data obtained in laboratory situations, were used in the analyzed studies. There needs to be empirical data on how energy use in large commercial systems will scale and develop.

## 3 Discussion

The LCA conducted in this study offers critical insights into the environmental impacts of CCS and CCU technologies. It underpins the urgent need for sustainable energy sources to power these technologies. Our findings highlight the challenges we must address to maximize the potential of CCS and CCU in effectively mitigating CO<sub>2</sub> emissions.

### 3.1 Energy Intensity and the Need for Renewable Energy

One of the most significant challenges highlighted by our analysis in Chapter 2.3 is the energy intensity of current CCS and CCU processes. The dependency on non-renewable energy sources not only undermines the overall carbon footprint reduction but also raises concerns about these technologies' sustainability and net environmental benefits. The transition to renewable energy sources is imperative to ensure that CCS and CCU technologies contribute positively to climate change mitigation efforts. This shift would align with the global push towards decarbonization and enhance the technologies' appeal from an environmental perspective.

### 3.2 Data Gaps and the Importance of Comprehensive Data Collection

As elaborated in Chapter 2.1, our study also reveals substantial gaps in the available data, particularly regarding up-to-date information on the energy consumption and environmental impacts of CCS and CCU processes. These gaps hinder the ability to make informed decisions and assess the technologies' viability and effectiveness. Therefore, there is a pressing need for standardized data collection methods and increased transparency in reporting to facilitate more robust and comprehensive LCAs. Our findings align with a consensus; most papers examined in the literature review share that collaboration among academia, industry, and regulatory bodies is essential to establish uniform data collection frameworks and databases.

### 3.3 Technological Innovation and Scalability

The tone of the examined papers in the detailed literature review also highlights the importance of technological innovation in improving the efficiency and scalability of CCS and CCU technologies. Advances in process optimization, material sciences, and system integration are critical to overcome current limitations and reducing costs. Furthermore, exploring novel CO<sub>2</sub> capture and conversion pathways could open up new avenues for carbon utilization, thereby expanding the potential applications and markets for CCU products. Continued investment in research and development is crucial to accelerating these innovations.

### 3.4 Policy Implications and the Role of Incentives

The findings from our study show a need for supportive regulatory frameworks and incentives to promote the adoption and development of CCS and CCU technologies. Policies aimed at internalizing the cost of carbon emissions, such as carbon pricing mechanisms, can enhance the economic viability of CCS and CCU. Additionally, targeted subsidies, tax incentives, and funding for research and development can accelerate further development.

## 4 Summary

This research report examines various studies on CCU and CCS. In addition to reviewing already completed literature analyses, we conducted a literature search for the years 2022-2024. Based on this, we created an overview of the prevailing technology landscape. This foundation enabled us to develop a meta-model and conduct life cycle assessments on various technologies. The LCA results show that the type of electricity used significantly affects the overall efficiency of the technologies, especially in reducing the carbon footprint.

We identified numerous challenges and points of criticism. These include incomplete or outdated data, methodological weaknesses, and a lack of research in certain areas. Nevertheless, the analysis shows that CCS and CCU could contribute to achieving the 1.5-degree target of the Paris Agreement. The paper underlines the importance of further research and development in this area to fully exploit the potential of CCS and CCU and achieve the goals of the Paris Agreement.

## 5 Outlook

Looking to the future of these technologies, it is clear that despite the progress made in developing CCS and CCU, there still needs to be more research. In particular, existing data gaps need to be closed to make informed decisions about implementing and scaling these technologies.

A key focus of future research should be on improving the accuracy and completeness of available data. Achieving this demands increased collaboration between government agencies, research institutions, and industry partners to establish uniform standards for data collection and provide comprehensive data sets.

In addition, we need methodological improvements to enhance the robustness of life cycle assessments and better understand potential environmental, economic, and social impacts. New modeling and simulation approaches could help capture the systems' complexity and provide more accurate results.

**Publication Remark.** This contribution is the revised version of the conference version published in *Tagungsband Langbeiträge ASIM SST 2024*, ARGESIM Report AR 47, ISBN ebook: 978-3-903347-65-6, p 19-26, DOI: 10.11128/arep.47.a4711

## References

- Bargiacchi E, Thonemann N, Geldermann J. Life cycle assessment of synthetic natural gas production from different CO<sub>2</sub> sources: A cradle-to-gate study. *Energies*, 13(17):4579, 2020. ISSN 1996-1073. DOI 10.3390/en13174579.
- Bodéan F, Bourgeois F, Petiot C. Ex situ mineral carbonation for CO<sub>2</sub> mitigation: Evaluation of mining waste resources, aqueous carbonation processability and life cycle assessment (Carmex project). *Minerals Engineering*, 59:52–63, 2014. ISSN 0892-6875. doi: DOI 10.1016/j.mineng.2014.01.011.
- Digulla FE, Bringezu S. Comparative life cycle assessment of carbon dioxide mineralization using industrial waste as feedstock to produce cement substitutes. *Energies*, 16(10):4118, 2023. DOI 10.3390/en16104118.
- ecoinvent. ecoinvent version 3.6, 2023. URL <https://support.ecoinvent.org/ecoinvent-version-3.6>.
- Eikeland E, Bank A, Blichfeld A, Tyrsted C. Optimized carbonation of magnesium silicate mineral for CO<sub>2</sub> storage. *ACS applied materials & interfaces*, 7(9):5258–5264, 2015. DOI 10.1021/am508432w.
- Fabian M, Shopska M, Paneva D. The influence of attrition milling on carbon dioxide sequestration on magnesium-iron silicate. *Minerals Engineering*, 23(8):616–620, 2010. ISSN 0892-6875. DOI 10.1016/j.mineng.2010.02.006.
- ifu. Umberto ICA software, 2024. URL <https://www.ifu.com/de/umberto>.
- ISO. Din en iso 14040:2021-02, umweltmanagement\_ökobilanz\_- grundsätze und rahmenbedingungen (iso\_14040:2006\_+ amd\_1:2020); deutsche fassung en\_iso\_14040:2006\_+ a1:2020, 2020a. URL <https://www.iso.org/standard/37456.html>.
- ISO. Din en iso 14044:2021-02, umweltmanagement\_ökobilanz\_- anforderungen und anleitungen (iso\_14044:2006\_+ amd\_1:2017\_+ amd\_2:2020); deutsche fassung en\_iso\_14044:2006\_+ a1:2018\_+ a2:2020, 2020b. URL <https://www.iso.org/standard/38498.html>.
- Kremer D, Dertmann C, Etzold S. Ex-situ mineral carbonation – a parameter study on carbon mineralisation in an autoclave as part of a large-scale utilisation process. *Journal of CO<sub>2</sub> Utilization*, 58:101928, 2022. ISSN 22129820. DOI 10.1016/j.jcou.2022.101928.
- Müller LJ, Kätelhön A, Bachmann M, Zimmermann A, Sternberg A, Bardow A. A guideline for life cycle assessment of carbon capture and utilization. *Frontiers in Energy Research*, 8:505883, 2020. ISSN 2296-598X. DOI 10.3389/fenrg.2020.00015.
- Naraharisetti PK, Yeo TY, Bu J. Factors influencing CO<sub>2</sub> and energy penalties of CO<sub>2</sub> mineralization processes. *Chemphyschem : a European journal of chemical physics and physical chemistry*, 18 (22):3189–3202, DOI 10.1002/cphc.201700565.
- Ostovari H, Sternberg A, Bardow A. Rock'n' use of CO<sub>2</sub>: carbon footprint of carbon capture and utilization by mineralization. *Sust. Energy & Fuels*, 4(9):4482–4496, DOI 10.1039/D0SE00190B.
- Pan SY, Chen YH, Chen CD. High-gravity carbonation process for enhancing CO<sub>2</sub> fixation and utilization exemplified by the steelmaking industry. *Environmental science & technology*, 49(20): 12380–12387. DOI 10.1021/acs.est.5b02210.
- Romão I, Nduagu E, Fagerlund J. CO<sub>2</sub> fixation using magnesium silicate minerals. part 2: Energy efficiency and integration with iron-and steelmaking. *Energy*, 41(1):203–211, 2012. ISSN 03605442. DOI 10.1016/j.energy.2011.08.026.
- Sanna A, Uibu M, Caramanna G. A review of mineral carbonation technologies to sequester CO<sub>2</sub>. *Chemical Society reviews*, 43(23):8049–8080, 2014. DOI 10.1039/C4CS00035H.
- Sanna A, Hall MR, Maroto-Valer M. Post-processing pathways in carbon capture and storage by mineral carbonation (CCSM) towards the introduction of carbon neutral materials. *Energy & Environmental Science*, 5(7):7781, 2012. ISSN 1754-5692. DOI 10.1039/c2ee03455g.
- Stokreef S, Sadri F, Stokreef A. Mineral carbonation of ultramafic tailings: A review of reaction mechanisms and kinetics, industry case studies, and modelling. *Cleaner Engineering and Technology*, 8: 100491, 2022. ISSN 2666-7908. DOI 10.1016/j.clet.2022.100491.
- United Nations. The Paris Agreement, 2015. URL <https://unfccc.int/process-and-meetings/the-paris-agreement>.
- Wang X, Maroto-Valer MM. Integration of CO<sub>2</sub> capture and mineral carbonation by using recyclable ammonium salts. *ChemSusChem*, 4(9):1291–1300, 2011. DOI 10.1002/cssc.201000441.
- O'Connor W, Dahlin DC, Rush GE, Gerdemann SJ, Penner LR, Nilsen DN. Aqueous mineral carbonation: Mineral availability, pretreatment, reaction parameters, and process studies, 2005.

# Mathematical Analysis of a Compartment Model

Aristeidis Niotis<sup>1</sup>, Kurt Chudej<sup>1,2\*</sup>

<sup>1</sup>Mathematisches Institut, Universität Bayreuth, 95440 Bayreuth, Germany

<sup>2</sup>Forschungszentrum Modellierung und Simulation (MODUS), Universität Bayreuth, 95440 Bayreuth, Germany;

\*kurt.chudej@uni-bayreuth.de

SNE 35(1), 2025, 17-24, DOI: 10.11128/sne.35.tn.10723  
 Selected ASIM SST 2024 Postconf. Publication: 2024-12-10  
 Received Revised: 2025-02-25; Accepted: 2025-02-28  
 SNE - Simulation Notes Europe, ARGESIM Publisher Vienna  
 ISSN Print 2305-9974, Online 2306-0271, www.sne-journal.org

**Abstract.** We give a theoretical investigation of a Covid model. This model was successfully used in the context of MPC control to keep the Covid pandemic manageable [1]. We compute especially a next generation basic reproduction number, a Lyapunov function and reveal some peculiarities if demography is skipped. Finally, we look at the model with two age groups.

## 1 Introduction

Epidemics and infectious diseases are often described using so-called compartment models in order to be able to make the best possible, realistic predictions about the course of the disease in larger population groups. A population is divided into different groups ("compartments") and the flow (inflows and outflows) between these compartments is examined more closely. A classic compartment model is the SIR model according to Kermack and McKendrick.

## 2 ODE Model

In [1] a detailed Covid model is developed and successfully used in the context of model predictive control (MPC) in order to mitigate the COVID-19 outbreak. The model was used with weekly updates of the parameters. Optimal mass-testing and age-dependent social distancing policies were determined [1].

Here a theoretical investigation of the mathematical properties of an autonomous version of this model is performed. At the beginning the model is simplified to one age class and enhanced with demography. Therefore the following autonomous mathematical compartment model is investigated in this research:

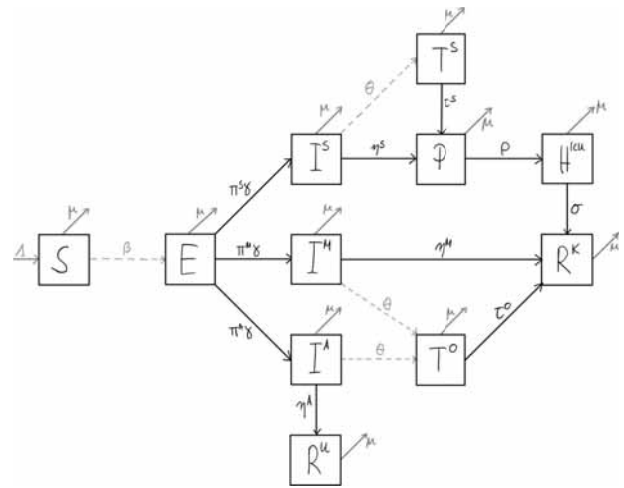


Figure 1: SEIPTHR model with demography.

### 2.1 ODE System

The associated ODE system with *mass action incidence* is given by

$$\begin{aligned} \dot{S} &= \Lambda - \beta S[I^S + I^M + I^A + T^S + T^O] - \mu S & (1a) \\ \dot{E} &= \beta S[I^S + I^M + I^A + T^S + T^O] - (\gamma + \mu)E & (1b) \\ \dot{I}^S &= \pi^S \gamma E - (\eta^S + \theta + \mu)I^S & (1c) \\ \dot{I}^M &= \pi^M \gamma E - (\eta^M + \theta + \mu)I^M & (1d) \\ \dot{I}^A &= \pi^A \gamma E - (\eta^A + \theta + \mu)I^A & (1e) \\ \dot{T}^S &= \theta I^S - (\tau^S + \mu)T^S & (1f) \\ \dot{T}^O &= \theta [I^M + I^A] - (\tau^O + \mu)T^O & (1g) \\ \dot{P} &= \eta^S I^S + \tau^S T^S - (\rho + \mu)P & (1h) \\ \dot{H}^{ICU} &= \rho P - (\sigma + \mu)H^{ICU} & (1i) \\ \dot{R}^K &= \eta^M I^M + \tau^O T^O + \sigma H^{ICU} - \mu R^K & (1j) \\ \dot{R}^U &= \eta^A I^A - \mu R^U & (1k) \end{aligned}$$

together with non-negative initial values

$$\begin{aligned}
 S(0) &= S_0, E(0) = E_0, I^S(0) = I_0^S, I^M(0) = I_0^M, \\
 I^A(0) &= I_0^A, T^S(0) = T_0^S, T^O(0) = T_0^O, P(0) = P_0, \\
 H^{ICU}(0) &= H_0^{ICU}, R^K(0) = R_0^K, R^U(0) = R_0^U. \quad (11)
 \end{aligned}$$

### 2.2 Model Description

The following compartments are introduced in [1]:

- $S(t), E(t)$ : Susceptible persons ( $S$ ) accumulate after infection with the pathogen in a compartment  $E$  (exposed), but are not yet infectious themselves.
- $I(t) = I^S(t) + I^M(t) + I^A(t)$ : The infectious compartment  $I$  is divided into three classes depending on the course of infection. A distinction is made between severe cases  $I^S$ , mild cases  $I^M$  and asymptomatic cases  $I^A$ .
- $T^S(t), T^O(t)$ : Infectious persons have the opportunity to be tested, in which we in turn differentiate according to the course of the disease.
- $P(t)$ : Seriously ill people will either go directly to a physician ( $P$ ) and go into quarantine or only after receiving a positive test result.
- $H^{ICU}(t)$ : After isolation in  $P$ , severely ill persons are transferred to an intensive care unit  $H^{ICU}$ .
- $R(t) = R^K(t) + R^U(t)$ : The compartment of recovered individuals  $R$  is divided into two classes depending on the course of infection: individuals who have actually been identified as infected are collected in  $R^K$  (known), the other ones recover in a natural way without having previously been identified as diseased ( $R^U$  - unknown).

In order to finally understand the interaction between the individual compartments, we need an overview of the parameters modelled in Table 1

Set  $\pi^S + \pi^M + \pi^A = 1$  and  $U := S + E + I^S + I^M + I^A + R^U$ . All constants in Table 1 are non-negative.

### 3 Mathematical Analysis

We decompose all compartments into the vector  $x = (E, I^S, I^M, I^A, T^S, T^O)$  of infected compartments and the remaining compartments  $y = (S, P, H^{ICU}, R^K, R^U)$ . All compartments are denoted by  $z = (x, y)$ .

Parameters	Description
$\beta > 0$	infection rate
$\gamma > 0$	average incubation time $\gamma^{-1}$ in days
$\pi^S > 0$	Proportion of severely ill patients
$\pi^M > 0$	Proportion of mildly ill patients
$\pi^A > 0$	Proportion of asymptomatic patients
$\theta \geq 0$	Test rate (Tests spread in $U$ per day)
$\eta^S > 0$	Recovery rate for severe course
$\eta^M > 0$	Recovery rate for mild course
$\eta^A > 0$	Recovery rate for asymptomatic course
$\tau^S > 0$	Rate at which tested persons recover (severe)
$\tau^O > 0$	Rate at which tested persons recover (others)
$\rho > 0$	average duration of isolation $\rho^{-1}$
$\sigma > 0$	average length of stay in ICU $\sigma^{-1}$

Table 1: Model parameters.

### 3.1 Positive Invariance and Existence of Solutions

Starting from our IVP (1), it is important that the biological relevance of the solutions is ensured. This requirement on the mathematical model is fulfilled by the *positive invariance* shown below:

**Theorem:** The non-negative orthant  $\mathbb{R}_{\geq 0}^{11}$  is a positive invariant set.

*Proof:* The r.h.s. of the ODE is quasipositive. Apply Theorem 4.2.2 in Prüss, Wilke [2], pp. 83–84.

The total population  $N(t) := \sum_{i=1}^{11} z_i(t)$  fulfills the initial value problem

$$\dot{N} = \Lambda - \mu N, \quad N(0) = N_0,$$

where  $N_0 := S_0 + E_0 + I_0^S + I_0^M + I_0^A + T_0^S + T_0^O + P_0 + H_0^{ICU} + R_0^K + R_0^U$ .

Its solution  $N(t) = \Lambda/\mu + e^{-\mu t}(N_0 - \Lambda/\mu)$  converges monotonically with  $t \rightarrow \infty$  to  $N_\infty := \Lambda/\mu$ .

Therefore  $N(t) \leq K := \max(N_0, N_\infty)$ .

This proves, that the polytop  $\Omega := \{z \in \mathbb{R}_{\geq 0}^{11} | N(t) \leq K\}$  is a positive invariant set of the IVP (1).

The next step is to ensure that there is indeed a solution of the IVP:

**Theorem:** The initial value problem (1) has a unique solution for  $t \in [0, \infty[$ .

*Proof:* On the compact set  $\Omega$  the IVP is globally Lipschitz continuous, due to the polynomial r.h.s. of the ODE. Apply Picard-Lindelöf.

Without loss of generality we set  $\Lambda = N_0 \cdot \mu = \mu$  for  $N_0 = 1$ , this implies  $N_\infty = 1$  and  $K = 1$ . This choice means that the total population at all times is constant equal to 1 and therefore fractions of the population are considered.

### 3.2 Next-Generation-Approach for the Basic Reproduction Number

Our next goal is to calculate a next-generation basic reproduction number according to [3]. For that we need the existence of a disease-free equilibrium of our ODE, which can be easily seen:

If  $\mu > 0$ , then there exists a unique disease-free equilibrium  $\mathcal{E}_{DFE}$  with compartment  $S = 1 := N$  and all other compartments equal to zero.

Using the decomposition of the compartments the initial value problem

$$\dot{z} = h(z), z(0) = z_0$$

is rewritten as

$$\begin{aligned} \dot{x} &= f(x, y) = \mathcal{F}(x, y) - \mathcal{V}(x, y), x(0) = x_0, \\ \dot{y} &= g(x, y), y(0) = y_0 \end{aligned}$$

with

$$\begin{aligned} \mathcal{F}(x, y) &= \begin{pmatrix} \beta S [I^S + I^M + I^A + T^S + T^O] \\ \mathbf{0} \end{pmatrix} \\ \mathcal{V}(x, y) &= \begin{pmatrix} (\gamma + \mu)E \\ (\eta^S + \theta + \mu)I^S - \pi^S \gamma E \\ (\eta^M + \theta + \mu)I^M - \pi^M \gamma E \\ (\eta^A + \theta + \mu)I^A - \pi^A \gamma E \\ (\tau^S + \mu)T^S - \theta I^S \\ (\tau^O + \mu)T^O - \theta [I^M + I^A] \end{pmatrix}. \end{aligned}$$

Let  $F = \frac{\partial \mathcal{F}}{\partial x}$  and  $V = \frac{\partial \mathcal{V}}{\partial x}$ . We will postpone the evaluation of the Jacobian matrices at the coordinates of the DFE to a later time.

The Jacobian matrices are given in this application by

$$\begin{aligned} F &= \frac{\partial \mathcal{F}}{\partial x} = \begin{pmatrix} 0 & \beta S \\ \mathbf{0} & & & & & \end{pmatrix} \\ V &= \frac{\partial \mathcal{V}}{\partial x} = \begin{pmatrix} r_1 & 0 & 0 & 0 & 0 & 0 \\ -\pi^S \gamma & r_2 & 0 & 0 & 0 & 0 \\ -\pi^M \gamma & 0 & r_3 & 0 & 0 & 0 \\ -\pi^A \gamma & 0 & 0 & r_4 & 0 & 0 \\ 0 & -\theta & 0 & 0 & r_5 & 0 \\ 0 & 0 & -\theta & -\theta & 0 & r_6 \end{pmatrix} \end{aligned}$$

with  $r_1 = \gamma + \mu$ ,  $r_2 = \eta^S + \theta + \mu$ ,  $r_3 = \eta^M + \theta + \mu$ ,  $r_4 = \eta^A + \theta + \mu$ ,  $r_5 = \tau^S + \mu$ ,  $r_6 = \tau^O + \mu$ .

For the next-generation matrix we need

$$V^{-1} = \begin{pmatrix} r_1^{-1} & 0 & 0 & 0 & 0 & 0 \\ m_1 & r_2^{-1} & 0 & 0 & 0 & 0 \\ m_2 & 0 & r_3^{-1} & 0 & 0 & 0 \\ m_3 & 0 & 0 & r_4^{-1} & 0 & 0 \\ m_4 & m_6 & 0 & 0 & r_5^{-1} & 0 \\ m_5 & 0 & m_7 & m_8 & 0 & r_6^{-1} \end{pmatrix}$$

where  $m_1 = \frac{\gamma}{\gamma + \mu} \frac{\pi^S}{\eta^S + \theta + \mu}$ ,  $m_2 = \frac{\gamma}{\gamma + \mu} \frac{\pi^M}{\eta^M + \theta + \mu}$ ,  $m_3 = \frac{\gamma}{\gamma + \mu} \frac{\pi^A}{\eta^A + \theta + \mu}$ ,  $m_4 = \frac{\gamma}{\gamma + \mu} \frac{\pi^S}{\eta^S + \theta + \mu} \frac{\theta}{\tau^S + \mu}$ ,  $m_5 = \frac{\gamma}{\gamma + \mu} \left( \frac{\pi^M}{\eta^M + \theta + \mu} \frac{\theta}{\tau^O + \mu} + \frac{\pi^A}{\eta^A + \theta + \mu} \frac{\theta}{\tau^O + \mu} \right)$ ,  $m_6 = \frac{\theta}{(\tau^S + \mu)(\eta^S + \theta + \mu)}$ ,  $m_7 = \frac{\theta}{(\tau^O + \mu)(\eta^M + \theta + \mu)}$ ,  $m_8 = \frac{\theta}{(\tau^O + \mu)(\eta^A + \theta + \mu)}$ .

The next-generation-matrix is computed as

$$K = FV^{-1} = \beta S \begin{pmatrix} K_1 & 0 & 0 & 0 & 0 & 0 \\ * & \mathbf{0} & & & & \end{pmatrix}^T$$

with

$$\begin{aligned} K_1 &= \frac{\gamma}{\gamma + \mu} \cdot \left( \frac{\pi^S}{\eta^S + \theta + \mu} + \frac{\pi^M}{\eta^M + \theta + \mu} \right. \\ &+ \frac{\pi^A}{\eta^A + \theta + \mu} + \frac{\pi^S}{\eta^S + \theta + \mu} \frac{\theta}{\tau^S + \mu} + \\ &+ \left. \frac{\pi^M}{\eta^M + \theta + \mu} \frac{\theta}{\tau^O + \mu} + \frac{\pi^A}{\eta^A + \theta + \mu} \frac{\theta}{\tau^O + \mu} \right). \end{aligned}$$

The spectral radius of  $K$  is given by  $\rho(K) = \beta S \cdot K_1$ , since  $K$  is a triangle matrix.

Finally the next generation basic reproduction number is given by

$$\mathcal{R}_0 = \rho(K)|_{DFE} = \beta N \cdot K_1 \stackrel{N=1}{=} \beta \cdot K_1.$$

### 3.3 Stability

In order to analyze the stability of our DFE  $(0, y_0)$ , it's helpful to write the partitioned linearized ODE as

$$\begin{aligned} \dot{x} &= J_1|_{DFE} \cdot x + J_2|_{DFE} \cdot (y - y_0) \\ \dot{y} &= J_3|_{DFE} \cdot x + J_4|_{DFE} \cdot (y - y_0). \end{aligned}$$

The relevant Jacobian matrices are given by  $J_1 = \frac{\partial f}{\partial x}$  and  $J_4 = \frac{\partial g}{\partial y}$ , an easy computation shows  $J_2|_{DFE} = \frac{\partial f}{\partial y}|_{DFE} = 0$ .

Note that  $F \geq 0$  (componentwise) and  $V$  is a regular M-matrix, since  $V^{-1}$  exists and  $V^{-1} \geq 0$  (componentwise). Therefore  $-J_1|_{DFE} = (V - F)|_{DFE}$  is a regular splitting due to Varga [4] p. 95, Def. 3.28.

Additionally we know [3, 4]:

If  $\mathcal{R}_0 < 1$ , then  $J_1|_{DFE}$  has only eigenvalues with negative real part.

If  $\mathcal{R}_0 > 1$ , then  $J_1|_{DFE}$  has at least one eigenvalue with positive real part.

The matrix  $J_4|_{DFE}$  has eigenvalues with negative real part, a simple calculation gives the eigenvalues  $-\mu$ ,  $-(\rho + \mu)$  and  $-(\sigma + \mu)$ .

Application of the linearization theorem gives the result a). A more complicated argument is required in order to prove b).

**Theorem:** The considered Covid model has the following properties:

- a) If  $\mathcal{R}_0 < 1$ , then the DFE is locally asymptotically stable.
- b) If  $\mathcal{R}_0 > 1$ , then the DFE is instable.

Following an idea of Shuai/van den Driessche [5] we compute a linear convex Lyapunov function for the case with  $\mathcal{R}_0 < 1$  in order to analyze the global stability of our DFE.

According to [5], we have to analyze first when  $\tilde{f}(x, y) = (F - V)|_{DFE} \cdot x - \mathcal{F}(x, y) + \mathcal{V}(x, y) \geq 0$  on a positive invariant set. For our model only the first component of  $\tilde{f}$  is not equal to zero, more precisely  $\tilde{f}_1(x, y) = \beta \cdot (N - S) \cdot [I^S + I^M + I^A + T^S + T^O]$ . Thus our positive invariant set is  $\bar{\Omega} = \{z \in \mathbb{R}_{\geq 0}^{11} | N(t) \leq N_\infty\} \subset \Omega$ .

Next we need a left eigenvector  $\omega^T$  of the non-negative matrix  $V^{-1}F$  to the eigenvalue  $\mathcal{R}_0 \geq 0$ .

This yields  $\omega^T = (0 \ 1 \ 1 \ 1 \ 1 \ 1)$ , where the  $E$ -component takes the value 0. Thus, the linear convex Lyapunov function on  $\bar{\Omega}$  is given by

$$Q(x) = \omega^T V^{-1}x = (K_1 \ q_1 \ q_2 \ q_3 \ q_4 \ q_5) \cdot x,$$

$$\text{with } q_1 = \frac{1}{\eta^S + \theta + \mu} + \frac{\theta}{(\tau^S + \mu)(\eta^S + \theta + \mu)}, q_2 = \frac{1}{\eta^M + \theta + \mu} + \frac{\theta}{(\tau^O + \mu)(\eta^M + \theta + \mu)}, q_3 = \frac{1}{\eta^A + \theta + \mu} + \frac{\theta}{(\tau^O + \mu)(\eta^A + \theta + \mu)}, q_4 = \frac{1}{\tau^S + \mu}, q_5 = \frac{1}{\tau^O + \mu}.$$

One can show, that the DFE is the largest invariant set in the set given by  $Q(x) = 0$ . Then apply LaSalle [6].

**Theorem:** The considered Covid model has the following properties:

If  $\mathcal{R}_0 < 1$ , then the DFE is globally asymptotically stable in  $\bar{\Omega}$ .

### 3.4 Numerical Solutions

Finally, we will consider numerical solutions for the ODE system. Two scenarios are investigated: with testing and without testing.

Consider the following IVP:

$$E_0 = 0.01, \ S_0 = 1 - E_0 = 0.99, \ I_0^S = \dots = R_0^U = 0$$

The following parameter selection for the age group of 15- to 60-year-olds was taken from [1]:

Parameter	Value
$\beta$	0.63
$\gamma$	0.19
$\pi^S$	$\frac{0.31}{100}$
$\pi^M$	$\frac{22.01}{100}$
$\pi^A$	$\frac{77.68}{100}$
$\eta^S$	0.25
$\eta^M$	0.25
$\eta^A$	0.17
$\tau^S$	0.75
$\tau^O$	0.92
$\rho^{-1}$	10.98
$\sigma^{-1}$	10.5

**Table 2:** Parameters for the simulation.

We set  $\mu = \frac{1}{365 \cdot 20}$ . Unfortunately, problems occur with the numerical solutions, because the solution curves leave the positive invariant set  $\Omega$  for a very large  $t$  value (see Figure 2).

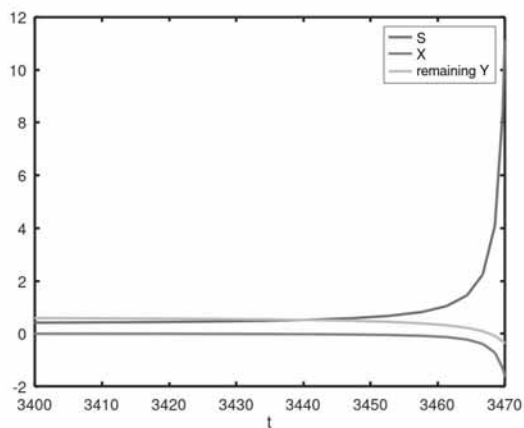
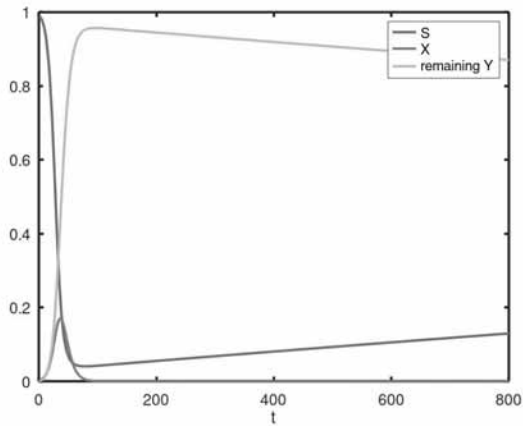


Figure 2: Simulation with demography, without testing.

An implicit stiff integrator can fix this problem (see Figure 3).  
 For the scenario without testing  $\mathcal{R}_0 \approx 3.44$  holds.  
 Finally, consider test measures with  $\theta = 0.4$ . The numeric solutions can be seen in Figure 4.  
 For this scenario we obtain a basic reproduction number of  $\mathcal{R}_0 \approx 1.54$

## 4 Model without Demography

We investigate now our model without demography, we set  $\mu = \Lambda = 0$ .

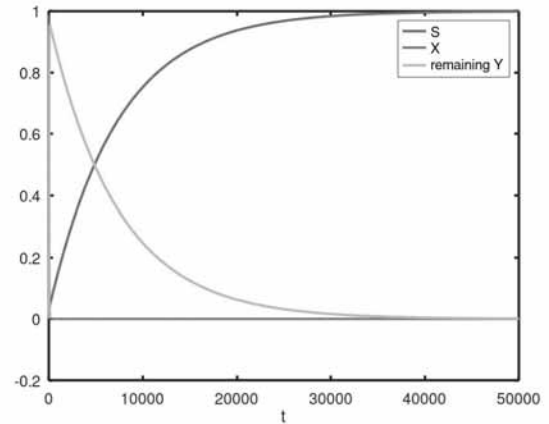


Figure 3: Simulation with demography, without testing, using an implicit stiff integrator.

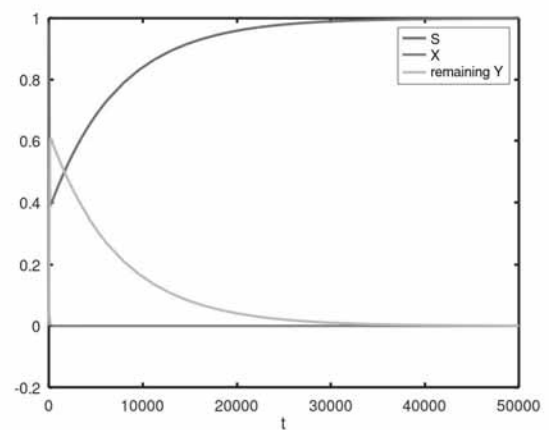
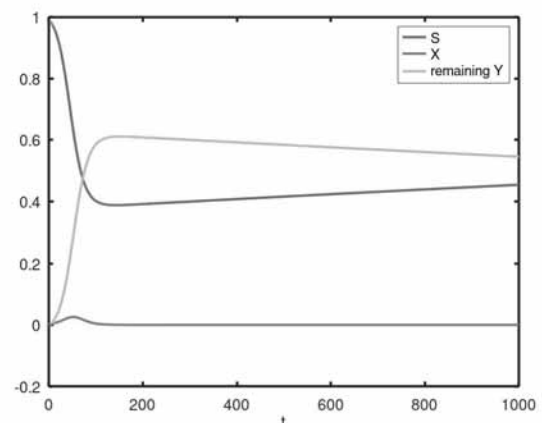


Figure 4: Simulation with demography, with testing,  $\theta = 0.4$ , using an implicit stiff integrator.

In contrast to the first model, this time there are peculiarities in the calculations for  $\mathcal{R}_0$ . Firstly, by analogy with the previous considerations, it can be shown that the non-negative orthant  $\mathbb{R}_{\geq 0}^{11}$  and the set  $\tilde{\Omega} := \{z \in \mathbb{R}_{> 0}^{11} \mid \sum_{i=1}^{11} z_i = 1\}$  are positive invariant for our second ODE.

Next, we need to ensure the existence of a DFE: the difference to the first model is that this equilibrium point is *no longer unique*. Simple calculations together with the positive invariance provide that all disease-free-equilibria fulfill the equation  $\tilde{S} + \tilde{R}^K + \tilde{R}^U = 1$ .

Therefore, there will be no unique basic reproduction number. The calculation of  $\mathcal{R}_0$  is similar to that of the first model: We get the same formulas as before, only with  $\Lambda = \mu = 0$ .

We obtain the next-generation-matrix

$$K = FV^{-1} = \beta S \begin{pmatrix} K_2 & 0 & 0 & 0 & 0 & 0 \\ * & & & & & \\ & & \mathbf{0} & & & \end{pmatrix}^T$$

with

$$K_2 = \frac{\pi^S}{\eta^S + \theta} + \frac{\pi^M}{\eta^M + \theta} + \frac{\pi^A}{\eta^A + \theta} + \frac{\pi^S}{\eta^S + \theta} \frac{\theta}{\tau^S} + \frac{\pi^M}{\eta^M + \theta} \frac{\theta}{\tau^O} + \frac{\pi^A}{\eta^A + \theta} \frac{\theta}{\tau^O}$$

The spectral radius of  $K$  is given by  $\rho(K) = \beta S \cdot K_2$ .

Finally, the next generation basic reproduction number is given by  $\mathcal{R}_0 = \rho(K)|_{DFE} = \beta \tilde{S} \cdot K_2$ .

Depending on the initial values of the unknown DFE-components, we calculate the limit value of  $S$  and choose it as  $\tilde{S}$ .

Another observation is that for  $\tilde{S} = 1 = N$  and  $\mu \rightarrow 0$  the basic reproduction numbers of both models coincide, which can be seen approximately for  $\mu = \frac{1}{365 \cdot 20}$  in the following table:

In contrast to the inclusion of demography in the first model, the linearization theorem cannot be used to investigate the local asymptotic stability of the DFE, since the corresponding matrix  $J_4|_{DFE}$  has the eigenvalue 0. Instead, we can again calculate a linear convex Lyapunov function for the case with  $\mathcal{R}_0 < 1$  of our DFE.

Again we have to analyze when the function  $\tilde{f}(x, y) = (F - V)|_{DFE} \cdot x - \mathcal{F}(x, y) + \mathcal{V}(x, y) \geq 0$ . For our second

$\beta$	$\mathcal{R}_0^{\text{with}}$	$\mathcal{R}_0^{\text{without}}$
0.1	0.545411144346408	0.546221176470588
0.4	2.18164457738563	2.18488470588235
0.8	4.36328915477126	4.36976941176471

**Table 3:** Basic reproduction numbers with/without demography, without testing.

model only the first component of  $\tilde{f}$  is not equal to zero, more precisely  $\tilde{f}_1(x, y) = \beta \cdot (\tilde{S} - S) \cdot [I^S + I^M + I^A + T^S + T^O]$ . Thus, we can consider a Lyapunov function on our positive invariant set  $\tilde{\Omega}$  only for  $S_0 \leq \tilde{S} \leq N_\infty = 1$ , since the  $S$ -component is monotonically decreasing.

Once again we get  $\omega^T = (0 \ 1 \ 1 \ 1 \ 1 \ 1)$ , where the  $E$ -component takes the value 0. Thus, the linear convex Lyapunov function is given by

$$Q(x) = \omega^T V^{-1} x = (K_2 \ q_1 \ q_2 \ q_3 \ q_4 \ q_5) \cdot x,$$

where  $q_1, q_2, q_3, q_4, q_5$  are given by the same formulas as before with  $\mu = 0$ .

Finally, we will consider again a numerical solution with the same parameter selection as in the previous simulations. We implement no testing ( $\theta = 0$ ) and set  $\tilde{S} = \lim_{t \rightarrow \infty} S(t) \approx 0.0358718761871864$ . The numeric solutions can be seen in Figure 5:

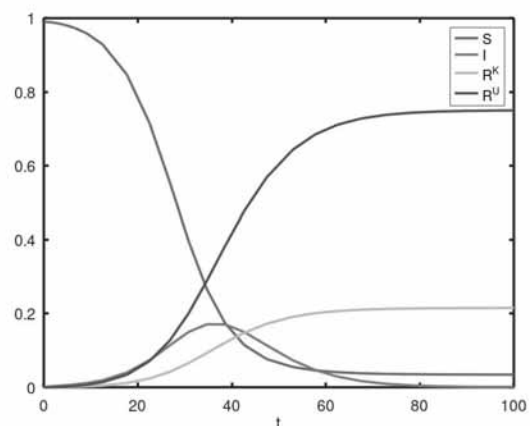


**Figure 5:** Simulation without demography, without testing.

For this scenario  $\mathcal{R}_0 \approx 0.123$  holds.

### 5 Model without Demography for two Age-groups

Finally, we examine the second model again, which we now expand to include another age group. The respective new infections now no longer depend only on the infected persons of the own age group, but also on those in the other age group, since contacts between population groups are taken into account.

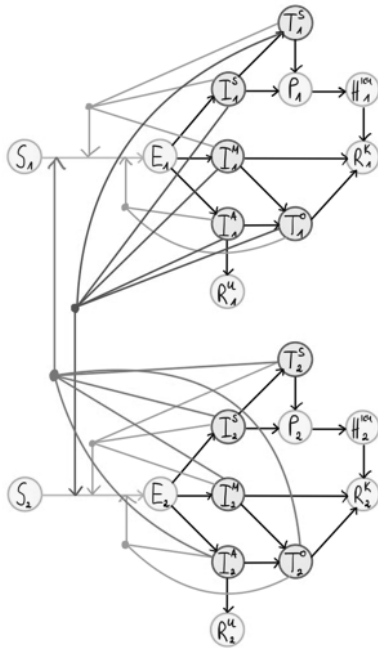


Figure 6: Model with two age groups, without demography.

In Figure 6 we see the mutual influence of the two age groups: The blue and purple arrows describe the influence on the new infections of the other group (orange). The grey arrows indicate the previous influence on the new infections of the own age group.

This extension of the model also changes the differential equation system, which doubles due to the additional compartments of the other age group. The ODE structure is the same for both groups:

We obtain for  $i = 1, 2$  the ODE system

$$\dot{S}_i = - \sum_{j=1}^2 \beta_{ij} S_i [I_j^S + I_j^M + I_j^A + T_j^S + T_j^O] \quad (2a)$$

$$\dot{E}_i = \sum_{j=1}^2 \beta_{ij} S_i [I_j^S + I_j^M + I_j^A + T_j^S + T_j^O] - \gamma E_i \quad (2b)$$

$$\dot{I}_i^S = \pi_i^S \gamma E_i - (\eta^S + \theta_i) I_i^S \quad (2c)$$

$$\dot{I}_i^M = \pi_i^M \gamma E_i - (\eta^M + \theta_i) I_i^M \quad (2d)$$

$$\dot{I}_i^A = \pi_i^A \gamma E_i - (\eta^A + \theta_i) I_i^A \quad (2e)$$

$$\dot{T}_i^S = \theta_i I_i^S - \tau^S T_i^S \quad (2f)$$

$$\dot{T}_i^O = \theta_i [I_i^M + I_i^A] - \tau^O T_i^O \quad (2g)$$

$$\dot{P}_i = \eta^S I_i^S + \tau^S T_i^S - \rho P_i \quad (2h)$$

$$H_i^{ICU} = \rho P_i - \sigma H_i^{ICU} \quad (2i)$$

$$\dot{R}_i^K = \eta^M I_i^M + \tau^O T_i^O + \sigma H_i^{ICU} \quad (2j)$$

$$\dot{R}_i^U = \eta^A I_i^A \quad (2k)$$

together with non-negative initial values. The calculation of the basic reproduction number now becomes a bit more complicated, the structure of the matrices changes a little compared to the second model. As before, due to the missing demography, we have the peculiarity of the non-unique DFE, so again we have to select an arbitrary equilibrium point with  $\tilde{S}_1 + \tilde{S}_2 + \tilde{R}_1^K + \tilde{R}_2^K + \tilde{R}_1^U + \tilde{R}_2^U = 1$ . In the following calculations, the corresponding placeholders are used again without presenting a detailed calculation option for the missing components as before.

We decompose the  $x$ -ODE using

$$\mathcal{F}(x, y) = \begin{pmatrix} \sum_{j=1}^2 \beta_{1j} S_1 [I_j^S + I_j^M + I_j^A + T_j^S + T_j^O] \\ \sum_{j=1}^2 \beta_{2j} S_2 [I_j^S + I_j^M + I_j^A + T_j^S + T_j^O] \\ \mathbf{0} \end{pmatrix}$$

and

$$\mathcal{V}(x, y) = \begin{pmatrix} \gamma E_1 \\ \gamma E_2 \\ (\eta^S + \theta_1) I_1^S - \pi_1^S \gamma E_1 \\ (\eta^S + \theta_2) I_2^S - \pi_2^S \gamma E_2 \\ (\eta^M + \theta_1) I_1^M - \pi_1^M \gamma E_1 \\ (\eta^M + \theta_2) I_2^M - \pi_2^M \gamma E_2 \\ (\eta^A + \theta_1) I_1^A - \pi_1^A \gamma E_1 \\ (\eta^A + \theta_2) I_2^A - \pi_2^A \gamma E_2 \\ \tau^S T_1^S - \theta_1 I_1^S \\ \tau^S T_2^S - \theta_2 I_2^S \\ \tau^O T_1^O - \theta_1 (I_1^M + I_1^A) \\ \tau^O T_2^O - \theta_2 (I_2^M + I_2^A) \end{pmatrix}$$

Both functions have values in  $\mathbb{R}^{12}$  and their entry structure is identical to that of the base model. The big Jacobian matrices are not included, since nothing fundamentally changed in the structure.

The next-generation matrix does not require all entries for the spectral radius, it has the following structure:

$$K = FV^{-1} = \begin{pmatrix} \mathcal{R}_{11}^{(S_1, \pi_1)} & \mathcal{R}_{12}^{(S_2, \pi_1)} & & \\ \mathcal{R}_{12}^{(S_1, \pi_2)} & \mathcal{R}_{22}^{(S_2, \pi_2)} & & \\ * & * & & \mathbf{0} \end{pmatrix},$$

where

$$\mathcal{R}_{ij}^{(S_k, \pi_l)} = \beta_{ij} \tilde{S}_k \cdot \left( \frac{\pi_l^S}{\eta^S + \theta_l} + \frac{\pi_l^M}{\eta^M + \theta_l} + \frac{\pi_l^A}{\eta^A + \theta_l} + \frac{\pi_l^S}{\eta^S + \theta_l} \frac{\theta_l}{\tau^S} + \frac{\pi_l^M}{\eta^M + \theta_l} \frac{\theta_l}{\tau^O} + \frac{\pi_l^A}{\eta^A + \theta_l} \frac{\theta_l}{\tau^O} \right).$$

Next,  $K$  is a  $12 \times 12$  matrix. For the spectral radius one needs the eigenvalues of  $K$ , which in this case must be calculated using the characteristic polynomial. The Laplace expansion for determinants provides:

$$\det(K - \lambda I) = \lambda^{10} \cdot \left[ \lambda^2 - \lambda \left( \mathcal{R}_{11}^{(S_1, \pi_1)} + \mathcal{R}_{22}^{(S_2, \pi_2)} \right) + \left( \mathcal{R}_{11}^{(S_1, \pi_1)} \mathcal{R}_{22}^{(S_2, \pi_2)} - \mathcal{R}_{12}^{(S_2, \pi_1)} \mathcal{R}_{12}^{(S_1, \pi_2)} \right) \right]$$

Thus,  $K$  has ten times the eigenvalue 0 and the two eigenvalues

$$\frac{\mathcal{R}_{11}^{(S_1, \pi_1)} + \mathcal{R}_{22}^{(S_2, \pi_2)} \pm \sqrt{A}}{2},$$

where

$$A = \left( \mathcal{R}_{11}^{(S_1, \pi_1)} + \mathcal{R}_{22}^{(S_2, \pi_2)} \right)^2 - 4 \left( \mathcal{R}_{11}^{(S_1, \pi_1)} \mathcal{R}_{22}^{(S_2, \pi_2)} - \mathcal{R}_{12}^{(S_2, \pi_1)} \mathcal{R}_{12}^{(S_1, \pi_2)} \right).$$

Therefore the basic reproduction number is defined by

$$\mathcal{R}_0 := \frac{\mathcal{R}_{11}^{(S_1, \pi_1)} + \mathcal{R}_{22}^{(S_2, \pi_2)} + \sqrt{A}}{2}.$$

If we start again from just one age group, then the following applies:

$$R := \mathcal{R}_{11}^{(S_1, \pi_1)} = \mathcal{R}_{22}^{(S_2, \pi_2)}, \quad 0 = \mathcal{R}_{12}^{(S_2, \pi_1)} = \mathcal{R}_{12}^{(S_1, \pi_2)}$$

and thus the basic reproduction number simplifies to

$$\mathcal{R}_0 = R,$$

which corresponds to the original  $\mathcal{R}_0$  of the second model.

Finally, we see that for several age groups our  $\mathcal{R}_0$  depends on the contacts within and between the individual groups, which would have made intuitive sense even without the calculations.

## 6 Conclusion

Enhancing the compartment model with demography simplifies the computation of the basic reproduction number. In this setting the disease free equilibria is unique. In the model predictive control setting of the original approach in [1] demography can be skipped, the solutions of the initial-value problem are only needed for one week, and demography changes the solutions only slightly. The advice is to skip demography in the model predictive control application if the time horizon is short but to use demography for the computation of the basic reproduction number and the Lyapunov function.

**Publication Remark.** This contribution is the revised version of the conference version published in *Tagungsband Langbeiträge ASIM SST 2024*, ARGESIM Report AR 47, ISBN ebook: 978-3-903347- 65-6, p 1-8, DOI: 10.11128/arep.47.a4707

## References

- [1] Grundel S, Heyder S, Hotz T, Ritschel TKS, Sauerteig P, Worthmann K. How Much Testing and Social Distancing is Required to Control COVID-19? Some Insight Based on an Age-Differentiated Compartmental Model. *SIAM Journal on Control and Optimization*. 2022; 60(2): S145–S169. doi: 10.1137/20M1377783.
- [2] Prüss JW, Wilke M. *Gewöhnliche Differentialgleichungen und dynamische Systeme*. 2nd Edition. Cham: Birkhäuser; 2019.
- [3] van den Driessche P, Watmough J. Reproduction numbers and sub-threshold endemic equilibria for compartmental models of disease transmission. *Mathematical Biosciences*. 2002; 180(1-2): 29–48. doi: 10.1016/s0025-5564(02)00108-6.
- [4] Varga RS. *Matrix Iterative Analysis*. 2nd Edition. Heidelberg: Springer; 2000.
- [5] Shuai Z, van den Driessche P. Global Stability of Infectious Disease Models Using Lyapunov Functions. *SIAM Journal on Applied Mathematics*. 2013; 73(4): 1513–1532. doi: 10.1137/120876642.
- [6] LaSalle J. Some Extensions of Liapunov’s Second Method. *IRE Transactions on Circuit Theory*. 1960; 7(4):520–527.

# Mathematical Model for Spatial and Temporal Risk Analysis of West Nile Virus Transmission in Bavaria, Germany

Oliver Chinonso Mbaoma<sup>1\*</sup>, Stephanie Margarete Thomas<sup>1,2</sup>, Carl Beierkuhnlein<sup>1,2,3</sup>

<sup>1</sup>Department of Biogeography, University of Bayreuth, Universitaetsstr. 30, 95447 Bayreuth, Germany;

\**oliver.mbaoma@uni-bayreuth.de*

<sup>2</sup>Bayreuth Center of Ecology and Environmental Research, BayCEER, University of Bayreuth, Universitaetsstr. 30, 95447 Bayreuth, Germany

<sup>3</sup>Geographical Institute of the University of Bayreuth, GIB, Universitaetsstr. 30, 95447 Bayreuth, Germany

SNE 35(1), 2025, 25-29, DOI: 10.11128/sne.35.sn.10724  
Selected ASIM SST 2024 Postconf. Publication: 2024-12-10  
Received Revised: 2025-02-17; Accepted: 2025-02-28  
SNE - Simulation Notes Europe, ARGESIM Publisher Vienna  
ISSN Print 2305-9974, Online 2306-0271, www.sne-journal.org

**Abstract.** The spatial and temporal trends of mosquito-borne diseases have been shifting. Recently, there has been an increase in cases of West Nile Fever across Germany. In this study, we investigated the spatial and temporal risk of West Nile virus transmission in Bavaria using a mathematical model. The model incorporated epidemiological, climatic, and bird distribution data. It generated spatially and temporally explicit graphs depicting the health states of mosquitoes and birds. Additionally, we produced risk maps identifying areas in Bavaria at heightened risk for West Nile virus transmission.

## Introduction

West Nile fever is an illness triggered by West Nile virus (WNV), a single strand RNA arbovirus from the Flaviviridae family and one of the most widely spread flaviviruses [1]. In 1937, the first case was isolated at West Nile district in Uganda and has since been occurred in all continents [2]. Although WNV normally circulates in a sylvatic cycle between mosquitoes and birds as hosts, mosquitoes can also spread the virus to humans and animals, including horses [2],[3]. Most of these animals and humans only experience mild viremia and are unable to serve as amplifying hosts for the virus [4]. In 2018, the virus was for the first time detected in 12 birds and 2 horses in eastern Germany [5]. The first human autochthonous case of the infection was detected in 2019 near Leipzig [6]. Suitable climatic conditions with high temperatures in summer was suspected to promote the spread of the virus.

While mosquitoes tend to spread the virus locally, migratory birds are suspected to play a role in disseminating the virus over long distances to new areas [5].

With information on bird surveillance for WNV, competence of vector mosquitoes and amplification suitability of hosts, we were able to develop a climate-driven process-based mechanistic model calibrated with functional traits of vector mosquito and host birds to predict the spatial and temporal risk of WNV infection in Bavaria.

## 1 Materials and Method

We adopted a similar approach applied to show the spatial and temporal pattern of WNV infection in Germany between 2018 and 2022 by Mbaoma et al, [7]. We applied the model in Bavaria and accounted for mosquito population, pathogen transmission in migratory and residential birds.

### 1.1 Materials

Climate and bird data were used to parameterize and force the model adequately. Cases of WNV infection were collected from the Animal Diseases Information System database of the FLI from 2018 to 2022 [5]. Bird distribution data was collected from E-bird online database [8]. Temperature, rainfall and humidity data used to drive our model were collected from E-OBS database [9].

### 1.2 Model Description

With a clear understanding of the entomology, life characteristics, and functional ecology of both the WNV vector and its hosts, we used the mechanistic approach which was developed by Mbaoma et al., 2024 [7] to generate spatial and temporal predictions of potential WNV infection outbreak in Bavaria.

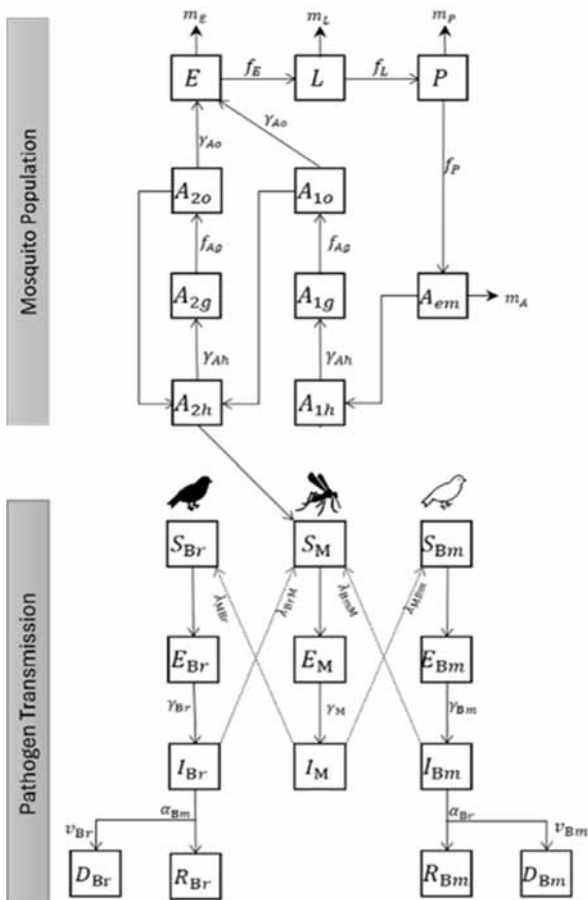


**Figure 1:** WNV epidemic model showing two sections depicting mosquito population and pathogen transmission between mosquito, resident bird and migratory bird with compartments:

- Eggs ( $E$ ), Larvae ( $L$ ), Pupa ( $P$ ), New adults ( $A_{em}$ ),
- Host-seeking adults ( $A_{1h}$ ), Gravid adults ( $A_{1g}$ ),
- Ovipositioning adults ( $A_{1o}$ ),
- Older host-seeking adults ( $A_{2h}$ ),
- Older gravid adults ( $A_{2g}$ ), Older ovipositioning adults ( $A_{2o}$ ),
- Susceptible mosquitoes ( $S_M$ ), Exposed mosquitoes ( $E_M$ ),
- Infected mosquitoes ( $I_M$ ),
- Susceptible residential birds ( $S_{Br}$ ),
- Susceptible migratory bird ( $S_{Bm}$ ),
- Exposed residential birds ( $E_{Br}$ ),
- Exposed migratory birds ( $E_{Bm}$ ),
- Infected residential birds ( $I_{Br}$ ),
- Infected migratory birds ( $I_{Bm}$ ),
- Removed residential birds ( $R_{Br}$ ),
- Removed migratory birds ( $R_{Bm}$ ),
- ..Dead residential birds ( $D_{Br}$ ),
- Dead migratory birds ( $D_{Bm}$ ).

Mathematical epidemiology and population biology were used to formulate the fundamentals of the compartmental model driven by several ordinary differential equations. The model consists of two sections: the first describing mosquito population while the second described pathogen transmission.

As described in the paper by Mbaoma et al. [7], disease-free mosquito population was explained by the several equations.

$$\begin{cases}
 \dot{E} = d\gamma_{Ao}(\beta_1 A_{1o} + \beta_2 A_{2o}) - (\mu_E + df_E)E \\
 \dot{L} = df_E E - (m_L(1 + L/k_L) + f_L)L \\
 \dot{P} = f_L L - (m_P + f_P)P \\
 \dot{A}_{em} = f_P P \sigma e \left( -\mu_{em} \left( 1 + \frac{P}{k_P} \right) \right) - (m_A + \gamma_{Aem})A_{em} \\
 \dot{A}_{1h} = \gamma_{Aem} A_{1h} - (m_A + \mu_r + \gamma_{Ah})A_{1h} \\
 \dot{A}_{1g} = \gamma_{Ah} A_{1h} - (m_A + \mu_{pr} + f_{Ag})A_{1g} \\
 \dot{A}_{1o} = f_{Ag} A_{1g} - (m_A + \mu_r + f_{Ao})A_{1o} \\
 \dot{A}_{2h} = f_{Ao}(A_{1o} + A_{2o}) - (m_A + \mu_r + \gamma_{Ah})A_{2h} \\
 \dot{A}_{2g} = \gamma_{Ah} A_{2h} - (m_A + \mu_{pr} + f_{Ag})A_{2g} \\
 \dot{A}_{2o} = f_{Ag} A_{2g} - (m_A + \mu_r + f_{Ao})A_{2o}
 \end{cases} \tag{1}$$

The process of infection between mosquito and bird population is explained by the following sets of Ordinary differential equations, with Equation 2,3 and 4 explaining health states of mosquitoes, migratory birds and residential birds respectively.

$$\begin{aligned}
 \frac{dS_M}{dt} &= -(\lambda_{BrM}(T) + \lambda_{BmM}(T))S_M + A_{2h} - m_A(T)S_M \\
 \frac{dE_M}{dt} &= (\lambda_{BrM}(T) + \lambda_{BmM}(T))S_M - \gamma_M(T)E_M - m_A(T)E_M
 \end{aligned} \tag{2}$$

$$\frac{dI_M}{dt} = \gamma_M(T)E_M - m_A(T)I_M$$

$$\begin{aligned}
 \frac{dS_{Br}}{dt} &= \left( b_{Br} - (b_{Br} - m_{Br}) \frac{N_{Br}}{K_{Br}} \right) N_{Br} - \lambda_{MBr}(T)S_{Br} - m_{Br}S_{Br} \\
 \frac{dE_{Br}}{dt} &= \lambda_{MBr}(T)S_{Br} - \gamma_{Br}E_{Br} - m_{Br}E_{Br}
 \end{aligned} \tag{3}$$

$$\frac{dI_{Br}}{dt} = \gamma_{Br}E_{Br} - \alpha_{Br}I_{Br} - m_{Br}I_{Br}$$

$$\begin{aligned}
 \frac{dR_{Br}}{dt} &= (1 - v_{Br})\alpha_{Br}I_{Br} - m_{Br}R_{Br} \\
 \frac{dD_{Br}}{dt} &= v_{Br}\alpha_{Br}I_{Br}
 \end{aligned}$$

$$\begin{aligned} \frac{dS_{Bm}}{dt} &= \left( b_{Bm} - (b_{Bm} - m_{Bm}) \frac{N_{Bm}}{K_{Bm}} \right) N_{Bm} - \lambda_{MBm}(T) S_{Bm} - m_{Bm} S_{Bm} \\ \frac{dE_{Bm}}{dt} &= \lambda_{MBm}(T) S_{Bm} - \gamma_{Bm} E_{Bm} - m_{Bm} E_{Bm} \\ \frac{dI_{Bm}}{dt} &= \gamma_{Bm} E_{Bm} - \alpha_{Bm} I_{Bm} - m_{Bm} I_{Bm} \\ \frac{dR_{Bm}}{dt} &= (1 - v_{Bm}) \alpha_{Bm} I_{Bm} - m_{Bm} R_{Bm} \\ \frac{dD_{Bm}}{dt} &= v_{Bm} \alpha_{Bm} I_{Bm} \end{aligned} \tag{4}$$

Cross infection between mosquitoes and amplifying hosts which are birds of interest was defined in Equations 5 to 8.

$$\lambda_{MBr}(T) = \delta_M F_b k(T) p_{MBr} \phi_{Br} \frac{I_M}{K_M} \tag{5}$$

$$\lambda_{MBm}(T) = \delta_M F_b k(T) p_{MBm} \phi_{Bm} \frac{I_M}{K_M} \tag{6}$$

$$\lambda_{BrM}(T) = \delta_M F_b k(T) p_{BrM} \frac{I_{Br}}{K_{Br}} \tag{7}$$

$$\lambda_{BmM}(T) = \delta_M F_b k(T) p_{BmM} \frac{I_{Bm}}{K_{Bm}} \tag{8}$$

Basic reproductive number was computed based on the next-generation matrix approach applied in the precursor model by Mbaoma et al [7] using the equation below:

$$R_0 = \sqrt{\left[ \frac{\gamma_M(T) \beta_{Mbr}(T) + \beta_{Mbm}(T)}{(\gamma_M(T) + m_M(T)) m_M(T)} \left( \frac{S_{Br}}{K_{Br}} + \frac{S_{Bm}}{K_{Bm}} \right) \right] + \left[ \frac{\gamma_{Br} \beta_{Br}(T)}{(\gamma_{Br} + m_{Br})(\alpha_{Br} + m_{Br}) K_{Br}} \frac{S_M}{K_{Br}} \right] + \left[ \frac{\gamma_{Bm} \beta_{Bm}(T)}{(\gamma_{Bm} + m_{Bm})(\alpha_{Bm} + m_{Bm}) K_{Bm}} \frac{S_M}{K_{Bm}} \right]}$$

### 1.3 State Variables, Parameters and Functions.

All state variables, parameters and functions used to develop this model, including calibration and validation processes have been described in a precursor publication for WNV epidemic model by Mbaoma et al. [7].

## 2 Results and Discussion

### 2.1 WNV Transmission Risk Projection for Bavaria

The inverse calibrated WNV epidemic model generated spatial and temporal abundance of mosquito. It also generated different health states for hosts of interests which include residential birds and migratory birds.

Due to limited occurrence recorded in Bavaria (just one case), we assumed our model was performing at optimum having been previously validated across Germany [7].

Functional traits of mosquito which includes fecundity, development rates, mortality rates, biting rates and extrinsic incubation rates of WNV pathogen all responded to deviations in temperature [10],[11]. The model was able to simulate various health states of mosquito and birds, with seasonal variation in Bavaria. Susceptible and parous host-seeking mosquitoes are especially of interest for the transmission potential (Figure 2). Also, we were able to simulate risk maps of WNV transmission for Bavaria between 2017 and 2022 at NUTS3 levels, identifying potential hotspots for WNV infection outbreaks (Figure 3).

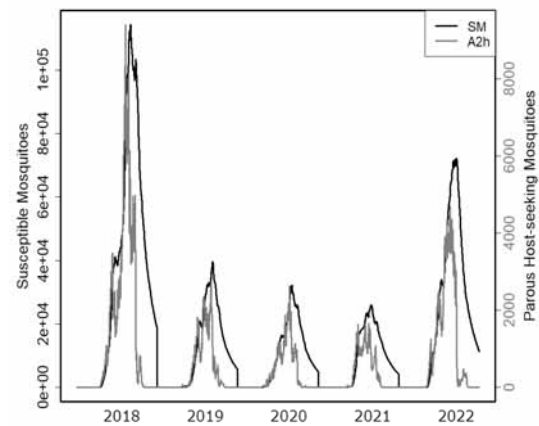
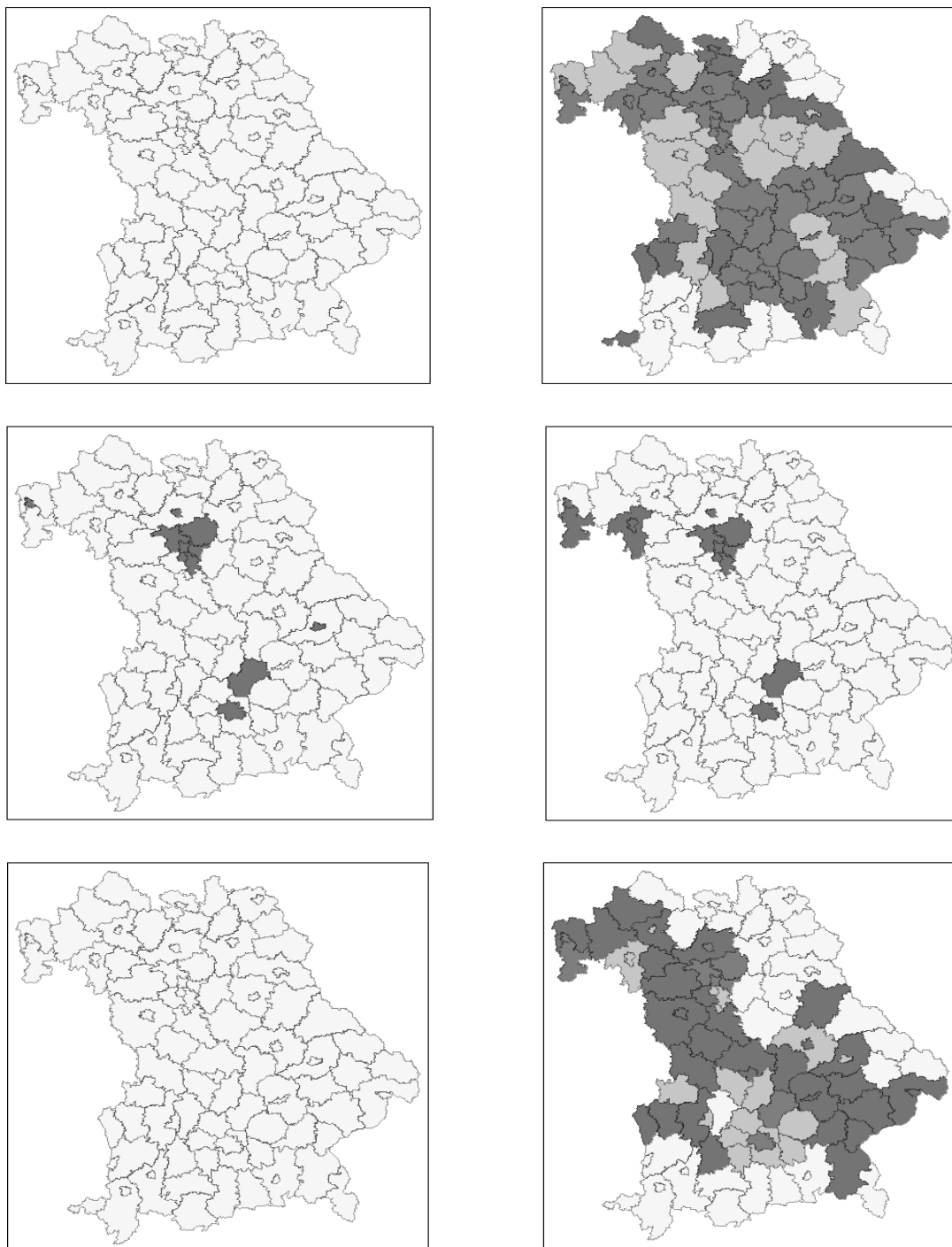


Figure 2: Simulated time series of health states for susceptible ( $S_M$ ) and parous host-seeking mosquitoes ( $A_{2h}$ ) between 2018 and 2022 in Bavaria.

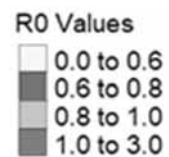
### 2.2 Seasonal Variation of WNV Infection Risk

Several climate sensitive mosquito-borne diseases display seasonal variation [12]. In our model, several factors, including vector population, vectoral capacity, vector competence and amplifying host competence influenced  $R_0$  rates.

Infection parameters, such as mosquito biting rate and extrinsic incubation rate were important drivers which was consistent with the role of environmental suitability in driving infectious disease transmission [10]. The model reasonable simulates seasonal trend of  $R_0$  values. The  $R_0$  values averaged across Bavaria show a low risk of WNV transmission in 2018 and 2022 (Figure 4).



**Figure 3:** WNV transmission risk across Bavaria at NUT3 level from 2017 to 2022 estimated from daily R0 values between August and October (week 30 to 42) when the peak of the WNV infections were reported by FLI.



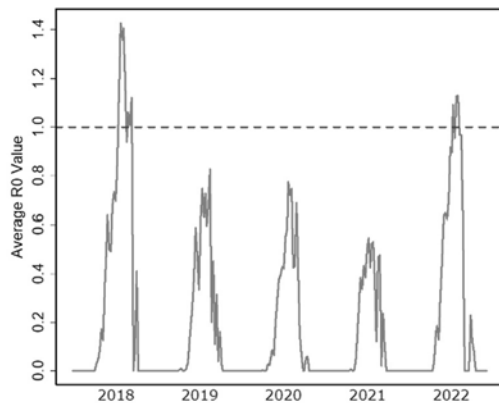


**Figure 4:** The risk of West Nile Virus (WNV) infection outbreaks, expressed as  $R_0$  values, was assessed across Bavaria from 2018 to 2022. The red line represents the simulated daily  $R_0$  values aggregated on a weekly basis, while the blue dashed horizontal line indicates the threshold at which secondary cases can be directly generated by the first case in a population where all individuals are susceptible to infection.

### 3 Conclusion

We developed a process based WNV epidemic model which was able to simulate areas prone to WNV transmission in Bavaria. From our results, it was obvious that WNV infection which is endemic in eastern Germany may likely spread to the South with several hotspots identified in Bavaria. Changing climate and migratory pattern of short distance migratory birds have been identified as key factors that could accelerate WNV infection spread. The model considered juvenile and adult stages of mosquito life cycle in several compartments, and two bird taxa with migratory and residential birds. Functional traits of mosquitoes were driven by climate. Host-feeding preference of vector, transmission probability and mosquito to host ratio were all accounted for in the model.

In addition, spatial heterogeneity of climate forcings, vectors and host species were considered. We developed a model that could be deployed at the backend of a warning system for *Culex pipiens* mosquito population occurrence and WNV transmission risk.

**Publication Remark.** This contribution is the revised version of the conference version published in *Tagungsband Kurzbeiträge ASIM SST 2024*, ARGESIM Report AR 46, ISBN ebook: 978-3-903347-64-9, DOI: 10.11128/arep.46 (volume DOI), p 5-8.

### References

- [1] De Filette M, Ulbert, Diamond S, et al. Recent progress in West Nile virus diagnosis and vaccination. *Vet Res* 43, 16 (2012). DOI 10.1186/1297-9716-43-16 .
- [2] Chancey C, Grinev A, Volkova E, Rios M. The global ecology and epidemiology of West Nile virus. *BioMed research international*. 2015, p. 376230. DOI 10.1155/2015/376230.
- [3] Holicki CM, Ziegler U, Răileanu C, Kampen H, Werner D, Schulz J, Silaghi C, Groschup MH, Vasić A. West Nile Virus Lineage 2 Vector Competence of Indigenous *Culex* and *Aedes* Mosquitoes from Germany at Temperate Climate Conditions. *Viruses*. 2020 May 19;12(5):561. DOI 10.3390/v12050561
- [4] Bowen RA, Nemeth NM. Experimental infections with West Nile virus. *Curr Opin Infect Dis*. Jun 2007, 20(3):293-7. DOI 10.1097/QCO.0b013e32816b5cad
- [5] Animal Diseases Information System TSIS. Available at: <https://tsis.fli.de/Reports/Info.aspx> (Acc. 12 2023).
- [6] Robert Koch Institut RKI (2019): [https://www.rki.de/DE/Content/Infekt/EpidBull/Archiv/2019/Ausgaben/40\\_19.pdf? blob=publicationFile](https://www.rki.de/DE/Content/Infekt/EpidBull/Archiv/2019/Ausgaben/40_19.pdf?blob=publicationFile).
- [7] Mbaoma OC, Thomas SM, Beierkuhnlein C. Spatio-temporally Explicit Epidemic Model for West Nile Virus Outbreak in Germany: An Inversely Calibrated Approach. *J. of epidemiology and global health* 14, 1052–1070 (2024). DOI 10.1007/s44197-024-00254-0
- [8] Sullivan BL, Wood CL, Iliff MJ, Bonney RE, Fink D, Kelling S. (2009). E-bird: A citizen-based bird observation network in the biological sciences. *Biological Conservation*, 142(10), 2282-2292 (2009). DOI 10.1016/j.biocon.2009.05.006
- [9] Cornes RC, van der Schrier G, van den Besselaar EJ, Jones PD. An ensemble version of the E-OBS temperature and precipitation data sets. *Journal of Geophysical Research: Atmospheres*, 123(17), 9391-9409 (2028).
- [10] Mordecai EA, Caldwell JM, Grossman MK, Lippi CA, Johnson LR, Neira M, Villena O. (2019). Thermal biology of mosquito-borne disease. *Ecology letters*, 22(10), 1690-1708 (2019). DOI 10.1111/ele.13335
- [11] Shocket MS, Verwillow AB, Numazu MG, Slamani H, Cohen JM, El Moustaid F, Rohr J, Johnson LR, Mordecai EA. (2020). Transmission of West Nile and five other temperate mosquito-borne viruses peaks at temperatures between 23°C and 26°C. *eLife*, 9, e58511 (2020). DOI 10.7554/eLife.58511
- [12] Tjaden NB, Caminade C, Beierkuhnlein C, Thomas SM. (2018). Mosquito-borne diseases: advances in modelling climate-change impacts. *Trends in parasitology*, 34(3), 227-245 (2018). DOI 10.1016/j.pt.2017.11.006



# Simulation-Based Analysis of Storage Strategies for an Inland Container Terminal

Maximilian Mowe\*, Jona Manemann, Lasse Jurgeleit,  
Maximilian Kiefer, Uwe Clausen

Institute of Transport Logistics, TU Dortmund University, Leonhard-Euler-Straße 2, 44227 Dortmund, Germany

\*[maximilian.mowe@tu-dortmund.de](mailto:maximilian.mowe@tu-dortmund.de)

SNE 35(1), 2025, 31-34, DOI: 10.11128/sne.35.sn.10725  
Selected ASIM SST 2024 Postconf. Publication: 2024-12-10  
Received Revised: 2025-02-28; Accepted: 2025-03-03  
SNE - Simulation Notes Europe, ARGESIM Publisher Vienna  
ISSN Print 2305-9974, Online 2306-0271, [www.sne-journal.org](http://www.sne-journal.org)

**Abstract.** Due to the transformation of the logistics sector, the use of trimodal container terminals is becoming increasingly important. This results in major challenges, such as managing the constantly increasing volume of shipments while simultaneously improving the efficiency of internal processes.

Adapting existing storage strategies has proven to offer great potential for raising productivity.

In this context, the following paper develops an alternative storage strategy for container terminals. For evaluation of its functionality, a simulation model for an exemplary trimodal container terminal is developed. In addition, potential is analysed, based on comparison with the currently used storing strategy.

## Introduction

The logistics sector is important to the economies worldwide and e.g. the third-largest economic sector in Germany with a total volume of €293 billion in 2021. Logistics service providers such as transportation and handling account for 50% of this [1]. Despite its economic importance and impressive figures, the logistics sector is facing major challenges.

Logistics has to fulfil customer requirements in an increasingly volatile environment and has failed so far to achieve sustainability targets. One lever in this respect is modal shift from road to combined rail-road-transport. A forecasted growth of rail by 73% by 2030 compared to 2010 in Germany is particularly attributable to rail/road trans-shipment as a key growth driver [2].

With freight transport accounting for 19.4% of Germany's total greenhouse gas emissions in 2021 [3] modal shift and other measures to reduce emissions are vital and operators of trimodal container terminal connecting road, rail, and water modes of transportation in container freight transport are in need of solutions to cope with growth efficiently.

One approach to overcoming these challenges for a trimodal container terminal is to improve internal processes. These range from improving the storage strategy to developing additional space and optimizing the use of resources. However, new strategies need to be tested before they are applied in reality. One method that makes this possible is simulation. Simulation makes it possible to create a virtual image of reality in order to test changes based on this image, which can then be transferred to reality [4].

In order to support those which facing these challenges, this paper aims to demonstrate the possibilities for optimizing operational strategies using simulation. Therefore, an exemplary container terminal is presented, which aims to compare two storage strategies by using simulation. The storage strategies to be compared differentiate as follows: the current situation with storage excluding the removal path, and the target situation with storage close to the delivery points.

For this purpose, our paper is divided into five sections. After a brief overview on current research on simulation for operational strategies of container terminals, the used simulation procedure is presented. Followed by developing the simulation model and conducting related experiments, an outlook on future work in this field of research is given.

## 1 Literature Review

A systematic literature review based on the guidelines of Durach et al. [5] is conducted to evaluate the common use of the method for planning operational strategies of container terminals.

The following search terms and combinations of these are used to identify relevant sources: “simulation”, “optimization”, “container terminal”, “stack”, “strategies”, and “terminal operation”. Publications from the databases Scopus, Web of Science, Google Scholar, and Science Direct are examined for this purpose.

After full-text analysis, 18 results emerged. The evaluation of the results shows that the methodological approach of simulation is used for optimizing operational strategies. However, no publication was found that deals specifically with the storage strategies. In a related study, Clausen et al. [6] constructed a simulation model to identify the optimal operational configuration for a terminal. The model determines the most effective combination of crane control and resource management strategies for each load the terminal can accommodate, based on a specific set of operational conditions. Novaes et al. [7] examine in their study the potential of data science to enhance container terminal operations, improve efficiency, boost throughput, and strengthen competitiveness in the shipping sector. Decision-making within container terminals, particularly in determining optimal container stacking locations, is a significant challenge due to the multitude of factors at play. By analyzing the datasets, new strategies and policies can be simulated to minimize container rehandling operations.

Overall, the papers identified indicate that simulation has applications in a variety of use cases in the area of planning the operating strategies of container terminals. For this reason, the simulation method is described below before the model developed for this use case is presented.

## 2 Method

“Simulation is the representation of a system with its dynamic processes in an experimentable model with the aim of reaching findings which are transferable to reality” [8]. To examine a system with simulation in a structured manner, multiple procedure models can be used (e.g. [4], [9], [10]). The procedure models provide users with information for appropriately carrying out simulation studies. In German-speaking countries VDI Guideline 3633 Sheet 1 is widely used and selected for this study because the system under investigation is located in Germany. The associated Verification and Validation (V&V) during the study follows Rabe et al. [11]. Their procedure model for V&V aligns with the phases of VDI 3633, which makes its application suitable for this study.

The phases defined by VDI 3633 guide users from task definition to the experiments and analysis. Within the procedure, there is a clear separation between data and model and each phase produces a result [4]. The intermediate results are the subject of the V&V. According to Rabe et al. [11], each phase is examined in itself and additionally with respect to or against previous phase results [11].

## 3 Simulation Modeling

According to the introduction, the objective is the analysis of a given storage strategy for container handling and its comparison with a zoning strategy. The investigations are conducted for two inland container terminals. CT1 is trimodal (see Figure 1) and CT2 is bimodal. CT2 contains a road and a rail lane, which are located next to each other. Prior to the actual strategy comparison, the preliminary goal is to model the terminals in their respective system state with sufficient accuracy. The subsequent comparison is aimed at the container movements and therefore focuses on the internal handling processes. Accordingly, the system under consideration ends with the entry and exit of transport vehicles.

For this study, CT’s activities are roughly divided into three handling processes. Incoming containers are stored and they are retrieved to leave the terminal. Additionally, a relocation process may be necessary for stacked containers. Containers enter the system by a mode of transportation (train, truck or ship).

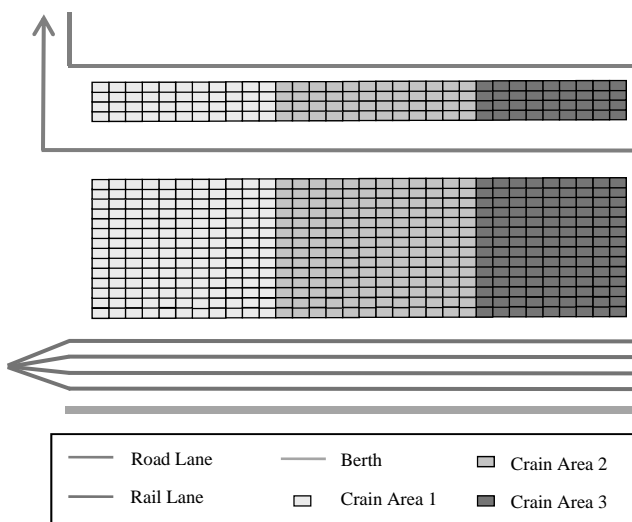


Figure 1: Schematic representation of container terminal 1.

For this study, CT’s activities are roughly divided into three handling processes. Incoming containers are stored and they are retrieved to leave the terminal. Additionally, a relocation process may be necessary for stacked containers. Containers enter the system by a mode of transportation (train, truck or ship).

Within the storing process, firstly a given strategy determines the position. Thereafter, a handling resource (e. g. portal crane) moves the container to its destination. The retrieval begins with the mode of transportation arriving at the terminal. The time of arrival may be known with a containers arrival or is defined while the container is already stored. Before moving the container it is checked if the container is movable (i. e. the container has no containers stacked above itself). Movable containers get loaded onto the mode of transportation and leave the system. For non-movable containers the relocation process for the container above is initiated before moving the desired container. At the beginning of the relocation process, it is also checked whether the container is movable. For movable containers the position get determined by the given storage strategy. For non-movable container the relocation process gets initiated for the container above and the desired container gets moved afterwards. Accordingly, the relocation process is recursive. For this study, we only consider relocations because of retrieval processes.

The handling resources, containers and modes of transport are being modeled as agents, which define their behavior within the terminal. The model including the described processes and agents is implemented with the simulation software AnyLogic 8.9 as a discrete event simulation using agents.

### 4 Experiments & Results

Within the experimental framework, the current terminal is analysed in the first simulation scenario using five different degrees of capacity utilisation with varying numbers of in- and outbound transport vehicles and containers. The second scenario implements the developed storing strategy with three different weighting factors. In order to achieve valid results, the confidence interval method is used to determine a number of 30 replications to be carried out per parameter variation. The duration of each simulation run lasts seven days with a two-day transient phase regarding to the method of Welch [12].

The developed storage strategy follows the existing requirements for container storage. Currently, the optimal storing location is identified based on the distance from its current position and under consideration of time restrictions such as the retrieval date.

Additionally, the new storage strategy also takes into account the distances for retrieving containers. For this purpose, the storage area is divided into various sections running along the road and rail lanes. According to this, the optimal storing location can be determined in order to ensure the shortest possible retrieval distance to the lanes. Therefore, our calculation is characterized by three elements. “A” indicates the distance of the container’s current location to the available storage position and “B” represents the direct retrieval distance to the lanes of truck and train. In addition, weighting of the retrieval distance is managed by factor “p”.

$$StoringPosition_Weighted = A + p * B \quad (1)$$

For validation of this equation, its functionality is verified in the simulation model. For this purpose, the straight distance between retrieval containers and the lane of truck and train is analysed. Since ships are mostly used for delivery of the containers, this mode of transport is not taken into account in the evaluation.

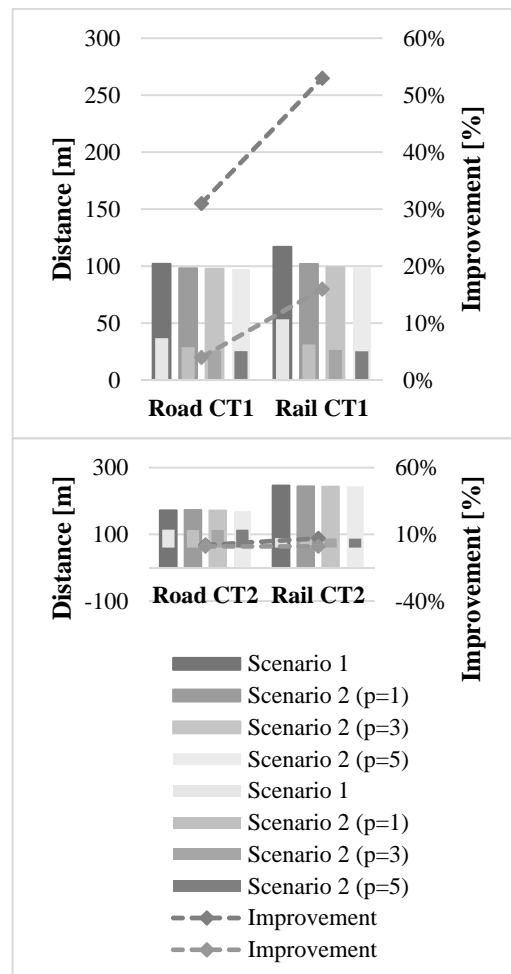


Figure 2: Comparison of covered distances for container retrieval.

From the grey-coloured bars in Figure 2, it can be observed that covered distances for retrieval at CT1 decreases for all weighting factors when applying the storing strategy compared to initial scenario 1. Depending on the mode of transportation, this improvement amounts to 31 % respectively 53 %, as shown by the grey dashed line. The improvement for CT2 is less significant. In general, containers are stored closer to the retrieval area, thus indicating that optimisation of the storing position by the equation works.

For a complete evaluation of its potential, the real distance from containers to the transport vehicles must be analysed. This is shown by the green bars in Figure 2 and indicates that the real distance is significantly greater. Furthermore, the green dashed line demonstrates that the improvement achieved compared to scenario 1 is not as great as previously suggested. At CT2, this positive effect is almost neutralised.

Furthermore, the total duration of dispatching processes for trucks and trains at both terminals will be analysed to validate the potential of the new storing strategy. However, at either location there has been no significant reduction for both modes of transport. For some scenarios, dispatching times have even increased.

Overall, results of the simulation scenarios indicate that the new storing strategy does not significantly improve internal processes of the container terminal. Due to a high utilisation of the lane, trucks can only stop in an assigned area but not at the level of containers storage location.

Although containers will be placed closer to the lane, it will not affect its distance to the real loading position of the truck. This difficulty also occurs when loading the trains, as each container is linked to a fixed railway wagon, which may not be positioned at the same level as containers storing location.

## 5 Conclusion

In this paper, two different storage strategies have been compared with focussing on increased productivity in a trimodal container terminal. To evaluate their potential in practice, simulation has been used. On the basis of VDI 3633 a simulation model was developed, which combines agent-based and discrete-event simulation. Evaluation based on industry-specific key performance indicators revealed that our newly developed storing strategy is working effectively and can improve internal processes.

However, due to specific infrastructural and operational conditions of both terminals considered in this example, the expected improvement can not be achieved. In order to fully realise its potential, further work must be conducted to apply the storing strategy in combination with scheduling of incoming modes of transportation. In addition, this strategy must be modified depending on the use case and its infrastructural conditions.

## References

- [1] BMDV: Masterplan Binnenschifffahrt. 2018.
- [2] Boysen J. et al.: Status quo des Güterverkehrssystems in Deutschland – eine Metastudie unter besonderer Betrachtung der Vernetzung des Verkehrs.
- [3] The Umweltbundesamt: Emissionen des Verkehrs. 2023.
- [4] VDI Association of German Engineers e.V.: Simulation of systems in materials handling, logistics and production: Part 1(VDI 3633). Berlin: Beuth, 2014.
- [5] Durach CF, et al.: A New Paradigm for Systematic Literature Reviews in Supply Chain Management. *J Supply Chain Manag*, 53 (4) 2017, p. 67–85. DOI 10.1111/jscm.12145
- [6] Clausen U, et al.: CONTSIM–Container Terminal Management with Simulation. *Procedia - Social and Behavioral Sciences*, 54 2012, p. 332–340. DOI 10.1016/j.sbspro.2012.09.752
- [7] Novaes MT, et al.: Operational performance evaluation of a container terminal using data mining and simulation. *Asian Transport Studies*, 10 2024, p. 100127. DOI 10.1016/j.eastsj.2024.100127
- [8] VDI Association of German Engineers e.V.: Simulation of systems in materials handling, logistics and production: Terms and Definitions (VDI 3633). Berlin: Beuth Verlag, 2018.
- [9] Law AM. Simulation modeling and analysis. New York, NY: McGraw Hill Education, 2015.
- [10] Banks J (ed). Handbook of simulation: Principles, methodology, advances, applications, and practice. New York: Wiley, 1998.
- [11] Rabe M, et al. A new procedure model for verification and validation in production and logistics simulation. In: Winter Simulation Conference, 2008 (Editor: S. J. Mason). Piscataway, NJ: IEEE, 2008, pp 1717–1726.
- [12] Welch PD. The statistical analysis of simulation results. *The Computer Performance Modeling* 1983, 1983:268–328.

**Publication Remark.** This contribution is the revised version of the conference version published in *Tagungsband Kurzbeiträge ASIM SST 2024*, ARGESIM Report AR 46, ISBN ebook: 978-3-903347-64-9, DOI: 10.11128/arep.46 (volume DOI), p 53-56.

# Simulation and Control of 2-Dimensional Anisotropic Heat Conduction

Stephan Scholz<sup>1a,2\*</sup>, Christopher Bonenberger<sup>1b,2</sup>, Nico Scheiter<sup>1</sup>, Lothar Berger<sup>1a</sup>

<sup>1</sup>Hochschule Ravensburg-Weingarten (RWU), 88250 Weingarten, Germany

\*[stephan.scholz@uni-ulm.de](mailto:stephan.scholz@uni-ulm.de), <sup>a</sup> Control and Process Engineering, <sup>b</sup> Institut für Künstliche Intelligenz

<sup>2</sup> Universität Ulm, 89081 Ulm, Germany

SNE 35(1), 2025, 35-39, DOI: 10.11128/sne.35.sn.10726  
 Selected ASIM SST 2024 Postconf. Publication: 2024-12-10  
 Received Revised: 2025-02-28; Accepted: 2025-03-03  
 SNE - Simulation Notes Europe, ARGESIM Publisher Vienna  
 ISSN Print 2305-9974, Online 2306-0271, [www.sne-journal.org](http://www.sne-journal.org)

**Abstract.** In this contribution, we provide a simulation and control approach for a two-dimensional heat conduction problem.

In particular, we spatially approximate the two-dimensional heat conduction problem with anisotropic thermal conductivity and transfer it via eigenvalue computation to a sampled-time state space model. Furthermore, we design a static feed-forward filter to reach a reference temperature and a full state feedback with linear-quadratic regulation to guarantee a stable closed-loop behavior.

Finally, we demonstrate the performance of our closed-loop heat conduction system.

## Introduction

Many industries, like semiconductor fabrication, require challenging thermal processing which need to be simulated and controlled very precisely, see e.g. [1]. The thermal dynamics modeling and its control design cover a wide range in the literature, depending on the geometry and research focus, see e.g. [1, 4] and [2, Ch. 2, 6, 8, 9]. The control design for small models can be simple and practical but they are limited for enhancements. In contrast, purely theoretical approaches might be too complex for realistic applications. In our contribution, we propose an extendable and easy-to-implement approach as a 2-dimensional geometry with multiple actuators along one boundary side and multiple sensors on the opposite. This is a simplified model of the realistic 3-dim. situation, see [3]. We approximate the spatial derivatives via finite differences and we obtain a high-dim. state space, which is solvable through eigenvalue computation in Section 1.

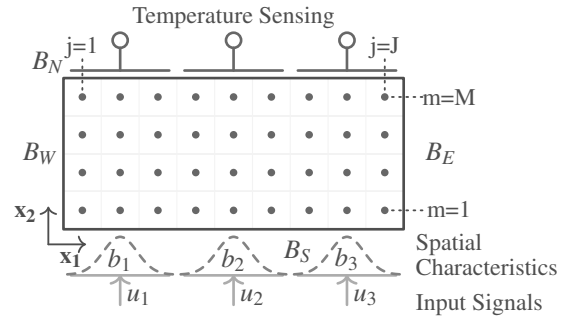


**Figure 1:** Geometry with finite difference nodes  $x_{j,m}$  actuation on  $B_S$  and measurement on  $B_N$ .

Based on these results, we derive the time discrete solution, the state feedback with linear-quadratic regulation and the reference tracking in Section 2. Finally, we visualize in Section 3 the proper operating closed-loop behavior.

## 1 Two-dimensional Heat Conduction

We assume a rectangle  $\Omega = (0, L) \times (0, W)$  with length  $L > 0$ , width  $W > 0$ , see Fig. 1. We note the position  $x = (x_1, x_2)^T \in \bar{\Omega}$ . The rectangle has the boundary  $\partial\Omega = \bar{\Omega} \setminus \Omega = B_W \cup B_E \cup B_S \cup B_N$  with the sides  $B_W = \{0\} \times [0, W]$  (west),  $B_E = \{L\} \times [0, W]$  (east),  $B_S = [0, L] \times \{0\}$  (south) and  $B_N = [0, L] \times \{W\}$  (north). The object consists of a solid material with density  $\rho > 0$ , specific heat capacity  $c > 0$  and anisotropic thermal conductivity  $\lambda_1 > 0$  along  $x_1$ -axis (or length) and  $\lambda_2 > 0$  along  $x_2$ -axis (or width).

The anisotropy describes the physical situation to conduct heat faster along one axis compared to the other axis. We summarize these material properties as diffusivity constants  $\alpha_1 := \frac{\lambda_1}{c\rho}$  and  $\alpha_2 := \frac{\lambda_2}{c\rho}$ .

The evolution of temperature in the plate  $\theta : [0, T] \times \Omega \rightarrow \mathbb{R}$  solves the two-dimensional heat equation

$$\frac{d}{dt} \theta(t, x) = \alpha_1 \frac{\partial^2}{\partial x_1^2} \theta(t, x) + \alpha_2 \frac{\partial^2}{\partial x_2^2} \theta(t, x) \quad (1)$$

for  $(t, x) \in (0, T_{final}] \times \Omega$ , with an initial temperature distribution  $\theta(0, x) = \theta_0(x)$  and boundary conditions

$$\lambda_1 \frac{\partial}{\partial x_1} \theta(t, x) = 0, \quad x \in B_W \cup B_E, \quad (2)$$

$$\lambda_2 \frac{\partial}{\partial x_2} \theta(t, x) = \begin{cases} -\phi_{in}(t, x) & \text{for } x \in B_S, \\ 0 & \text{for } x \in B_N. \end{cases} \quad (3)$$

The boundary conditions in Eq. (2, 3) describe a thermal insulation (no thermal losses) and heat can only be supplied along boundary  $B_S$  via the heat flux

$$\phi_{in}(t, x) = \sum_{n=1}^{N_u} b_n(x) u_n(t) \quad (4)$$

with  $N_u \geq 1$  as the number of actuators. We assume that the boundary side  $B_S$  consists of segments  $\beta_n \subseteq B_S$  such that  $B_S = \bigcup_{n=1}^{N_u} \beta_n$  and each actuator operates only on its segment and has the spatial characteristics

$$b_n(x) = \begin{cases} m_n \exp(-\|M_n [x - x_{c,n}]\|^{2\nu_n}) & \text{for } x \in \beta_n \\ 0 & \text{for } x \in B_S \setminus \beta_n \end{cases}$$

with  $m_n \in [0, 1]$ ,  $M_n > 0$  and  $\nu_n \in \mathbb{N}_{>0}$  for  $n \in \{1, \dots, N_u\}$ . Furthermore, we assume an arbitrary positive input signal  $u_n : [0, T] \rightarrow \mathbb{R}_{>0}$ . Analog to the actuator setup, we consider temperature measurements on boundary side  $B_N$ . Each temperature sensor operates only on its segment  $\gamma_n \subseteq B_N$  with  $B_N = \bigcup_{n=1}^{N_y} \gamma_n$  where  $N_y \geq 1$  denotes the number of sensors. We assume the temperature measurement

$$y_n(t) = \frac{1}{\int_{\gamma_n} g_n(x) dx} \int_{\gamma_n} g_n(x) \theta(t, x) dx \quad (5)$$

for  $n \in \{1, \dots, N_y\}$  and with the sensor characterization  $g_n : \gamma_n \rightarrow [0, 1]$  analog to  $b_n$ . We approximate the spatially derivatives in heat equation (1) next, to derive the large-scale state space system. The heat conduction modeling approach with the actuator and sensor characteristics is also described in [3, 4].

We assume that all finite difference nodes are inside the rectangle as  $x_{j,m} := ([j - \frac{1}{2}]\Delta x_1, [m - \frac{1}{2}]\Delta x_2)^\top$  for  $j \in \{1, 2, \dots, J\}$  and  $m \in \{1, 2, \dots, M\}$  with  $J > 0$  and  $M > 0$ , see the dots in Fig. 1. We introduce the global index  $i(j, k) := j + (k - 1) J$  and the temperature vector of the nodes  $\Theta(t) := (\theta(t, x_1), \dots, \theta(t, x_i), \theta(t, x_{N_c}))$  with totals number of nodes  $N_c = J M$ . We approximate the second-order derivatives with finite differences  $\frac{\partial^2}{\partial x_1^2} \approx \frac{1}{\Delta x_1^2} D_1$  in  $x_1$ -direction with  $D_1 = \text{diag}(\underbrace{\tilde{D}_1, \dots, \tilde{D}_1}_{M \text{ matrix blocks}})$  and

$$\tilde{D}_1 = \begin{pmatrix} -1 & 1 & & & & \\ 1 & -2 & 1 & & & \\ & \ddots & \ddots & \ddots & & \\ & & & 1 & -2 & 1 \\ & & & & 1 & -1 \end{pmatrix} \in \mathbb{R}^{J \times J}$$

and for the  $x_2$ -direction we find  $\frac{\partial^2}{\partial x_2^2} \approx \frac{1}{\Delta x_2^2} D_2$  with

$$D_2 = \begin{pmatrix} -I_J & I_J & & & & \\ I_J & -2I_J & I_J & & & \\ & \ddots & \ddots & \ddots & & \\ & & & I_J & -2I_J & I_J \\ & & & & I_J & -I_J \end{pmatrix}.$$

Summing up  $D_1$  and  $D_2$  with its coefficients, we note the system matrix as

$$A = \frac{\alpha_1}{\Delta x_1^2} D_1 + \frac{\alpha_2}{\Delta x_2^2} D_2. \quad (6)$$

In the matrices  $\tilde{D}_1$  and  $D_2$ , we already consider the thermally insulated boundary conditions but we have to include also the heat supply via

$$B = \frac{\alpha_2}{\lambda_2 \Delta x_2} (\tilde{b}_1, \dots, \tilde{b}_{N_u})$$

with vectors  $\tilde{b}_n := (b_n(x_{1,1}), \dots, b_n(x_{J,1}), 0_{J(M-1)})^\top$ . So, we formulate the state space formulation

$$\frac{d}{dt} \Theta(t) = A \Theta(t) + B u(t). \quad (7)$$

with the temperature measurement  $y(t) = C \Theta(t)$  from Eq. (5).

The output matrix is noted as  $C = (\tilde{c}_1, \dots, \tilde{c}_{N_y})^\top$  with  $\tilde{c}_n := (0_{J \times (M-1)}, \bar{g}_1, \dots, \bar{g}_{N_y})$  and elements  $\bar{g}_{n,j} = g_n(x_{j,M}) / \sum_{j=1}^J g_n(x_{j,M})$ . We know that we can find the analytical solution of Eq. (7) as

$$\Theta(t) = e^{A[t-t_0]} \Theta(0) + \int_{t_0}^t e^{A[t-\tau]} B u(\tau) d\tau. \quad (8)$$

However, as the size of matrix  $A$  grows quadratically by  $N_c$ , the exact and fast computation of  $\exp(A)$  might be a problem for large systems  $N_c \gg 1$ . If we know the eigenvalues  $\mu_i$  and eigenvectors  $\psi_i$  of  $A$  for  $i \in \{1, \dots, N_c\}$ , then we find the matrix exponential as

$$\exp(A t) = V^{-1} \text{diag}(e^{\mu_1 t}, \dots, e^{\mu_{N_c} t}) V \quad (9)$$

with  $V = [\psi_1, \dots, \psi_{N_c}]$ . The article [5] states explicit formulas for the pair  $(\mu_i, \psi_i)$  for a 1-dim. heat equation problem and we extend this concept for our 2-dim. problem. We assume  $f(z, n) := \cos(z(2n-1)\pi)$  and we state the eigenvalues of the 2-dim. problem as

$$\begin{aligned} \mu_{j,m} = & -2p_1 [1 - f((j-1)/J, 1)] \\ & -2p_2 [1 - f((m-1)/M, 1)] \end{aligned} \quad (10)$$

with  $(j, m) \in \{1, \dots, J\} \times \{1, \dots, M\}$ ,  $p_l = \alpha_l / \Delta x_l^2$  and  $l \in \{1, 2\}$ . We note the eigenvectors

$$\psi_i = (\psi_{i,1}, \dots, \psi_{i,JM})^\top$$

with vector elements

$$\psi_{(j,m),(\tilde{n}_j, \tilde{n}_m)} = f\left(\frac{j-1}{2J}, \tilde{n}_j\right) f\left(\frac{m-1}{2M}, \tilde{n}_m\right) \quad (11)$$

for the indices  $(\tilde{n}_j, \tilde{n}_m) \in \{1, \dots, J\} \times \{1, \dots, M\}$ . The proof of this assumption is omitted here, the correctness of  $(\mu_i, \psi_i)$  can be verified by evaluating  $A\psi = \mu\psi$  with cosine identities.

## 2 Controller Design

We sample the temperature in time as  $\Theta(n\Delta T) =: \Theta(n)$  for  $n \in \{0, \dots, \lfloor \frac{T}{\Delta T} \rfloor\}$  with sampling time  $\Delta T > 0$  and we derive from Eqs. (8-11) the time-sampled system

$$\Theta(n+1) = A_D \Theta(n) + B_D u(n) \quad (12)$$

with matrices

$$\begin{aligned} A_D &:= \exp(A\Delta T) = V^{-1} \text{diag}(e^{\mu_1 \Delta T}, \dots, e^{\mu_{N_c} \Delta T}) V, \\ B_D &:= \int_0^{\Delta T} \exp(A[\Delta T - \tau]) B d\tau. \end{aligned}$$

The input signal  $u(n) := -K \Theta(n) + W r(n)$  is designed such that a state feedback  $K \in \mathbb{R}^{N_u \times J K}$  stabilizes the system and a static feed-forward filter  $W \in \mathbb{R}^{N_u \times N_y}$  steers the measured temperatures to a static reference signal  $r \in \mathbb{R}^{N_y}$ . Feedback matrix  $K$  is found by solving the discrete infinite-horizon linear-quadratic regulator problem

$$\min_u \sum_{n=1}^{\infty} \Theta(n)^\top Q \Theta(n) + u(n)^\top R u(n) \quad (13)$$

with subject to Eq. (12). The optimal control problem (13) leads to the discrete time algebraic Riccati equation

$$P = Q + A_D^\top P A_D - [A_D^\top P B_D] [R + B_D^\top P B_D]^{-1} [B_D^\top P A_D]$$

where we compute matrix  $P$  to obtain the feedback gain

$$K = [R + B_D^\top P B_D]^{-1} B_D^\top P A_D.$$

If the number of actuators and sensors coincide,  $N_u \equiv N_y$ , then we find the filter matrix  $W$  to drive the thermal dynamics to a constant reference value  $r$ . We assume for  $n \rightarrow \infty$  an uniform temperature distribution

$$[A_D - B_D K] \Theta(n) + B_D W r = \Theta(n) \quad (14)$$

and a constant output

$$y(n) = C \Theta(n) = r. \quad (15)$$

We identify  $\Theta$  in Eq. (15) with Eq. (14) and we use the reference tracking  $y \equiv r$  to formulate the filter

$$W = -[C(A_d - B_d K - I)^{-1} B_d]^{-1}.$$

For more details on the control design, we refer to introductory text books, e.g. [6, Ch. 7].

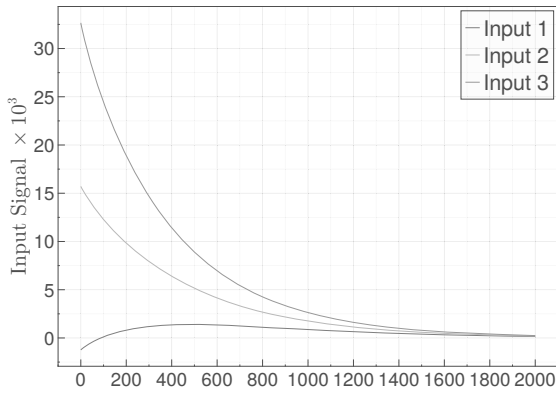


**Figure 2:** Input signals  $u_n$  with  $n \in \{1, 2, 3\}$  applied on boundary side  $B_S$ , time  $t$  in [s].

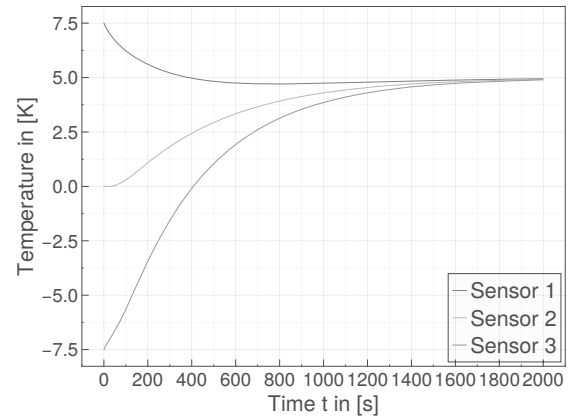


**Figure 3:** Measured temperatures  $y_n$  with  $n \in \{1, 2, 3\}$  on boundary side  $B_N$ .

### 3 Simulation Case Study

We apply the proposed concepts on an example of a steel plate with model parameters as in Table 1 and controller configuration as in Table 2.

The initial temperature distribution is  $\theta_0(x_1, x_2) = 10 \sin(2\pi \frac{x_1}{L})$ . We design the controller such that it is forced to act quickly  $Q \gg R$  and the static filter shall steer the three measured temperatures towards the reference value  $r = (5, 5, 5)^T$ .

The computed input signal  $u(t)$  and the resulting measurement temperatures  $y(t)$  are depicted in Figure 2 and Figure 3. The input signals  $u_2$  and  $u_3$  start with high initial values compared to  $u_1$  because they have to increase the temperatures of  $y_2$  and  $y_3$ , see Figure 3. All temperatures along boundary side  $B_N$  converge in Figure 4 after ca. 1200 seconds. We implemented the simulation with JULIA programming language [7] and solved the algebraic Riccati equation with the library MATRIXEQUATIONS.JL [8]. The full source code is available [9].

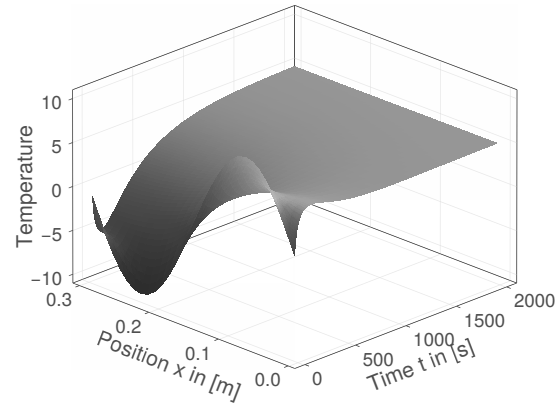


**Figure 4:** Temperature evolution on boundary side  $B_N$ .

$L$	$W$	$J$	$K$	$(\lambda_1, \lambda_2)$	$\rho$	$c$
0.3	0.1	30	10	(40, 60)	8000	400

**Table 1:** System Parameters for Simulation.

Actuators		Sensors		$\Delta T$	$Q$	$R$
$N_u$	$(m, M, v)$	$N_y$	$(m, M, v)$			
3	(1, 40, 2)	3	(1, 20, 1)	2	$10^5 I$	$I$

**Table 2:** Controller Parameters for Simulation.

### Discussion & Conclusion

In real world applications, we have to deal with thermal emissions like convection and radiation on each boundary side, which we did not consider in this contribution. Moreover, in 3-dim. objects we can only measure the temperatures on the boundary, not inside the object. However, as we require access to all temperatures for the full state feedback, we have to compute them with a state observer. In a nutshell, we derived a state space control design for a 2-dim. heat equation and we exemplified its performance. Further research will focus on the extension of our approach for systems with thermal emissions and 3-dim. geometries.

## References

- [1] Tay A, Tan KK, Zhao S, Lee TH. Predictive Ratio Control of Multizone Thermal Processing System in Lithography, *IFAC Proceedings Volumes*. 2008; 41(2): 10863–10868.
- [2] Meurer T. Control of higher-dimensional PDEs: Flatness and backstepping designs. Springer Science & Business Media, 2012.
- [3] Scholz S, Berger L. Hestia. jl: A Julia Library for Heat Conduction Modeling with Boundary Actuation. *Simul. Notes Eur.* 2023; 33(1): 27–30, DOI 10.11128/sne.33.sn.10634.
- [4] Scholz S, Berger L. Optimization-based Reference Tracking for Two-Dimensional Multiple Source Heating, *2024 IEEE 63rd Conference on Decision and Control*. 2024. DOI 10.1109/CDC56724.2024.10886335
- [5] Yueh WC, Eigenvalues of several tridiagonal matrices. *Applied Mathematics E-Notes [electronic only]*. 2005; 5: 66–74.
- [6] Åström KJ, Murray R. Feedback systems: an introduction for scientists and engineers. Princeton university press, 2021.
- [7] Bezanson J, Edelman A, Karpinski S, Shah VB. Julia: A fresh approach to numerical computing. *SIAM Review*. 2017; 59(1): 65-98.
- [8] Varga A, Karrasch D, Legat B, Aluthge D. andreasvarga/MatrixEquations.jl: v2.4.2 (v2.4.2). Zenodo. 2024. Available: DOI 10.5281/zenodo.10546715
- [9] Scholz S. stephans3/StateSpace2DHeatConduction.jl: StateSpace2DHeatConduction.jl v0.1.0 (v0.1.0). Zenodo. 2024. Available: DOI 10.5281/zenodo.11350656

**Publication Remark.** This contribution is the revised version of the conference version published in *Tagungsband Kurzbeiträge ASIM SST 2024*, ARGESIM Report AR 46, ISBN ebook: 978-3-903347-64-9, DOI: 10.11128/arep.46 (volume DOI), pp 45-48.



# Comparing Different Pruning Strategies for the Evaluation Task of Virtual Stochastic Sensors

Dávid Bodnár\*, Claudia Krull

Institut für Simulation und Graphik, Otto-von-Guericke-Universität Magdeburg, Universitätsplatz 2, 39106 Magdeburg, Germany; \*[david.bodnar.ovgu@gmail.com](mailto:david.bodnar.ovgu@gmail.com)

SNE 35(1), 2025, 41-48, DOI: 10.11128/sne.35.tn.10727  
 Selected ASIM SST 2024 Postconf. Publication: 2024-12-10  
 Received Revised: 2025-02-28; Accepted: 2025-03-03  
 SNE - Simulation Notes Europe, ARGESIM Publisher Vienna  
 ISSN Print 2305-9974, Online 2306-0271, [www.sne-journal.org](http://www.sne-journal.org)

**Abstract.** Virtual Stochastic Sensors calculate statistically relevant estimates in indirectly observable discrete stochastic systems. This is done by the proxel-based analysis that aims to reconstruct the relevant part of the state space with an iterative process. Strategically removing non-relevant proxels from the analysis (pruning) to reduce runtime overhead might potentially affect the results. And while the impact on the decoding problem has already been analysed in detail, the effect on the evaluation problem was not yet discussed.

The paper discusses three pruning strategies and compares their properties in case of the evaluation task. The theoretical statements are empirically proven using a car rental agency model in form of a Conservative Hidden non-Markovian Model.

The results show that in case of well chosen parameters all three pruning strategies are able to reach the same accuracy. The major difference between the strategies is due to their runtime properties which need to be carefully aligned with the use-case to reach optimal behavior. Based on the results the *fixed number of proxels pruning* strategy provides highly predictable execution time, while the *fixed threshold pruning* is very good at discovering a broader spectrum of the state space. The *variable pruning* is a very good trade-off between the previous strategies enabling lower thresholds and thorough state space analysis while maintaining acceptable execution times at the cost of more complex parametrisation.

**Keywords:** Virtual Stochastic Sensor, Hidden non-Markovian Model, Proxel-based Simulation, Pruning, Evaluation

## Introduction

Virtual Stochastic Sensors (VSSs), introduced in [1], utilize the proxel-based analysis [2] to analyse partially observable discrete stochastic systems. The proxels, which represent a given system state at a given point in time, build a so-called proxel tree to reconstruct and represent the relevant part of the state space during the analysis. The insignificant part is pruned away.

There are different pruning strategies to define what is insignificant. In this paper three of them, *fixed threshold pruning*, *fixed number of proxels pruning* and *variable pruning*, will be discussed in detail. Similarly to [3] we aim to give an overview of the influence of the different pruning strategies on the evaluation results of VSSs. This is motivated by the generalisation and further development of the Change Adaptation Algorithm (CAA) described in [4].

As in [3], this paper utilizes the same car rental service model, presented in [5], for the evaluation. In this model, customers arrive in a premium or ordinary queue based on their membership. They use the same door for entering and leaving the shop area and this door is being observed (opening creates a signal) by the analysis. A single employee is serving both queues. Premium customers have priority over ordinary ones, but a customer is always served to the end if the processing has been started. Both queues are limited to 50 customers. Figure 1 shows the Augmented Stochastic Petri Net (ASPN) [5] of the system. ASPNs are modified Petri nets [6] that can model the emission of symbols when a transition fires. This model will also be used as an example in the following to demonstrate the different concepts and tools used in this paper.

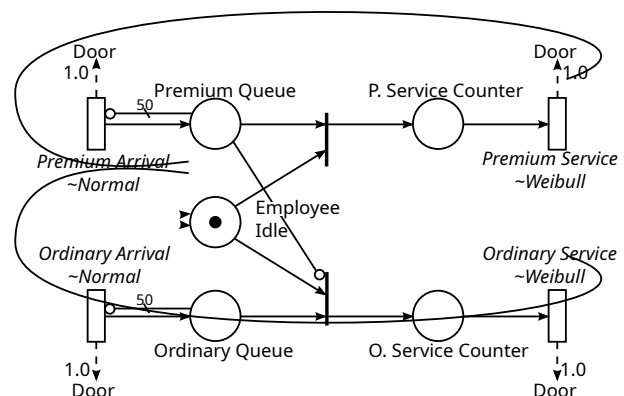


**Figure 1:** Car rental service Example as ASPN.

This paper compares three pruning strategies in theory and using the above presented experiment for the evaluation problem of Conversive Hidden non-Markovian Models (CHnMMs). The results show that after a given threshold there is no significant difference in the resulting probabilities, however, other major properties vary for each strategy so choosing one or the other for a given problem will always depend on the use-case.

## 1 Related Work

Virtual Sensors (VSs) [7] aim to collect system information that is hard or expensive to obtain in a direct way. If we combine them with stochastic processes a so-called VSS can be constructed which calculates statistically relevant estimates of system parameters that are similarly hard, inefficient and/or expensive to measure.

In this section, an introduction will be provided to such a stochastic process, the so-called CHnMM [8] and its solution algorithm, the proxel-based analysis. Additionally, proxel merging will be discussed.

### 1.1 Conversive Hidden non-Markovian Model

The concept of CHnMMs originates from the well-known Hidden Markov Models (HMMs) [9], where a hidden or partially hidden system is analyzed by probabilistic symbol emissions. This idea was extended to Hidden non-Markovian Models (HnMMs) by [10] to overcome the limitations of the discrete-time Markov chain in the background. HnMMs use arbitrary continuous distribution functions to describe the state changes and to create time dependence between them.

Similarly to HMMs, the HnMMs also try to solve the evaluation and the decoding problem. The decoding problem, finding the most probable generator state sequence to a given trace, and the impact of the different pruning strategies on it have already been discussed in [3]. This paper is focusing on the evaluation problem, e.g. finding the probability that a trace has been generated by a given model.

A specific subclass of HnMMs are the so-called CHnMMs which allow additional performance optimizations of the algorithm due to the fact that every state change results in an observable symbol emission. Those optimizations are powerful enough to make CHnMMs the perfect experiment environment to test and verify new ideas in an efficient way. That is why this paper also limits its scope to CHnMMs.

In case of the presented car rental shop the hidden internal system state is the length of (the number of customers in) the ordinary and premium queues. Every state change (a customer entering or leaving the queue) results in a door opening (signal emission). This effectively means that by solving the evaluation problem, the goal of this project is to find the probability of a given door-opening signal protocol.

### 1.2 Proxels-based analysis

CHnMMs also need a solution algorithm. However, instead of using the forward algorithm [11] or the Viterbi algorithm [12] the so-called proxel-based analysis [2] can be used. The technique utilizes the encapsulation of a possible system state description (system state  $m$ , age vector  $\vec{\tau}$ , the probability of that state  $p$ , a timestamp  $t$ , etc.) into a so-called proxel object as it can be seen in Equation 1. One can use a collection of those proxels to describe all possible system states at a given point in time, including the ages of the relevant non-Markovian transitions. Then by creating a parent-child relationship between the timesteps one can derive the possible system states for the future timesteps in an iterative way. Of course, the proxel definition can be extended to carry additional information through the analysis. Referring back to the example model, a specific proxel represents a given number of customers in the premium and ordinary queues ( $m$ ), the durations since the last customers entered each queue and while one is being served ( $\vec{\tau}$ ) and the probability ( $p$ ) of ending up in the represented state at the current simulation time ( $t$ ).

$$P_x = (m, \vec{\tau}, p, t) \quad (1)$$

The mentioned parent-child relation is described by the Hazard Rate Function (HRF) in Equation 2 using the Probability Density Function (PDF)  $f(\tau)$  and the Cumulative Distribution Function (CDF)  $F(\tau)$  of a possible state change. The equation describes the current state change rate for a given state change if this one has been active for  $\tau$  and has not happened yet. So in case of our example model this translates to for example, what is the probability of a customer service being finished in this timestep, if he/she is being served right now. Or similarly, what is the probability of the next customer entering the shop now?

$$H(\tau) = \frac{f(\tau)}{1 - F(\tau)} \quad (2)$$

To keep the proxel tree at a reasonable size, very unlikely proxels can be pruned from the tree. Different strategies exist to perform this operation. They will be further discussed in Section 2.

Proxel probabilities are represented on a logarithmic scale to preserve precision as in case we represent them on normal scale, they would disappear due to arithmetic underflow very soon after the analysis was started.

### 1.3 Merging proxels

In case of the evaluation problem, we are not interested in the history of a given proxel, because we are only trying to compute the probability of a given system state at time  $t$ . This means that after a couple of timesteps after starting the proxel-based analysis we can find proxels in the proxel tree, that represent the same system state, but they have been generated by different routes. These proxels can be merged by adding their probabilities (which are logarithmic probabilities, as stated before, represented by  $\tilde{p}_1$  and  $\tilde{p}_2$ , where  $\tilde{p}_1 > \tilde{p}_2$ ) using the Kingsbury-Rayner formula [9] shown in Equation 3. By performing this merging operation one can keep the size of the proxel tree under control very efficiently.

$$\tilde{p}_1 +_{\log} \tilde{p}_2 = \tilde{p}_1 - \ln\left(1 + e^{-(\tilde{p}_2 - \tilde{p}_1)}\right) \quad (3)$$

The Kingsbury-Rayner formula additionally provides an opportunity to efficiently add probabilities that are on a different magnitude.

An example of a merging opportunity is presented in Figure 2, where the discovered state space of a three state system ( $m_0$ ,  $m_1$ ,  $m_2$ ) is represented over three timesteps. The two proxels marked with red at  $t = 2\Delta$  represent the same internal system state with different probabilities but they were reached through different routes, so they can be merged.

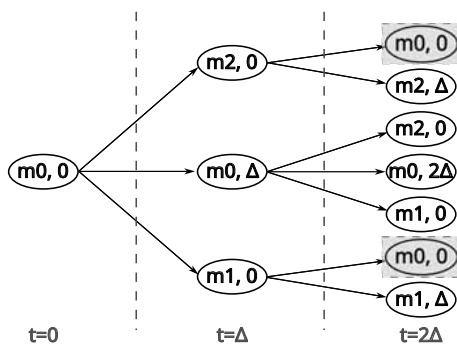


Figure 2: Example of mergable proxels.

As stated before, in case of the evaluation problem only the current system state is a subject of interest. This means, that in many cases different customer enter sequences (P - premium customer, O - ordinary customer), for example "PPOPO" and "POPPO", can be represented by a single common proxel.

Merging significantly reduces the number of existing proxels over time. This also means that much less strict pruning configurations can be used than for example in case of the decoding task. These will be shown later in Section 3.2.

Until now, we have introduced CHnMMs and the proxel-based analysis as two base concepts of our research. We also gave a brief overview about the possibility of merging as the main method to keep the proxel tree under control in case of the evaluation problem. In the next section the concept of pruning and the different pruning strategies will be introduced as the main research interest of this paper.

## 2 Pruning Strategies for Evaluation

Pruning is a concept of the proxel-based analysis, in which the algorithm classifies a part of the proxel tree as irrelevant for further analysis and removes it. The different strategies encapsulate a set of logical steps to be performed on the proxel tree in order to identify and prune the irrelevant proxels.

There are two major events that can render a proxel based analysis infeasible. One of them is state space explosion, when the proxel tree grows exponentially and reaches a state where the next step is enormously expensive to compute or the resources of the computer running the analysis are fully consumed. The other one is the exact opposite, the proxel tree can die out. In this case the remaining proxels, for example due to extreme pruning, encounter an observed symbol that cannot be emitted by their current system state and with that the proxel becomes impossible and is removed from the analysis. If all the proxels are removed from the tree, the tree dies out. Merging and a pruning strategy needs to be devised to prevent both of these extreme cases from happening

As already mentioned at the end of the previous section, merging does an excellent job at keeping the proxel tree under control. But sooner or later the analysis reaches the point where additional intervention is needed in the form of pruning.

Still, merging makes it possible to use less strict pruning strategies than in case of the decoding problem [3]. This also results in the fact that state space explosions or died out proxel trees are not common for simple models. However, with increasing system complexity a state space explosion might occur, but it is extremely unlikely.

In this section a brief overview will be given of the three investigated pruning strategies. But before diving into the details, we should list the properties of a good pruning algorithm.

These are in case of the evaluation problem in our experience, the following:

1. High proxel processing throughput
2. Small amount of lost (pruned) probability
3. Prevents state space explosion
4. Scales the proxel tree up and down depending on how „interesting” the current part of the trace is
5. Guarantees predictable execution times
6. Is easily customizable for different needs
7. Is overall robust, which means that it does not react very differently to similar traces

These criteria will be used to evaluate the different pruning strategies.

## 2.1 Fixed Threshold Pruning

The *fixed threshold pruning* is a simple concept defining a pruning probability threshold  $p(P_{pruned,t_i})$ . Below that value every proxel is considered to be irrelevant and is then removed from the proxel tree.

The threshold is defined compared to the probability of the most probable proxel  $\max(p(P_{x,t_i}))$  in the proxel tree for a given time  $t_i$ . It is described by a ratio  $r$  as it can be seen in the Equation 4. The parameter  $r$  is a freely selectable value with the limits  $0 < r \leq 1$ .

$$p(P_{pruned,t_i}) < r \max(p(P_{x,t_i})) \quad (4)$$

This pruning strategy is the most vulnerable to state space explosions and other instabilities as described in [3]. However, combined with merging it is possible to use extremely low pruning thresholds, as it will be shown in Section 3.2.

This strategy scales the proxel tree overall well and as a simple algorithm, it provides a high proxel processing throughput. But due to the unpredictable number of proxels in the proxel tree, the execution time has a high fluctuation when the threshold is low.

## 2.2 Fixed Number of Proxels Pruning

The *fixed number of proxels pruning* is another simple strategy for keeping, as the name suggests, only a predefined number of proxels at the end of every timestep keeping the higher probability proxels and pruning the less likely ones. This property is the major advantage of the strategy, as it is very easy to parametrize and very robust against disturbances. However, the algorithm itself has some drawbacks.

The optimal proxel storage in case of the evaluation problem is a hash table [13], because due to the merging described in Section 1.3 one wants to retrieve proxels as efficiently as possible. The cost of it is the hash table's average search complexity,  $O(1)$ . However, a hash table cannot be sorted, so in order to perform the pruning, one needs to put all the proxels into a sorted array-like structure which is an additional overhead to the already complex sorting operation of  $O(n \log(n))$  [13].

Of course, one can perform some implementation tricks, like storing a pointer to the proxel in the proxel storage instead of the object itself, to speed up the moving and sorting operation significantly. But in the end, one still needs to perform the moving and sorting of the entries and with a potentially higher number of proxels to keep, these can become too expensive for the analysis. Similarly, not all tricks might be universally available in every programming language.

This strategy provides a simple single parameter customization and very predictable execution times, but it fails to scale the proxel tree, so one really needs to find the perfect parameter with this strategy before running a long-time analysis.

## 2.3 Variable Pruning

*Variable pruning* was introduced in [4] due to the limitations of the *fixed threshold pruning* in case of the decoding problem. It is basically combining the previously discussed pruning strategies by creating a relationship between the current number of proxels in the proxel tree and the pruning threshold.

This is done by defining a minimum number of proxels ( $r_{min}$ ) - pruning threshold ( $\#P_{min}$ ) pair, which prune the really unlikely proxels. Additionally, one selects a maximum number of proxels ( $r_{max}$ ) - pruning threshold ( $\#P_{max}$ ) pair to drastically prune the tree if the proxel tree becomes too large. The two points must be connected by a strictly monotonically increasing continuous function ( $r(\#P_{x,t_i})$ ) to guarantee a smooth transition between the two behaviors. The definition is shown in Equation 5:

$$r = \begin{cases} r_{min} & \text{if } \#P_{x,t_i} < \#P_{min} \\ r(\#P_{x,t_i}) & \text{if } \#P_{min} \leq \#P_{x,t_i} \leq \#P_{max} \\ r_{max} & \text{if } \#P_{x,t_i} > \#P_{max} \end{cases} \quad (5)$$

Even though the strategy is slightly more complex than the previous strategies due to the high factor of customization (different minimum and maximum pairs, different equations), it is a good trade-off between the advantages and disadvantages of the previous strategies. One can use overall much lower pruning thresholds while maintaining high throughput, lower risk of state space explosion and reducing the fluctuation of execution time compared to the *fixed threshold pruning*.

### 3 Experiments

In this section, the previously discussed properties of the different pruning strategies will be shown in an empirical way. First the experiment setup and the parametrization will be briefly discussed before describing the experiment results in details.

#### 3.1 Experiment Setup

A car rental service, presented in the introduction, was fed with the same input data as presented in [3] previously to make the result easily comparable.

A Personal Computer (PC) equipped with an AMD Ryzen 7 3800X and 64 GB of RAM has been used for the experiment execution. The RAM was sufficient to prevent swapping, which made the experiments performed easily comparable. The implementation code utilized the C++20 standard and it was compiled using GCC 11.4.0 with the highest optimization level enabled. The application was containerized using Docker. The PC was running Manjaro Linux with the kernel 6.1.69.

#### 3.2 Parameter Selection

The experiment has been run 1620 times for every given pruning strategy with a defined parametrization, which includes 162 different model parameters with 10 randomly generated traces each. These models include only stable models, further discussed in [5].

The different pruning strategies were parametrized based on different logic. The *fixed threshold pruning* strategy (abbreviated with „th” in the following figures) was tested with various thresholds in the range of  $[1e-1, 1e-150]$ . Similarly, a wide range of sizes between  $[50, 2500]$  were used to test the *fixed number of proxels pruning* strategy (abbreviated with „size” in the following figures). For the *variable pruning* (abbreviated with „var” in the following figures) five different equations were used, all with the minimum threshold ( $r_{min}$ ) of  $1e-300$  for proxel tree sizes below 1000 ( $\#P_{min}$ ), and a maximum threshold ( $r_{max}$ ) of 0.1 above proxel tree size of 100000 ( $\#P_{max}$ ). All equations describe a mapping between the pruning threshold and the logarithm of the current tree size. We are omitting the equations here due to space reasons.

Figure 3 visualizes the previous equations between the previously described minimum and maximum pairs to make them easier to follow for the reader. Please be aware that the x and the y axis are using logarithmic scale.

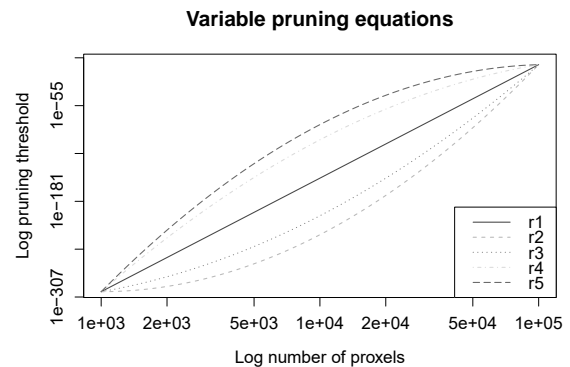


Figure 3: Variable pruning equations.

The different equations make it possible to scale the *variable pruning* with different „speed” between the minimum and maximum values. As the results in the next subsection will show, this was already enough to reach significantly different behavior.

### 3.3 Experiment Results

For easier representation, the experiment results were visualized in the Figures 4 - 6 in a unified way. Yellow background („th” on the X-axis) marks the *fixed threshold pruning* strategies with different thresholds in scientific notation. Green background („size” on the X-axis) marks the *fixed number of proxels pruning* strategies with different fixed proxel tree sizes, while blue background („var” on the X-axis) marks the *variable pruning* strategies with different equation IDs.

During the tests, we did not experience any state space explosions, even with extremely small pruning thresholds. This means that the merging efficiently eliminates this problem, however, this is not a proof that in case of a more complex model we would not experience any problems with the *fixed threshold pruning* strategy, as this is the most vulnerable strategy regarding state space explosions.

Figure 4 visualizes the performance criteria of the experiment. Here we see that the *fixed threshold pruning* needs to deal with an extreme uncertainty regarding the number of proxels with decreasing pruning threshold. This leads to a similar fluctuation/variation in the execution time. The *variable pruning* efficiently copes with this problem while using a significantly lower minimal threshold. The *fixed number of proxels pruning* maintains predictable and low execution times.

In case of the proxel processing efficiency (Figure 4, top right) the *variable pruning* and the *fixed threshold pruning* with lower thresholds outperform the *fixed number of proxels pruning* by about 25 – 30%. This results from the fact that sorting the proxel tree is an operation that is hard to parallelize.

The last graph in the Figure 4 visualizes the probability lost through pruning. Please be aware that the probabilities are visualized on a logarithmic scale. One would like to minimize that in order to get the possibly most complete analysis of the state space. However, the first steps in case of the analysis play a crucial role in this case, because the proxel probabilities are decreasing drastically over the analysis time domain. This means that the proxels pruned away first basically determine the amount of probability lost. As we can see in the picture, the *fixed number of proxels pruning* has a really high spread for these values.

This shows that it could potentially throw away important proxels. The *fixed threshold pruning* copes with the problem well at lower pruning thresholds.

The *variable pruning* provides the best values with somewhat higher spread than the *fixed threshold pruning*. This is the indicator of being a good trade-off between the two other techniques.

Evaluation tries to compute the probability that a given trace has been generated by a given model. Interestingly enough, most of the strategies provided the same result to that question as it can be seen in Figure 5. Only the *fixed threshold pruning* strategies with the thresholds  $1e-1$  and  $1e-2$  failed to reach the same results, but in these cases only 1 or 2 proxels survived the timesteps on average. In case of the fixed pruning threshold  $1e-10$ , which is the first test case that came to the common solution, on average about 35 proxels survived the timestep after pruning, so we expect that a *fixed number of proxels pruning* with values under 50 could have also reached this result.

Not being able to reach a better result by processing more proxels has to do with the fact that the proxel probabilities are represented on a logarithmic scale. At the end of the analysis a subset of proxels became dominant (they had significantly higher probabilities) over the remaining proxels. That part of the proxel tree computationally defined the results.

This means that there is a sweet spot in the computation and with an optimal number of proxels one is able to compute the end result of the analysis very efficiently. In our case this sweet spot is somewhere between 35 – 50 proxels. However, this cannot be stated universally, because more complex systems might have a higher optimal proxel number. Generally said, with a threshold based pruning strategy one can get to the optimum more easily than with the *fixed number of proxels pruning* strategy, because it is very hard to find the optimal number of proxels without performing multiple experiments.

Another important aspect is to keep enough proxels in the tree to support diversity and to prevent the proxel tree from dying out if something very unexpected happens, for example due to very strong pruning all the existing proxels become impossible in the next timestep. This quality can be visualized with the pruning ratio, so which amount of the proxels are kept on average after the pruning step. This can be seen in Figure 6.

Here we see that the strategies that failed to reach the common probability result have thrown away more than 50% of the proxels on average from timestep to timestep.

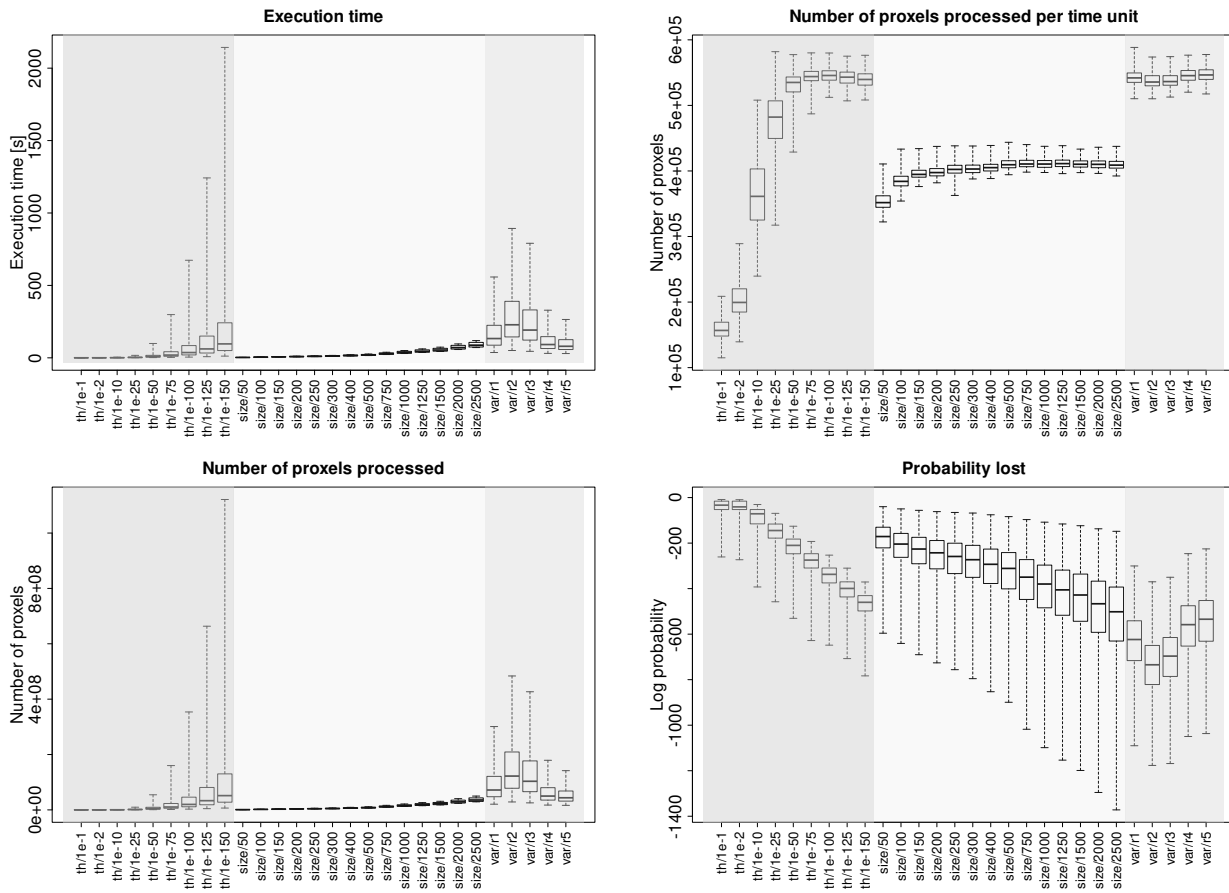


**Figure 4:** Quality Measures of Different Pruning Strategies.

Note: Yellow background („th” on the X-axis) marks the *fixed threshold pruning* strategies with different thresholds.  
 Green background („size” on the X-axis) marks the *fixed number of proixels pruning* strategies with different sizes.  
 Blue background („var” on the X-axis) marks the *variable pruning* strategies with different equations.

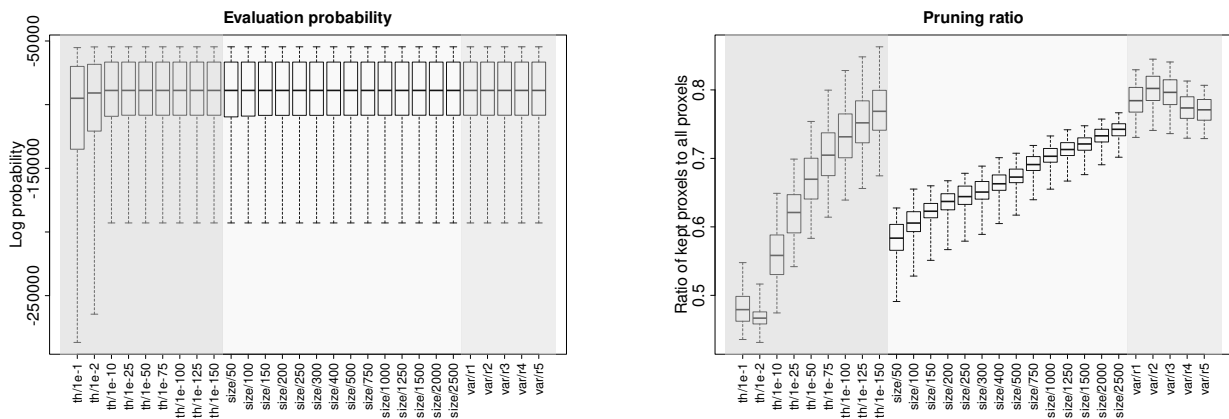


**Figure 5:** Probability of a given door protocol.

Note: Information about the colors and abbreviations can be found in the note below the caption of Figure 4.

**Figure 6:** Pruning rate with different prunings.

Note: Information about the colors and abbreviations can be found in the note below the caption of Figure 4.

Generally, this is caused by the relatively small number of proxels. Of course, with the increasing number of proxels the different strategies are keeping a higher amount of proxels. This generally means also higher fault tolerance toward very unlikely events in the proxel-based analysis and also indicates higher robustness for similar traces.

## 4 Discussion & Conclusion

The goal of this paper was to give a general overview of different pruning strategies for the evaluation problem and to compare their properties.

All three of the analyzed pruning strategies are suitable for the evaluation problem. Problems like state space explosion or dying out proxel trees are very unlikely, as merging keeps the proxel tree under control enabling the use of less strict pruning strategies compared to the decoding problem [3]. We have not encountered them during our experiments. This generally also shows that the pruning strategy has a smaller impact on the results in case of the evaluation problem, as long as they are parametrized in a reasonable way.

There is generally an optimum where the proxel-based analysis reaches the final evaluation result with a minimum number of proxels. However, finding this sweet spot is not trivial and it surely requires multiple test runs, which is not always possible in the real world.

In case of all three strategies the parameters need to be chosen carefully. But with a good rule of thumb solution like „one should keep at least 50 – 100 proxels on average, but one should aim for more” one should be on the safe side to get a good general solution with acceptable execution times. However, for more complex systems a higher number of proxels might be needed.

The *fixed number of proxels pruning* performs good enough to be a robust solution if one values highly predictable execution times over other properties. However, the proxel processing throughput might be a limiting factor. If the desired property of the analysis is to explore the state space as thoroughly as possible, one should use the *fixed threshold pruning* or tweak the *variable pruning* to speed up the execution time and get some additional advantages, like less lost probability, more diverse proxel tree, etc.

From a practical point of view there is no real limitation that would prevent the user from utilizing any of these pruning strategies in an experiment with artificial data or in real world use-cases.

## References

- [1] Krull C, Buchholz R, Horton G. Virtual Stochastic Sensors: How to gain insight into partially observable discrete stochastic systems. *The 30th IASTED International Conference on Modelling*. 2011.
- [2] Lazarova-Molnar S. *The Proxel-Based Method: Formalisation, Analysis and Applications*. Magdeburg: Otto-von-Guericke-Universität. 2005.
- [3] Bodnár D, Krull C. Comparing Different Pruning Strategies for the Decoding Task using Virtual Stochastic Sensors. In: *The European Simulation and Modelling Conference 2023*, eds Vingerhoeds R, de Saqui-Sannes P. Toulouse: EUROSIS-ETI. 2023; pp. 37–42.
- [4] Bodnár D, Krull C. Adapting to Change of Model Transitions in Proxel Based Simulation of CHnMMs. In: *Proceedings Langbeiträge ASIM SST 2022, 26. Symposium Simulationstechnik*, edited by Breitenecker F. Vienna: TU Wien. 2022; pp. 101–108.
- [5] Krull C. *Virtual Stochastic Sensors: Formal Background and Example Applications: Reconstructing the Behavior of Partially Observable Discrete and Hybrid Stochastic Systems*. Shaker. 2021.
- [6] Bobbio A, Puliafito A, Telek M, Trivedi KS. Recent Developments in Non-Markovian Stochastic Petri Nets. *Journal of Systems Circuits and Computers*. 1998; 8(1):119–158.
- [7] Wilson E. Virtual sensor technology for process optimization. 1997. Presentation at the ISSCAC 1997.
- [8] Buchholz R. *Conversive Hidden non-Markovian Models*. Magdeburg: Otto-von-Guericke-Univ. 2012.
- [9] Fink GA. *Markov Models for Pattern Recognition*. London: Springer London. 2014.
- [10] Krull C, Horton G. Hidden non-Markovian Models: Formalization and solution approaches. *6th Vienna Intern. Conference on Mathematical Modelling*. 2009.
- [11] Rabiner L. A tutorial on hidden Markov models and selected applications in speech recognition. *Proceedings of the IEEE*. 1989;77(2):257–286.
- [12] Viterbi A. Error Bounds for Convolutional Codes and an Asymptotically Optimum Decoding Algorithm. *Information Theory, IEEE Transactions on*. 1967; 13:260 – 269.
- [13] Skiena SS. *The Algorithm Design Manual*. Cham: Springer International Publishing. 2020.

**Publication Remark.** This contribution is the revised version of the conference version published in *Tagungsband Langbeiträge ASIM SST 2024*, ARGESIM Report AR 47, ISBN ebook: 978-3-903347- 65-6, p 113-120, DOI: 10.11128/arep.47.a4704

# Development of a Simulation Model for Predicting Energy Consumption of Battery-Electric Buses

Anja Konzept\*, Arne Hitz, Benedikt Reick

Institute for e-mobility, Ravensburg-Weingarten University of applied sciences, Doggenriedstraße 70, 88250 Weingarten, Germany; \*[anja.konzept@rwu.de](mailto:anja.konzept@rwu.de)

SNE 35(1), 2025, 49-53, DOI: 10.11128/sne.35.sn.10728  
 Selected ASIM SST 2024 Postconf. Publication: 2024-12-10  
 Received Revised: 2025-03-03; Accepted: 2025-03-05  
 SNE - Simulation Notes Europe, ARGESIM Publisher Vienna  
 ISSN Print 2305-9974, Online 2306-0271, [www.sne-journal.org](http://www.sne-journal.org)

**Abstract.** This paper presents the development of a simulation model for battery-electric public transportation buses aimed at accurately predicting energy consumption and state of charge with minimal input data. The model considers driving resistances, elevation profiles, temperatures, and load conditions to closely replicate real-world operational scenarios. Validation with data from a Swiss public transport company shows high accuracy in the prediction of energy consumption and state of charge. The model facilitates precise route and charging infrastructure planning, enhancing efficiency and optimizing costs for public transport operators.

## Introduction

In order to reduce CO<sub>2</sub> emissions at European level, as outlined in the Paris Agreement, the EU Climate and Energy Framework, and the White Paper on Transport, an increasing number of companies in the public transportation sector are transitioning from combustion engine buses to battery-electric buses.

This transition represents an important shift in the transportation sector [1, 2]. A significant challenge in this context is the variability in range depending on the driven route (elevation profile, rural track, urban track), temperature, and load [3].

To facilitate an effective transition to electromobility in public transport, it is important to consider the energy supply of the buses in advance [2].

To enable precise planning of the charging strategy (depot or opportunity charging) and the associated charging stations as well as network utilization, even

before the ordering of a new fleet, a simulation model of an electric bus is created as part of this publication. A challenge in this task is that the transport companies usually have limited technical data and information about the electric buses.

Thus, the planning of fleets size and charging stations is often done by assuming average consumption values determined in Standardized On Road Test cycles (SORT) [4, 5]. These data are often very inaccurate and do not reflect worst case scenarios or the exact local conditions (e.g. low environmental temperatures or elevations).

The aim of this work is to develop a bus model with few data that reflects as accurately as possible the consumption and state of charge (SoC) of a battery-electric bus, including powertrain data, heating, air conditioning, and auxiliary consumers for different route sections taking into account altitude data, outside temperature and load. This should enable precise mapping of route sections, schedules, and extreme scenarios. The model should also be easily adaptable to different bus types. In the following sections, the functions and individual components of the simulation model are described in more detail. Furthermore, the input parameters and the verification of the model are discussed, an outlook for improvements and further applications is given.

## 1 Model Overview

This section provides an overview of the simulation model. The structure and individual components are described in more detail. The first step in developing the model is to identify the available data and determine how detailed the model should be.

For the initial setup of the model, the MAN Lion's City 12 E low-floor bus is selected, as data for verification purposes are available from a battery-electric bus fleet that is already in operation.

The model is designed so it can be easily re-parameterized for other bus models through an initialization script. Due to the limited availability of technical data, electric drive train components such as the inverters are not physically simulated in detail, this also ensures fast computation times. Instead, an efficiency map based, purely longitudinal dynamic model was developed. Since the main focus is energy consumption, the longitudinal dynamics prove to be sufficiently accurate, as can be seen in the verification process.

Figure 1 provides an overview of the model. The model inputs are a speed profile over time, elevation profile over the distance traveled and average outside temperature. Due to the monitoring system, the fleet operators in this study have only access to sparsely sampled GPS positions (5.3 samples per minute) without altitude information. Consequently, these GPS points require a special preprocessing methodology to reconstruct the route data (including speed and road slope) to a sufficient sampling frequency of 1 Hz. The detailed methodology employed is described in [6].

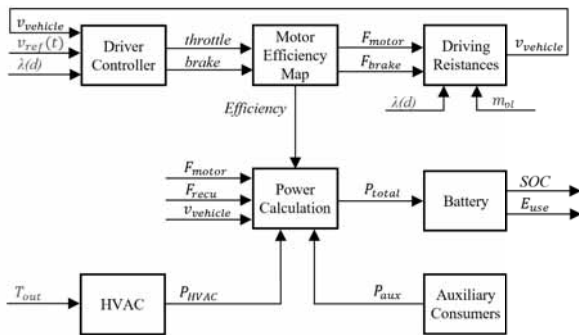


Figure 1: Simulation model overview.

As driver controller, the "Longitudinal Driver" component of the Simulink vehicle dynamics blockset is used as a PI controller [7]. This controls the vehicle speed and outputs throttle and brake pedal position. In the motor efficiency block, the current motor torque is then determined using the accelerator pedal position and the maximum possible torque for the current operating point. The maximum torque can be determined from a motor map using the motor speed calculated from the vehicle speed and the gear ratio. From the motor torque, the motor force  $F_{motor}$  that drives the vehicle is then calculated using tire radius and gear ratio. The recuperation force  $F_{recu}$  of the motor is also calculated in this way. For strong decelerations, an additional mechanical brake is used.

This results in the total braking force  $F_{brake}$ . Furthermore, the efficiency during driving and recuperation is determined using the motor map stored in a lookup table. As the specific motors installed in the MAN bus are not known, the map of an asynchronous electric motor with similar power data is used. Exemplary motor maps are available in publications e.g. [8, 9] or can be generated via simulation tools such as Matlab or Motor CAD. The driving resistances block uses  $F_{motor}$ , the total braking force  $F_{brake}$ , and the road gradient  $\lambda(d)$  as inputs. Here, all necessary driving resistances of the bus are calculated. These are rolling resistance  $F_{RW}$ , air resistance  $F_{RA}$ , gradient resistance  $F_{RC}$ , and inertia resistance  $F_{RI}$ . This results in the total driving resistance  $F_R$  calculated in equation 1 using the individual resistances from equation 2. [10]

$$F_R = F_{RW} + F_{RA} + F_{RC} + F_{RI} \quad (1)$$

$$\begin{aligned} F_{RW} &= m_{ges} * g * \mu \\ F_{RA} &= c_w * A * \frac{\rho_A}{2} * v^2 \\ F_{RC} &= m_{ges} * g * \sin(\lambda) \\ F_{RI} &= a_x * (e_i * m_{net} + m_{pl}) \end{aligned} \quad (2)$$

The result is the longitudinal vehicle velocity, which is fed back into the driver controller as  $v_{vehicle}$ . Since there are certain deviations between  $v_{ref}$  and  $v_{vehicle}$  due to the driver controller, the road gradient  $\lambda(d)$  is given over distance and not over time. This way, the actual distance traveled can be calculated by integrating the vehicle velocity, and the appropriate road gradient at that position can be used.

To map power and energy consumption of the vehicle, the power calculation block is introduced. The driving power is initially calculated from motor force ( $F_{motor}$ ), recuperated force ( $F_{recu}$ ), and vehicle velocity ( $v_{vehicle}$ ). Additionally, motor efficiency, determined from the efficiency map, is used to calculate the required driving power. For the gearbox and power electronics, a constant efficiency is assumed.

The consumption of the Heating-Ventilation Air Conditioning (HVAC) components also have a significant impact on the range of electrically operated buses. Consequently, the power of the heat pump is mapped depending on outside temperature via a lookup table [11].

Auxiliary consumers such as display boards, doors, and compressors are taken into account with a constant power consumption. The power of HVAC ( $P_{HVAC}$ ) and auxiliary consumers ( $P_{aux}$ ) are introduced into the power calculation block.

Thus, the total power ( $P_{total}$ ) can be determined by summing the power of the different components. By integrating  $P_{total}$ , it is also possible to determine the energy ( $E_{use}$ ) consumed for the driven cycle.

### 1.1 Battery Model

To be able to simulate the SOC of the vehicle, a battery model is added to the simulation model. Here, the table-based battery model from the Simscape library is used and populated with parameters from a nickel-manganese-cobalt battery cell, which was used in a previous work [12]. The cell has a maximum Open-circuit voltage (OCV) of 4.15 V ( $V_{ocv}$ ) and a capacity of 14.44 Ah ( $C_{nom}$ ).

In the battery model, the OCV is calculated as a function of the SoC and temperature. The internal resistance also depends on the SoC and temperature (T) [13]. Self-discharge and aging are initially neglected.

Only limited information is available about the battery installed in the MAN Lion's City, though it is known to be an 800 V system with 65 % of the 480 kWh battery capacity usable. Since the Simscape battery model is an electrical model, a current must be calculated from the previously determined total vehicle power ( $P_{total}$ ). This is done using equation 3.

$$I_{bat} = \frac{P_{total}}{U_{bat}} \quad (3)$$

Here  $P_{total}$  is the total power of all consumers determined in the power calculation block.  $U_{bat}$  is the battery voltage measured at the battery model and delayed by one time step. This approximates the battery current. A controlled current source is then used to charge or discharge the battery model. The SoC of the battery is then calculated in the Simscape block using equation 4.

$$SoC(t) = SoC(t=0) - \frac{1}{C_{nom}(T)} \int_0^t (I_{bat}(t)) dt \quad (4)$$

This enables simulation of any route sections and calculation of energy consumption as well as battery SoC.

### 1.2 Verification

To verify the functionality and parameterization of the model, precise data must be collected. For this purpose, data is provided by the Swiss transport company "Verkehrsbetriebe Zürich" which is already operating numerous electric buses and has a detailed monitoring system.

The data used for verification are GPS position, vehicle speed, elevation profile, outside temperature, power of the heatpump, power of the powertrain, energy of auxiliary consumers and the SoC. With this data, the exact consumption, divided into drivetrain (driving and recuperation), heat pump depending on the route and auxiliary consumers can be determined. The same routes are also simulated with the longitudinal bus model.

A comparison between the consumption for driving, recuperation, air conditioning, and auxiliary consumers, as well as the SoC is made. Since the available test data was collected in winter, the installed diesel heater was often recorded as active (activated at temperatures below 7 °C). The energy consumed by the heatpump is therefore very low.

Further verification of the HVAC modeling for other seasons is planned. Figure 2 shows the SoC progression of the real vehicle compared to the SoC progression of the simulation model. For this comparison, the speed recorded by the monitoring system is used as the input for the simulation model. Additionally, the altitude data is used to determine the incline over distance and also serves as input. The environmental temperature is also taken into account in the simulation. Here it can be seen that the two SOC curves show only small deviations.

As route input, a round trip of 44 km length until a charger is approached is used. To quantify the differences, the maximum deviation and the Mean Squared Error (MSE) is calculated. The maximum deviation between the two SoC curves is 1.4469%. The calculated MSE is 0.31737, which indicates a high level of concordance between the two datasets.

Table 1 presents the energy consumption of the buses main consumers on the same 44 km round trip as in figure 2, broken down by drivetrain, HVAC and auxiliary consumers. This data also demonstrates that the energy consumption per component in the simulation model corresponds to the real-world data.

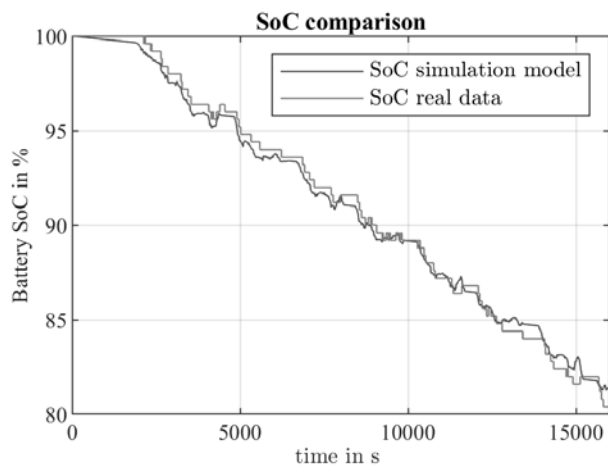


**Figure 2:** State of charge of the battery model compared to real vehicle data driving the same route.

	$E_{\text{drivetrain}}$	$E_{\text{HVAC}}$	$E_{\text{aux}}$
<b>Real data</b>	57.07 kWh	0.84 kWh	11.98 kWh
<b>Simulation</b>	57.56 kWh	0 kWh	11.34 kWh

**Table 1:** Energy consumption by component for simulation and real data.

## 2 Discussion

In this paper, a simulation model for a battery-electric bus is presented. This model is capable of accurately predicting energy consumption and state of charge with minimal input data. By considering driving resistances, elevation profiles, temperatures, velocity and various load conditions, a model is created which accurately represents a real electric bus. The validation of the model with data from a Swiss public transport company demonstrates high accuracy, highlighting the model’s relevance and reliability, although only a minimal set of parameters are available.

The model enables public transport operators to precisely plan their bus routes, battery sizing and charging infrastructure before electrifying their fleets. This not only enhances efficiency but also optimizes costs and relieves the power grid. Additionally, the model allows for the simulation of extreme scenarios, such as full load at cold temperatures, which would not be possible with average consumption values.

In the future, the model is to be extended and includes battery aging, enabling better assessment of long-term performance.

This will determine whether an old bus is still capable of covering all routes with the available charging points. Furthermore, additional parameter files for other buses should follow. Moreover, adding a more intelligent controller that can map different driver types is conceivable. Integrating different driving styles is a valuable addition to simulate the impact of driving behavior on energy consumption.

Overall, this battery-electric bus model represents a powerful tool for planning and optimizing electric bus fleets, supporting the sustainable transformation of public transport, as the application in the project FreeE-Bus funded by Interreg Alpenrhein-Bodensee-Hochrhein shows.

## References

- [1] Bundesministerium für Digitales und Verkehr. *Gesetzeskarte Elektromobilität im ÖPNV*. Berlin; 2022.
- [2] Statista. *Anzahl der elektrifizierten Busse im öffentlichen Personennahverkehr in Deutschland nach Antriebsart von 2019 bis 2022*. retrieved: 05.28.2024, <https://de.statista.com/statistik/daten/studie/1048269/umfrage/anzahl-der-elektrobuse-in-deutschland-nach-antriebsart/>
- [3] Zank P, Heining P. *VDE Renewables GmbH: Elektrifizierung von KMU-Busunternehmen*. Alzenau; 2023.
- [4] Seeliger A, et al. *Elektrobuse im ÖPNV - Eine technisch/wirtschaftliche Analyse unter Berücksichtigung praktischer Anwendungsbeispiele*. Hochschule Niederrhein, Krefeld; 2016.
- [5] Jahic A, et al. *Energy Consumption of Battery-Electric Buses: Review of Influential Parameters and Modelling Approaches*. B&H Electr. Eng.; 2023. doi: 10.2478/bhee-2023-0007.
- [6] Hitz A, Konzept A, Reick B, Rheinberger K (in press). *Efficient GPS route matching method for battery electric bus fleets*. SAE Technical Paper; 2024.
- [7] Mathworks. *Longitudinal Driver*; retrieved: 05.28.2024, <https://de.mathworks.com/help/autoblks/ref/longitudinaldriver.html>
- [8] Hayes G. J, Goodarzi A. G. *Electric Powertrain: Energy Systems, Power Electronics and Drives for Hybrid, Electric and Fuel Cell Vehicles*. John Wiley & Sons Ltd; 2017. doi: 10.1002/9781119063681.
- [9] Winzer P, Doppelbauer M. *Berechnung von Wirkungsgradkennfeldern von Asynchronmaschinen mit Hilfe der Finite-Elemente-Methode*. Karlsruhe Institute of Technology (KIT); 2013.

- [10] Mitschke M, Wallentowitz H. *Dynamik der kraftfahrzeuge*. Springer Vieweg Wiesbaden; 2014. doi: 10.1007/978-3-658-05068-9.
- [11] Heß L, et al. *Analysis of the Specific Energy Consumption of Battery-Driven Electrical Buses for Heating and Cooling in Dependence on the Technical Equipment and Operating Conditions*. World Electric Vehicle Journal; 2023. doi:10.3390/wevj14050126.
- [12] Konzept A, Reick B, Pintaric I, Osorio C. *HIL based Real-Time Co-Simulation for BEV Fault Injection Testing*. SAE Technical Paper; 2023. doi: 10.4271/2023-24-0181.
- [13] Mathworks, *Battery(Table-Based)*; retrieved: 05.28.2024, <https://de.mathworks.com/help/sps/ref/batterytablebased.html>

## Appendix

A	Cross sectional area
$a_x$	Acceleration in x direction
$C_{nom}$	Nominal battery capacity
CO <sub>2</sub>	carbon dioxide
cw	Drag coefficient
$E_{aux}$	Energy consumption of auxiliary consumers
$E_{drivetrain}$	Energy consumption of drivetrain
$E_{HVAC}$	Energy consumption of HVAC components
$e_i$	Moment of inertia addition-factor
$E_{use}$	Energy consumption total
$F_{brake}$	Brake force
$F_{motor}$	Motor Force
$F_R$	Total driving resistance
$F_{RA}$	Aerodynamic drag
$F_{RC}$	Climbing resistance
$F_{recu}$	Recuperation force
$F_{RI}$	Inertial resistance
$F_{RW}$	Wheel resistance
$I_{bat}$	Battery current
$m_{ges}$	Total vehicle mass with load
$m_{net}$	Vehicle mass without load
$m_{pl}$	Mass of load
MSE	Mean Squared Error
OCV	Open circuit voltage
$P_{aux}$	Power auxiliary consumers
$P_{HVAC}$	Power Heating-Ventilation, Air Conditioning
$P_{total}$	Total power
SoC	State of Charge
SORT	Standardized On Road Test cycle
$T_{out}$	Environmental Temperature
$U_{bat}$	Battery voltage
$v_{vehicle}$	Vehicle longitudinal velocity
$v_{ref}$	Reference velocity
$\lambda(d)$	Road gradient as a function of distance
$\rho_A$	Air density

**Publication Remark.** This contribution is the revised version of the conference version published in *Tagungsband Langbeiträge ASIM SST 2024*, ARGESIM Report AR 47, ISBN ebook: 978-3-903347- 65-6, p 137-141, DOI: 10.11128/arep.47.a4737



# Data-adaptive Dynamic Simulation via Structured Dynamic Mode Decomposition

Christopher Bonenberger<sup>1,2\*</sup>, Stephan Scholz<sup>1,2</sup>, Nico Scheiter<sup>1</sup>

<sup>1</sup>Ravensburg-Weingarten University of Applied Sciences (RWU), 88250 Weingarten, Germany

<sup>2</sup>Ulm University, 89081 Ulm, Germany; \*[bonenbch@rwu.de](mailto:bonenbch@rwu.de)

SNE 35(1), 2025, 55-59, DOI: 10.11128/sne.35.sn.10729  
 Selected ASIM SST 2024 Postconf. Publication: 2024-12-10  
 Received Revised: 2025-03-03; Accepted: 2025-03-05  
 SNE - Simulation Notes Europe, ARGESIM Publisher Vienna  
 ISSN Print 2305-9974, Online 2306-0271, [www.sne-journal.org](http://www.sne-journal.org)

**Abstract.** We consider the task of system identification and simulation via Dynamic Mode Decomposition (DMD) and physics-informed DMD for a simple heat conduction problem. In this regard, we consider the trade-off between data-driven and model-based simulation at the example of the one-dimensional heat equation. Thereby, we highlight the similarities between *dynamic simulation* and *data-driven modeling*. More precisely, we show how *physics-informed DMD* can be used to learn a data-adaptive finite-difference model and how this relates to the inherent limitations of finite-difference simulation.

## Introduction

In recent years the scientific community has witnessed remarkable progress in data-driven modeling based on different machine learning (ML) models. However, the universality and effectiveness of these models—most often *Deep Learning* (DL) models—usually comes at the price of explainability and the need for large data sets. Scientific machine learning (SciML) tackles these issues by task-specific modifications of classical ML algorithms (e.g. incorporating prior knowledge leads to *domain-aware* or *physics-guided ML*). These techniques allow to utilize information provided through available data while leveraging prior knowledge about the system at hand.

This ideally results in interpretable and robust models, which are able to incorporate physical laws and allow for effective use of data.

In the following we consider simulation (and model design in particular) at the intersection of data-driven and model-driven approaches.

Based on the prominent example of heat conduction (e.g. [1], p. 475) we use several types of Dynamic Mode Decomposition (DMD, [2]) that implement different levels of *informedness* up to a data-adaptive method that basically implements a finite-difference model as known from dynamic simulation (e.g. [3]).

The resulting scenario allows an almost seamless transition of decided system modeling to data-adaptive system identification. In this setting, we show how well-known results from numerical analysis and computer simulation can help to understand and improve the use of ML techniques.

## 1 Methods

In the following we briefly review the required methodologies. For the sake of brevity a detailed consideration of basic DMD, physics-informed DMD and finite-difference methods is foregone. Instead reference is made to [2], [1], [4] and [3] respectively.

### 1.1 DMD, Physics-informed & Structured DMD

In short, *basic DMD* is concerned with data-driven estimation of a linear operator that approximates the dynamics of a system at hand.

More precisely, assume we are given data  $\mathbf{X} \in \mathbb{R}^{N \times T}$  consisting of  $T$  observations  $\mathbf{x}_t \in \mathbb{R}^N$  that are equidistantly sampled in time.

The system dynamics that map  $\mathbf{x}_t$  to  $\mathbf{x}_{t+1}$  may now be approximated by solving the optimization problem

$$\min_{\mathbf{A} \in \mathbb{R}^{N \times N}} \left\{ \sum_{t=1}^{T-1} \|\mathbf{x}_{t+1} - \mathbf{A}\mathbf{x}_t\|_2^2 \right\}. \quad (1)$$

The goal function may be rewritten as  $\|\mathbf{X}_2 - \mathbf{A}\mathbf{X}_1\|_F$ , where  $\mathbf{X}_1, \mathbf{X}_2 \in \mathbb{R}^{N \times T-1}$  hold the first and last  $T-1$  columns of  $\mathbf{X}$  respectively and  $\|\cdot\|_F$  denotes the Frobenius norm.

Now the direct least-squares solution may be written in terms of the pseudo-inverse  $\mathbf{X}_1^\dagger = \mathbf{V}\Sigma^\dagger\mathbf{U}^\top$  using the Singular Value Decomposition (SVD)  $\mathbf{X}_1 = \mathbf{U}\Sigma\mathbf{V}^\top$  (e.g. [2]).

Typically, a low-rank approximation  $\mathbf{A}_r$  of  $\mathbf{A}$  is found by projection onto the leading left singular vectors, which amounts to  $\mathbf{A}_r = \mathbf{U}_r\mathbf{A}\mathbf{U}_r$ . In this regard the columns of  $\Psi = \mathbf{U}\Phi$ , where  $\Phi$  are eigenvectors  $\mathbf{A}_r\Phi = \Phi\Lambda_r$ , are referred to as *dynamic modes*.<sup>1</sup> With regard to the choice of  $r$  we follow [5].

Now, *physics-informed DMD* (piDMD, see [4]) is a regularized form of basic DMD. In short, we solve Eq. (1) subordinate to certain constraints on  $\mathbf{A}$ , which implement prior knowledge about the system at hand. As an example, constraining  $\mathbf{A}$  to be unitary implements a conservative system.

In the following, we will make use of piDMD for *spatially local* systems, i.e. we constrain  $\mathbf{A}$  to be a banded matrix in order to model local dependencies of diffusive systems (cf. [4]).

Finally, we make use of *structured DMD* (sDMD, see [6]), which sort of regularizes basic DMD by writing  $\mathbf{A}$  in terms of  $Q$  elementary matrices  $\mathbf{S}_q$  and seeking an associated coefficient vector  $\mathbf{a} \in \mathbb{R}^q$ , i.e.

$$\min_{\mathbf{a} \in \mathbb{R}^q} \left\{ \sum_{t=1}^{T-1} \left\| \mathbf{x}_{t+1} - \left( \sum_{q=1}^Q a_q \mathbf{S}_q \right) \mathbf{x}_t \right\|_2^2 \right\}.$$

This amounts to solving the linear system  $\mathbf{Z}\mathbf{a} = \mathbf{c}$  with

$$[\mathbf{Z}]_{i,j} = \sum_{t=1}^{T-1} \mathbf{x}_t^\top \mathbf{S}_j^\top \mathbf{S}_i \mathbf{x}_t \text{ and } [\mathbf{c}]_i = \sum_{t=1}^{T-1} \mathbf{x}_t^\top \mathbf{S}_i^\top \mathbf{x}_{t+1} \quad (2)$$

with  $\mathbf{Z} \in \mathbb{R}^{Q \times Q}$  (see [6]). By choosing appropriate elementary matrices  $\mathbf{S}_q$ , sDMD can be used to incorporate prior knowledge, e.g. choosing Toeplitz matrices  $\mathbf{S}_q$  leads to a spatially shift-invariant system. In fact, this formalism is based on ideas from shift-invariant time-series analysis.

A broader view on “structured” learning in different contexts is provided in [7]. Here, we use this formalism in order to realize data-adaptive system identification based on the finite-difference methods.

<sup>1</sup>In general, approximating system dynamics by a linear operator is tied Koopman operator theory, which allows to trade nonlinear finite-dimensional systems for infinite-dimensional linear systems (provided an appropriate *observable function*). However, in this work we are dealing with linear systems only.

## 1.2 Diffusive Systems, Solutions & Simulation

We consider a simple one-dimensional insulated diffusive system, namely heat conduction on a bar of length  $L$ . This implies Neumann boundaries, i.e.  $x'(t,0) = x'(t,L) = 0$ , for the diffusion equation

$$\frac{\partial x(t,s)}{\partial t} = \alpha \frac{\partial^2 x(t,s)}{\partial s^2} \quad s \in [0,L], t > 0, \quad (3)$$

where  $x(t,s)$  denotes the temperature at point  $s$  and time  $t$  and  $\alpha \in \mathbb{R}^+$  is the *diffusivity constant*. The analytical solution is found from the convolution integral  $g(t,s) * x(0,s) = x(t,s)$ , where  $x(0,s)$  denotes the initial distribution and  $g(t,s)$  denotes a Gaussian distribution (e.g. [1], p. 475 et seqq.). The spatial convolution amounts to pointwise multiplication in frequency domain and considering the boundary conditions yields

$$x(t,s) = \sum_{\gamma=0}^{\infty} \hat{c}_\gamma \exp\left(-4\alpha t \left(\frac{\pi\gamma}{2L}\right)^2\right) \cos\left(\frac{2\pi\gamma s}{2L}\right), \quad (4)$$

where  $\hat{c}_\gamma$  denotes the cosine Fourier series coefficients<sup>2</sup> of the initial distribution  $x(0,s)$ .

Beneath the analytical solution we consider numerical solutions to Eq. (3) based on finite differences (e.g. [3], p. 179). A one dimensional centered space finite difference scheme can be written as

$$\mathbf{x}_{k+1} = \frac{\alpha\Delta t}{(\Delta s)^2} \mathbf{D}\mathbf{x}_k + \mathbf{x}_k, \quad k \in \mathbb{N}, \quad (5)$$

where  $\mathbf{x}_k := \mathbf{x}((k+1)\Delta t)$ ,  $\Delta t$  and  $\Delta s$  denote temporal and spatial sampling intervals and  $\mathbf{D}$  is a tridiagonal matrix that is *almost* Toeplitz (except for the boundaries terms), i.e.

$$\mathbf{D} = \begin{bmatrix} -2 & 2 & 0 & \dots & 0 \\ 1 & -2 & 1 & 0 & \dots & 0 \\ & & & \ddots & & \\ 0 & \dots & 0 & 1 & -2 & 1 \\ 0 & \dots & & 0 & 2 & -2 \end{bmatrix} \in \mathbb{R}^{N \times N}. \quad (6)$$

Thereby the condition on stability is (cf. [3], p. 181)

$$C = \frac{2\alpha\Delta t}{(\Delta s)^2} \leq 1 \text{ or rather } \Delta t \leq \frac{(\Delta s)^2}{2\alpha}. \quad (7)$$

<sup>2</sup> $x(0,s)$  can be expressed by such a series via symmetric extension, leading to  $2L$  instead of  $L$  in the denominators of Eq. (4).

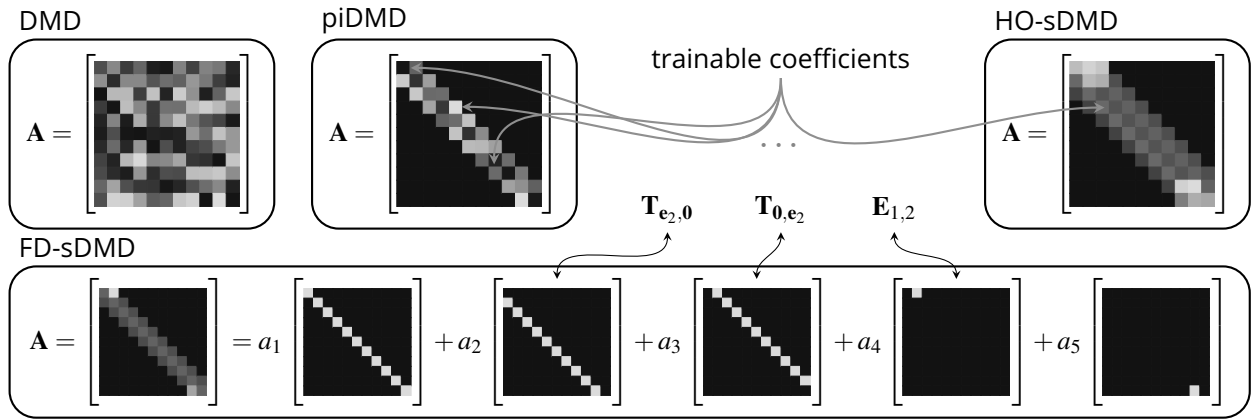


**Figure 1:** An overview about the different variants of DMD and coefficients that are trained (with  $N = 11$ ). In the matrices  $\mathbf{A}$  each color represents a different trainable coefficient. For FD-sDMD the sum of elementary matrices is explicitly shown.

### 1.3 piDMD and sDMD for Diffusive Systems

In the context diffusive systems as described above, it is reasonable to use piDMD for spatially local systems (cf. [4]). In respect of Eq. (5), particularly the matrix  $\mathbf{D}$ , we impose tri-diagonality constraints on  $\mathbf{A}$ . A solution to this kind of piDMD is provided in [4], p. 15.

A more specific modeling is possible via sDMD. Here, we focus on the following three different variants.

**FD-sDMD** Let  $\mathbf{T}_{\mathbf{c},\mathbf{r}} \in \mathbb{R}^{N \times N}$  denote a quadratic Toeplitz matrix defined by the vectors  $\mathbf{c}, \mathbf{r} \in \mathbb{R}^N$ , its first column and row respectively (necessarily their first components are equal, i.e.  $[\mathbf{c}]_1 = [\mathbf{r}]_1$ ).

Moreover, let  $\mathbf{E}_{i,j} \in \mathbb{R}^{N \times N}$  denote a zero matrix with a single component in row  $i$  and column  $j$  being one, i.e.  $[\mathbf{E}_{i,j}]_{i,j} = 1$ . Finally,  $\mathbf{I}$  is the identity matrix and  $\mathbf{e}_k$  denotes its  $k$ -th column.

Now, we may express the structure of Eq. (5) via sDMD in terms of the elementary matrices

$$\mathbf{S}_1 = \mathbf{I}, \mathbf{S}_2 = \mathbf{T}_{\mathbf{e}_2, \mathbf{0}}, \mathbf{S}_3 = \mathbf{T}_{\mathbf{0}, \mathbf{e}_2}, \mathbf{S}_4 = \mathbf{E}_{1,2}, \mathbf{S}_5 = \mathbf{E}_{N,N-1}.$$

In this setting, sDMD yields an adaptive finite-difference model and that also learns boundary conditions from data (FD-sDMD, see Fig. 1).

**PE-sDMD.** On top of sDMD one might incorporate more prior knowledge about the discretized system  $\mathbf{D}$  (this implies knowledge about the boundary conditions).

In this case sDMD reduces to parameter estimation (PE-sDMD), since we solely consider a single structure matrix  $\mathbf{S}_1 = \mathbf{D}$  (cf. Eq. (6)). More precisely, in consideration of Eq. (5) we solve

$$\min_{a_1 \in \mathbb{R}} \left\{ \sum_{t=1}^{T-1} \|\mathbf{x}_{t+1} - a_1 \mathbf{S}_1 \mathbf{x}_t - \mathbf{x}_t\|_2^2 \right\},$$

such that  $a_1 = \sum_t \mathbf{x}_t^T \mathbf{S}_1^T (\mathbf{x}_{t+1} - \mathbf{x}_t) / \sum_t \mathbf{x}_t^T \mathbf{S}_1^T \mathbf{S}_1 \mathbf{x}_t$  (cf. Eq. (2)) and  $\mathbf{A} = a_1 \mathbf{S}_1 + \mathbf{I}$ .

**HO-sDMD.** In contrast to the refinement of FD-sDMD to PE-sDMD, we might also be interested in more flexible structures. As there are countless possibilities, it is reasonable to follow familiar models. Here we consider a structure that loosely resembles a higher-order finite difference scheme (HO-sDMD) via

$$\mathbf{S}_1 = \mathbf{I}, \mathbf{S}_2 = \mathbf{T}_{\mathbf{e}_2, \mathbf{0}}, \mathbf{S}_3 = \mathbf{T}_{\mathbf{0}, \mathbf{e}_2}, \mathbf{S}_4 = \mathbf{T}_{\mathbf{e}_3, \mathbf{0}}, \mathbf{S}_5 = \mathbf{T}_{\mathbf{0}, \mathbf{e}_3}$$

and  $\mathbf{S}_6, \dots, \mathbf{S}_{15}$  being matrices  $\mathbf{E}_{i,j}$  that dissolve the Toeplitz structure at the boundaries. Visualizations of the structures resulting from DMD, piDMD and the different variants of sDMD are provided in Fig. 1.

## 2 Experiments & Discussion

Now, we present some results of a detailed comparison of the aforementioned variants of DMD and finite-difference simulation at the example of flow prediction for a simple diffusive system.

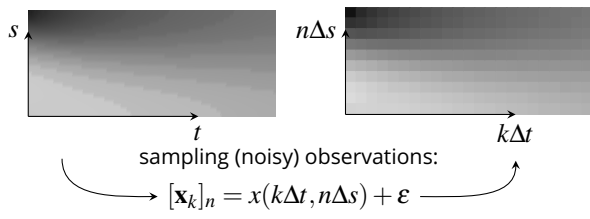


**Figure 2:** Analytical solution of a 1D heat conduction problem (left panel) and sampled data with  $N = 11$  and  $\Delta t \approx 0.043\text{s}$  such that  $C = 1$ . The measurement noise is modeled via additive Gaussian noise, i.e.  $\epsilon \sim \mathcal{N}(0, \sigma^2)$  (by default  $\sigma^2 = 0.005$ ).

The special aspect of this setup is our ability to bring together these two different paradigms in a novel way, i.e. we are able to *interpolate* between data-driven and model-driven simulation.<sup>3</sup>

**Experimental Setup.** We consider the problem of heat conduction at the example of a unit length copper rod, i.e. we fix  $L = 1\text{m}$  and set  $\alpha$  based on the specific thermal capacity, thermal conductance and density of copper ( $\alpha \approx 0.1\text{m}^2\text{s}^{-1}$ ).

Moreover, we consider the time interval  $t \in [0, 1]$ . For all following numerical evaluations the initial (heat) distribution is described by a second order polynomial with random coefficients, i.e.

$$x(0, s) = p_0 + p_1s + p_2s^2, \quad p_0, p_1, p_2 \sim \mathcal{N}(0, 1),$$

where  $\mathcal{N}(0, 1)$  denotes a zero mean and unit variance normal distribution. Exemplary spatiotemporal data is shown in Fig. 2. The analytical solution is computed according to Section 1.2 using the discrete Fourier transform to approximate the coefficients of the initial distribution.

Discrete data is generated by equidistant sampling of the analytical solution at  $N$  points in space. Temporal sampling is bound to Eq. (7) and we consider different stability settings by adjusting  $C$  (cf. Fig. 3). As indicated in Fig. 2 the sampling process is combined with additive noise.

As usual for data-adaptive algorithms, we perform a train-test split, i.e. given  $T$  observations  $\mathbf{x}_t \in \mathbb{R}^N$  a fraction of  $\lceil RT \rceil$  observations is used for training and remaining data is used to evaluate performance. We measure the average relative prediction error over all test samples. Simulation-based predictions use the last available training sample.

**Results.** The different graphs in Fig. 3 show relative prediction errors for varying train-test ratio, noise level and sampling respectively. The top graph shows that model-driven prediction is clearly superior to data-driven models although the latter improve with increasing train-test ratio  $R$ .

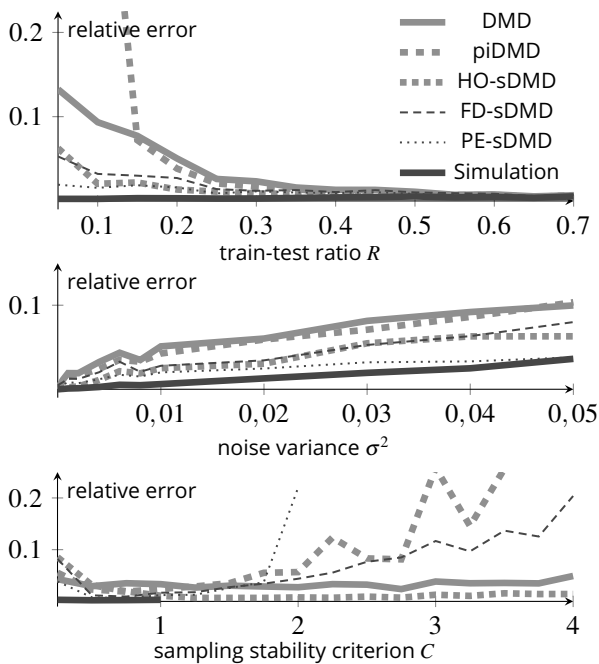


**Figure 3:** Relative prediction error—the median of 100 runs—for different parameter sweeps. Missing values indicate numerical instability. By default we use  $C = 1, \sigma^2 = 0.005$  and  $R = 0.25$  (with  $N = 21$ ).

<sup>3</sup>Code is available under <https://github.com/cmab92/ASIM2024-DD-MD-DMD>.

The middle panel indicates that model-building also pays off in the presence of noise and again more structure increases performance. Finally, the results in the lower panel allow to draw the conclusion that especially the compromise between data-driven and model-driven solutions can be very effective.

Notably FD-sDMD is quite robust against a violation of the stability condition.

**Outlook.** Our results are a first attempt to “simulation-informed DMD”. We have shown at a simple example, that DMD and piDMD can be improved by incorporating techniques that are typically used in dynamic simulation.

The results are promising and we believe that a similar approach can be used for different ML algorithms. However, future work should focus on an evaluation of the proposed technique in more complex real-world applications.

**Publication Remark.** This contribution is the revised version of the conference version published in *Tagungsband Kurzbeiträge ASIM SST 2024*, ARGESIM Report AR 46, ISBN ebook: 978-3-903347-64-9, DOI: 10.11128/arep.46 (volume DOI), p 41-44.

## References

- [1] Bracewell R. *The Fourier transform and its applications*, vol. 3. McGraw-Hill. 2000.
- [2] Schmid PJ. Dynamic mode decomposition and its variants. *Annual Review of Fluid Mechanics*. 2022;54:225–254.
- [3] Özişik MN, Orlande HR, Colaço MJ, Cotta RM. *Finite difference methods in heat transfer*. CRC press. 2017.
- [4] Baddoo PJ, Herrmann B, McKeon BJ, Nathan Kutz J, Brunton SL. Physics-informed dynamic mode decomposition. *Proceedings of the Royal Society A*. 2023; 479(2271):20220576.
- [5] Gavish M, Donoho DL. The optimal hard threshold for singular values is  $4/\sqrt{3}$ . *IEEE Transactions on Information Theory*. 2014;60(8):5040–5053.
- [6] Bonenberg C, Scholz S, Schneider M. From Data-Driven to Model-Driven Learning via Structured Dynamic Mode Decomposition. In: *2024 IEEE 63rd Conference on Decision and Control (CDC)*. 2024; pp. 2144–2149.
- [7] Bonenberg C. Time series analysis via maximum variance frames. Universität Ulm. 2025.



# Towards Imaginative Robots: A Generative Pipeline for Simulated Environments

Christopher May\*, Lorenz Suchy, Jörg Franke, Sebastian Reitelshöfer

Institute for Factory Automation and Production Systems (FAPS), Friedrich-Alexander-Universität Erlangen – Nürnberg, Egerlandstr. 7-9, 91058 Erlangen, Germany; \*[christopher.may@faps.fau.de](mailto:christopher.may@faps.fau.de)

SNE 35(1), 2025, 61-70, DOI: 10.11128/sne.35.tn.10720  
Selected ASIM SST 2024 Postconf. Publication: 2024-12-10  
Received Improved: 2025-03-07; Accepted: 2025-03-09  
SNE - Simulation Notes Europe, ARGESIM Publisher Vienna  
ISSN Print 2305-9974, Online 2306-0271, [www.sne-journal.org](http://www.sne-journal.org)

**Abstract.** Autonomous Mobile Systems (AMS) offer significant advantages for industry and private sectors by adapting to diverse and dynamic environments. To train these systems, large amounts of data are required, typically obtained from simulated environments. However, the creation of these environments is often labor-intensive. Here, we propose a generative pipeline that provides a streamlined approach to virtual training and testing while allowing users to apply automated methods including generative AI.

Our pipeline consists of four, partly iterative main steps. The pipeline spans from the creation of individual assets to the utilization of the simulated environments. The pipeline is then implemented for an exemplary scenario, utilizing multiple methods including generative AI.

Furthermore, we propose a novel application of our pipeline to provide robots with the capabilities to “imagine” virtual experiences based on anticipated tasks.

The presented pipeline not only simplifies the process of generating simulated environments, but also resembles a scalable framework for developing increasingly complex AMS.

## Introduction

Mobile robots, and in particular Autonomous Mobile Systems (AMS), are transforming the world. While transport robots are already well-established in industry, they have not yet reached their peak. In the coming years companies will expand their fleets and applications with new systems, increasingly powered by AI. [1]

Developing and training AI models requires massive amounts of data to ensure performance in the demanding, large, dynamic, and diverse operating environments of AMS. One solution to reduce the effort associated with collection and annotation of the required data is simulation. In simulated environments, the possibilities to generate synthetic data are virtually unlimited. However, generating data for all kinds of imaginable scenarios, is still related with large human efforts. Recent breakthroughs in generative AI could enable developers of AMS to reduce the needed effort while improving the quality of synthetic data from robotics simulation.

Most of the existing work on the generation of simulated robot training environments focuses on reinforcement learning in small manipulation scenarios [2, 3]. Those do not lie within the scope of our work. One notable exception has been presented by Bonetto et al. Their approach focuses on “Generating Realistic Animated Dynamic Environments for Robotics Research”, abbreviated “GRADE” [4]. GRADE requires an existing set of assets. Bonetto et al. have, among others, proven that synthetic data from simulated environments can be sufficient to train and validate vision-based robots [5, 6]. Another related approach that utilizes generative AI has been presented in the position paper “Towards Generalist Robots: A Promising Paradigm via Generative Simulation” [7]. Their related work “RoboGen” [3] focuses on motion planning for stationary robots. Xian et al. define the term ‘generative simulation’. Their concept is supposed to generate scenes with accompanying robot tasks and at the same time include training supervision. Although the authors discuss multiple ideas and claim to be able to generate infinite data for various robots in various environments, at the time of writing this paper, the work of Xian et al. remains primarily a literature review without actual implementation. While an interesting physics simulator, GENESIS is currently missing the promised aspects of ‘generative simulation’. [8]

In this paper, we first identify methods that are relevant in the context of simulated environments for AMS. We then present a generative pipeline for the creation of simulated environments for AMS. The pipeline consists of four main steps, which are partially iterative. In this modular approach, different methods can be employed in different steps of the pipeline. This applies to both conventional methods and generative AI-methods. We furthermore present an exemplary implementation of our pipeline that utilizes several of the methods discussed to create simulated environments, fully populated with AI-generated assets. Finally, we introduce the concept of *imaginative robots* and propose the application of our pipeline to enable robots to prepare for new and unknown situations autonomously.

## 1 Methods for the Creation of Simulated Environments

Before defining a pipeline for creating simulated environments, it is important to clarify the relevant methods. We identify four general methods that are relevant to simulated operating environments. These methods can incorporate existing models, databases, etc. Although these methods can be used in conjunction with each other, for the purpose of this discussion, we treat them as isolated from one another. We limit ourselves to a rather general evaluation, which is intended to provide general guidance. The presented methods may yield different results when specific approaches are evaluated. In this paper we focus on static, unarticulated environments. Customizability of assets and environments is still a relevant aspect for specific scenarios and with articulated models in mind for future work.

### 1.1 Manual Methods

The first and most obvious class of methods is manual methods. This classification includes all approaches where substantial work is done manually using tools such as Blender and Autodesk Maya [9, 10]. Although manual methods can utilize these tools, they do not involve automation. Users have control and may modify every aspect of their workpiece to fit within the requirements, as long as it is supported by the tools utilized.

While manual methods can produce high-quality handcrafted results, the trade-off is that they are largely time consuming. Therefore, they are not suitable for large-scale simulated environments.

### 1.2 Automated Reconstruction Methods

Due to the time-intensity of manual methods, the application of automated methods is attractive. A class of automated methods are methods for automated reconstruction. They are proven to be suitable for efficiently reconstructing larger scale outdoor but also indoor environments. [11]

Automated reconstruction approaches are often implemented as photogrammetric methods based on RGB data, but might also incorporate depth data. The gathered data is then combined into photorealistic 3D models that accurately represent their real-world counterpart. [11, 12]

A significant disadvantage of automated reconstruction methods is limited modifiability of the generated models. This hinders the application of photogrammetric methods in the context of generating new data for training and validation of AMS. Possible applications include the reconstruction of individual assets or the reconstruction of empty “base” environments that can be populated later on.

### 1.3 Procedural Methods

Methods for automated reconstruction cannot create new environments and therefore might be helpful in some aspects, but not to tackle the core problem of new and diverse data. Manual methods can build upon human imagination to create new content - however strongly impeded by the necessary manual labor. Hence, we will now shift towards methods that are able to create entirely new assets and environments with minimal human intervention.

Procedural methods generate content algorithmically within predefined constraints, without the need for manual input after an initial setup. These methods can produce a vast amount of diverse and complex data automatically, both in a deterministic manner but also by incorporating random elements. The absence of a manual input apart from the initial setup is a core feature of those procedural methods.

Procedural methods are well established in computer games, where they are used to generate expansive virtual worlds, such as in commonly known Minecraft. They also find application in robotics simulation: NVIDIA Omniverse includes a “Domain Randomizer”, able to alter multiple parameters of a simulated scene randomly [13]. Further procedural approaches in robotics simulation include Cropcraft [14] for generating simulated crop fields or the already mentioned GRADE [4]. [15, 16]

## 1.4 Generative AI-based Methods

The next class of relevant methods is based on generative AI. Similar to procedural methods, generative AI-methods are able to computationally generate new content. Unlike procedural methods, they are generally not constrained to algorithmically predefined content.

There are several popular approaches to implementing generative AI, such as Generative Adversarial Networks (GANs), Variational Autoencoder (VAEs) or Transformer Models [17–19]. The latter might be the most publicly known type of model for being the basis of LLMs like ChatGPT.

Another relevant approach involves diffusion models. Diffusion models start with random noise and iteratively refine it into a detailed output, guided by a prompt. Inspired by the physical diffusion process, these models reverse noise addition, leveraging conditioning information – like the provided prompt – to shape the noisy base towards the desired content. This approach enables the generation of high-quality outputs. [20, 21]

A further notable approach are Neural Radiance Fields (NeRFs). NeRFs synthesize 3D scenes from 2D images by using deep neural networks to gain a volumetric representation of a scene. They are able to generate high quality scenes, but at the cost of computational inefficiency. [22]

## 1.5 Summary of Relevant Methods

All of the methods discussed in this chapter are relevant and usable for creating simulated environments. However, each of them has specific advantages and disadvantages. Users have to choose a fitting method based on their specific needs. To summarize the findings of this chapter and to ease the decision-making process, Table 1 provides a generalized comparison of the methods mentioned.

All methods are compared in five categories and rated from -- (worst) up to ++ (best):

- Human Effort involved, less is better
- Quality of results assets
- Customizability of assets for specific requirements, e.g. rigged objects
- Hardware requirements imposed by the method; lower requirements are rated better
- Originality, meaning the capability to generate new content

	Manual	Recon- struction	Proce- dural	Gen-AI
Effort	--	0	+	++
Quality	++	+	+	-
Customiza- bility	++	-	-	0
Hardware require- ments	0	-	-	--
Originality	++	--	0	+

**Table 1:** The four discussed methods for creating simulated environments are compared in regards to effort, quality, customizability, hardware requirements and originality.

## 2 Introduction of the Generative Pipeline

In the following we introduce a pipeline which enables its users to create, compose and harness simulated environments. All methods compared in the previous chapter can be applied throughout the pipeline. They may also be combined and different approaches might be used in different steps.

The pipeline shown in Figure 1 consists of four steps, which are explained in a generic manner in this chapter. An exemplary implementation is described in the following chapter.



**Figure 1:** The proposed pipeline for the generation of simulated environments consists of four steps.

The foundation of every virtual environment are its individual components, which we refer to as assets. Hence the first step of the pipeline is the “Creation” step, where assets are generated. Those are 3D models of individual items, e.g., a machine or a table. They should be stored in a standardized and widely compatible format to ensure future usability.

The assets created in step one need to be classified and rated. This is done in step two, “Classification and Rating”. Depending on the method applied for creation of the assets, this step varies in complexity. The goal is to obtain a database of assets, classified at least by type and quality.

An extensive, high quality model database is crucial for a successful implementation of later steps. Users might also incorporate existing and purchasable sets, needing to keep in mind the reduced control over the assets.

Building upon the assets created and classified in the previous steps, we can proceed to the third step of “Composition”. Here the simulated environments are composed from the models in the asset database. This step can vary greatly in complexity, depending on the size and complexity of the desired operating environment of the AMS in question.

The fourth step represents the application or actual use of the simulated environment and does not lie within the scope of our work. Typical applications include the generation of synthetic data, validation of the AMS software or reinforcement learning [5, 23].

Notably, the pipeline shown in Figure 1 does not end here. Instead, an iterative process is started after the application step: The pipeline returns to the environment composition step. Here, a new simulated environment is created and then used for the desired application. This can be done over and over again.

Compared to existing domain randomization approaches in robotics simulators, an entirely new environment can be created with minimal effort. The application can thus benefit from experiences in diverse and virtually unlimited environments. This is a core component of our approach and allows users to take full advantage of the work done in the first two steps.

### 3 Exemplary Implementation of the generative Pipeline

For the validation of the proposed pipeline, we chose a practically relevant scenario: An electronics production environment, which is to be used for the validation of an autonomous tow truck. In the following, we present an exemplary implementation of the pipeline using various methods.

We chose to focus the application of generative AI on the first step of the pipeline.

The second step is conducted manually due to the nature of the results from the previous step. For step three we present and apply a highly adaptable procedural approach. In this publication the fourth step is limited to a qualitative evaluation of exemplary generated environments.

For implementation we chose – independently from [4] – to use the .usd-format and NVIDIA Isaac Sim as simulation software. NVIDIA Isaac Sim offers significant benefits in regards to graphics and thus evaluation of vision-based algorithms over the established Gazebo simulator [4, 24].

#### 3.1 Creation of Assets through Generative AI

In the first step of asset creation, we apply generative AI. After applying multiple AI-models and optimizing their settings, we settled on using MV Dream and Magic3D [25, 26]. Both were used through the threestudio framework [27].

With the goal in mind of generating models that are as diverse as possible, Magic3D appears to be the better solution. Therefore, depending on the assets to be generated, one has to find a trade-off between higher quality or diverse assets. Generally, both approaches are able to generate 3D-models in usable quality as Figure 2 illustrates. The left section of the figure displays textured renderings, while the right section represents the normals of the meshes.

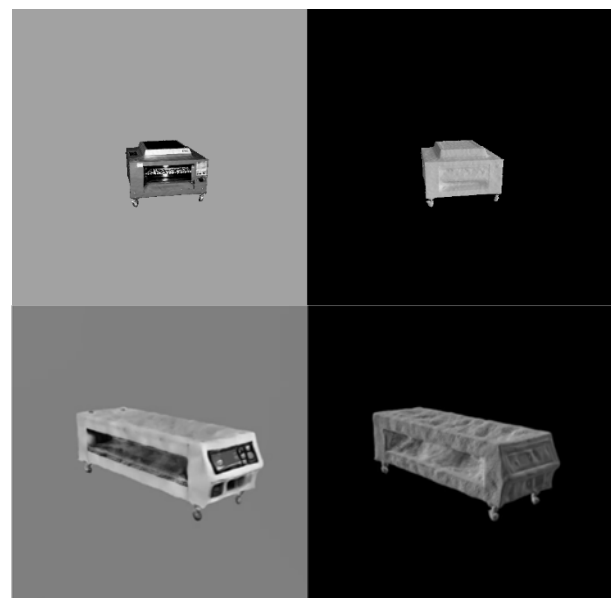


**Figure 2:** Both 3D models depicted are generated with the prompt “Industrial Reflow Oven”. The upper oven is created by Magic3D, the lower one by MVDream.

To ease the creation of a large number of assets, we use a script that automatically launches the AI model using a list of predefined prompts. The importance of using the right prompt when generating an asset is even more important than in 2D use cases. A prompt like “a pencil” likely won’t yield a usable result. A more promising prompt would be “an upright standing pencil”.

### 3.2 Manual Classification and Rating of Components

Due to the high hardware requirements of the AI models used in the first step, we were only able to generate a limited number of 300 assets over the course of multiple months. This low number of assets allows us to conduct the second step of the pipeline manually. It is simplified by the fact, that no classification of assets is needed due to the known prompts used for their creation.

However, the quality of the generated assets varies significantly, even within models generated with the same prompt. The models are categorized into three different categories. “Good” are all useable models, “bad” are models where the mesh or texture have significant problems and “failed” for assets where the AI completely failed. Around 30% of the models are rated “good” and thus deemed usable.

The models generated in the first step and rated “good” in this step form the basis for the next step of environment composition. Figure 3 shows a comparison of two models rated “bad” and “good”, created with the same prompt.

Additional work is necessary for AI generated assets, since the AI-models we use are not aware of absolute scales. We thus have to scale and rotate the generated assets manually.

### 3.3 Procedural Environment Composition

For environment composition, we present a procedural approach that uses environment subdivision and provides interfaces to the methods outlined above through a modular approach. For our implementation, we rely solely on our AI-generated model database. The environment composition can be divided into three substeps which are displayed in order in Figure 4.

During layout generation, the available space is defined. A randomly sized rectangle is defined as the base for the layout.

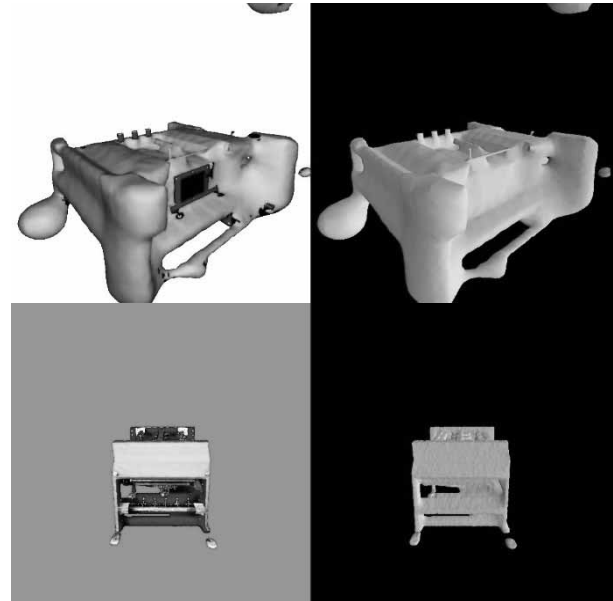


**Figure 3:** Even with the same prompt, the resulting assets can vary greatly in quality, as illustrated in this comparison of results from Magic3D with the prompt “Pick and Place Machine”. The upper model is rated as “bad”, the lower one as “good”.



**Figure 4:** The environment composition step can be broken down into the three substeps of layout generation, definition of bounding spaces and asset placement.

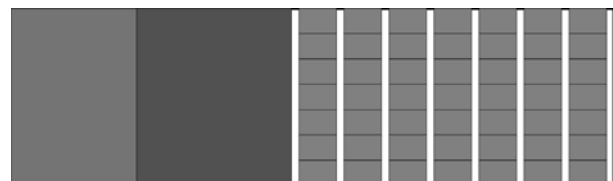


**Figure 5:** This exemplary procedurally generated floor layout consists of an office space (green), storage space (blue) and multiple production lines (red).

Next, the generated space is subdivided – also randomly – into the available classes of space. For our implementation, those are:

- Office space
- Storage space
- Production space

The latter is further divided into multiple production lines, depending on the size of the plant. An exemplary result of this process is shown in Figure 5.

Subsequently, the defined spaces are further partitioned into bounding spaces. They are defined by their size, position and subtype. An iterative algorithm divides the spaces defined by the layout into smaller rectangular bounding spaces. Their size is chosen randomly within predefined bounds that are dependent on the class of the space. An exception is made for the production lines: To achieve a more realistic, uniform layout, their size is only generated once for each layout and thus identical.

Each bounding space is then equipped with a procedurally generated group of assets. For this purpose, a sub-function is called for each bounding space. This function generates a fitting group of assets within the given space. In our implementation, the function is defined among others for workplaces, storage racks, and production lines. An exemplary, randomly generated production line is shown in Figure 6.

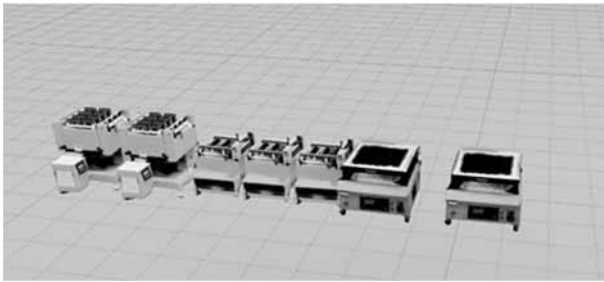


**Figure 6:** The depicted exemplary production line composed within step three consists of three different AI-generated machines, which are used two or three times.

For the placement of the production lines in our environments, a modification has been made: While the sub-function generally generates a new group of assets for each bounding space, this is not fitting for the production lines. In practice, a production plant often operates several identical production lines. Therefore, a number of types of production lines is randomly chosen after space partitioning. The different lines – such as the one in Figure 6 – are stored separately from the main .usd file. Instead of generating a new production line for each defined space, one is then randomly chosen from the pre-generated lines and placed within the available space including a randomized offset. By adding the modifications for the production lines to our implementation, we are both able to generate random environments and also to obtain areas where a specific structure is necessary.

### 3.4 Assessment of Generated Environments

In this paper we restrict the application step to a qualitative assessment of environments generated by the pipeline. An advanced application is discussed in chapter 4.2. Figure 7, Figure 8, and Figure 9 represent examples of each kind of area defined in our implementation.

From the exemplary screenshots we conclude that the presented pipeline and its implementation are suitable for the generation of simulated environments for AMS. The generated environments do not yet reach the same level of detail as handcrafted simulated environments. However, while composing an environment by hand would take hours or days, our pipeline is capable of composing environments in minutes on a standard desktop computer. We expect that advances in generative AI and further improvements to the pipeline will make it possible to generate environments and their assets with higher quality and more resource efficient in the near future.



**Figure 7:** This screenshot from an environment generated by our implementation of the pipeline depicts an office area composed with AI-generated workplaces. There are multiple different desks present, picked randomly from the asset database.



**Figure 8:** This screenshot from an environment generated by our implementation of the pipeline depicts a storage area with a number of AI-generated storage racks.



**Figure 9:** This screenshot from an environment generated by our implementation of the pipeline shows a production area consisting of multiple production lines with AI-generated machines. The lines on the left are identical and have been procedurally composed within step three.

## 4 Imaginative Robots

Imagination is a key capability that signifies advanced intelligence. Humans, along with few other species, possess the ability to foresee the outcomes of events they have not experienced by mentally simulating them. This ability to mentally simulate novel scenarios is closely linked to high cognitive flexibility and problem-solving capabilities. [28, 29] This translates to robots as well: While humans can anticipate and adapt based on imagined events, autonomous robots can hardly generalize and remain limited to explicitly programmed or learnt behaviours. Based on two well-established definitions of imagination from the Oxford English Dictionary [30] and the Oxford Dictionary of Philosophy [31], we define an *imaginative robot* as follows:

An *imaginative robot* is a robot capable of independently generating new interactive models of environments and situations that the system does not actually perceive, while combining knowledge in novel ways and anticipating possible scenarios.

We argue that building on the capabilities of the presented pipeline, *imaginative robots* could be realized and substantially improve the adaptability and flexibility of AMS. In the following, we lay out a concept and path towards *imaginative robots*.

### 4.1 Perception

Like all autonomous systems [32], an *imaginative robot* needs to gather knowledge about its environment through perception.

A key requirement of *imaginative robots* is a semantically rich and multimodal environment perception. While a simple Lidar-sensor might be sufficient for basic navigation tasks, modern AMS including humanoid robots need more additional information such as provided by cameras.

Meaningful information needs to be extracted and processed semantically. A key challenge is identifying relevant information and discarding irrelevant data. While modern foundation models such as Grounding-DINO [33] are in theory capable of identifying arbitrary objects, the necessary computing power and storage hinder their widespread and continuous application. [34]

### 4.2 Memory and Anticipation

The second key component of an *imaginative robot* is its memory. This memory goes beyond classical maps for mobile robots and introduces multiple new components.

Our concept involves building a comprehensive database of environmental information and contexts extracted from reality on the one hand, and storing the robot's capabilities and related experiences on the other. This memory will need to comprise of a combination of vector- and graph-based databases to facilitate the efficient storage and retrieval of necessary information. It also needs to rank the importance of information and allow for forgetting information, eg. by frequency of occurrence as well as impact on the system. This approach forms the basis for a key capability of *imaginative robots*: Anticipation.

Based on past experiences and current information – such as sensory input or a high-level task to solve – an *imaginative robot* can make assumptions about future events and tasks. A crucial element of anticipation is to take action or prepare prior to the expected event [35]. This takes the form of thought experiments based on the pipeline presented in this paper and is the reason for calling this concept *imaginative robots*.

### 4.3 Thought Experiments

As a thought experiment in the context of *imaginative robots* we define the intelligent generation of simulated environments in preparation for anticipated events. Using the modular generation process described previously, the system can target specific performance or knowledge gaps by constructing scenarios tailored to the robot's needs.

To improve domain adaptation and reduce the Sim2-Real gap, memorized real-world relationships and objects are integrated directly into the simulations.

An *imaginative robot* repeatedly invokes these thought experiments to learn from them, thereby improving task performance. Rather than stopping after a fixed number of trials, the system continuously monitors key metrics to determine when additional simulations are required – a concept related to curriculum learning and active learning [36, 37].

Because a large number of experiments can be run with minimal effort, the robot can focus on areas that need improvement while also testing a wide range of possible outcomes for upcoming scenarios. Once performance in these thought experiments reaches a satisfactory level, the robot stops them and completes the anticipation process. This way, a continually learning and self-improving system could be implemented that closely resembles natural mechanisms for imagination and anticipation.

## 5 Discussion

The validation of the generative pipeline presented in this paper underscores the pivotal role that generative AI plays in the future development of AMS. The structured and modular approach proves to be essential as it allows for updates in step with advances in AI technology, ensuring that new and more advanced solutions can be seamlessly integrated.

The pipeline can generate diverse and virtually unlimited environments with minimal human input, although it does not fully replace human design expertise. It provides a scalable solution to the data generation challenges encountered in AMS training and validation, and enables rapid synthetic data production.

The current implementation has several important limitations. Environment generation is restricted to strictly rectangular layouts with limited room classifications, while asset placement functions must be manually coded, which limits both variety and realism in the simulated environments.

Furthermore, the manual evaluation process for generated assets, while feasible for the limited scale demonstrated, is likely to be unsustainable for larger-scale implementations.

The computational requirements also hinder wider application, as the generative AI models required approximately 40 GB of VRAM, taking two to three hours per asset on an NVIDIA RTX 6000 ADA graphics card.

The usage of generative AI thus represents significant hardware acquisition and operational costs.

Despite these limitations, the pipeline offers a solid foundation for future work. Its design enables the incorporation of newer AI models and the potential automation of asset evaluation and improvement of layout generation. Such enhancements would reduce manual intervention, improve overall quality, and expand the range of scenarios that can be simulated. The concept of *imaginative robots*, while currently in a preliminary stage, is also supported by this approach, hinting at a future where autonomous systems can generate and adapt to novel virtual experiences based on anticipated tasks.

## 6 Conclusion and Future Work

In this paper, we introduced a pipeline designed for generating simulated environments for AMS. This pipeline covers the entire spectrum from the creation of individual assets to the generation of complete simulated environments. It enables the rapid generation of large amounts of synthetic data, which is invaluable for robot training and validation.

Special attention was paid to advances in generative AI, which offer significant improvements over traditional methods. To validate our proposed pipeline, we implemented it and successfully generated a wide range of electronics manufacturing environments, populated by AI-generated assets. In addition, we introduced an innovative concept aimed at creating *imaginative robots*.

To exploit the full potential of our pipeline, we anticipate further developments in generative AI, which is advancing at a remarkable pace. Our ongoing efforts will focus on integrating newer AI models, such as LATTE3D or TRELIS [38, 39]. Initial tests have already shown gains in both efficiency and quality. Additionally, we foresee the application of generative AI at various stages of the pipeline, including asset evaluation and layout generation, thereby broadening the range of scenarios and domains the pipeline can address. In addition, interactive, physically simulated objects would expand the potential applications of the generated environments.

Building on these advancements, we aim to fully realize the concept of *imaginative robots*. Currently, this is achievable to some extent, but as our pipeline evolves to generate new assets and types of environments on the go, its full potential will be unlocked.

Until then, the use of existing assets and predefined environment classifications provides a sufficient interim solution.

### Acknowledgement

This publication was written as part of the research project “POV.OS – Hardware and Software Platform for Mobile Machinery”, funded by the German Federal Ministry for Economic Affairs and Climate Action on the basis of a resolution of the German Bundestag.

### Publication Remark.

This contribution is the improved version of the conference version published in *Tagungsband Langbeiträge ASIM SST 2024*, ARGESIM Report AR 47, ISBN ebook: 978-3-903347-65-6, pp 159-166, DOI 10.11128/arep.47.a4708

## 7 References

- [1] Gartner. Gartner Hype Cycle Shows Supply Chain Adoption of Mobile Robots Will Far Outpace Drones Over Next Three Years. Accessed: Mar. 25, 2024. [Online]. Available: <https://www.gartner.com/en/newsroom/press-releases/2023-08-17-gartner-hype-cycle-shows-supply-chain-adoption-of-mobile-robots-will-far-outpace-drones-over-next-three-years>
- [2] Katara P, Xian Z, Fragkiadaki K. Gen2Sim: Scaling up Robot Learning in Simulation with Generative Models. 2023, DOI 10.48550/arXiv.2310.18308
- [3] Wang et al. RoboGen: Towards Unleashing Infinite Data for Automated Robot Learning via Generative Simulation. Nov. 2023, [Online]. Available: <http://arxiv.org/pdf/2311.01455v2>
- [4] Bonetto E, Xu C, Ahmad A. GRADE: Generating Realistic Animated Dynamic Environments for Robotics Research. 2023, DOI 10.48550/arXiv.2303.04466
- [5] Bonetto E, Xu C, Ahmad A. Learning from synthetic data generated with GRADE. 2023. DOI 10.48550/arXiv.2305.04282
- [6] Metzner M, et al. "Virtual training and commissioning of industrial bin picking systems using synthetic sensor data and simulation. *Int. Journal of Computer Integrated Manufacturing*, vol. 35, 4-5, pp. 483–492, 2022. DOI 10.1080/0951192X.2021.2004618
- [7] Xian Z, Gervet T, Xu Z, Qiao YL, Wang TH, Wang Y. Towards Generalist Robots: A Promising Paradigm via Generative Simulation. May 2023, [Online]. Available: <http://arxiv.org/pdf/2305.10455v3>
- [8] Genesis Authors. Genesis: A Universal and Generative Physics Engine for Robotics and Beyond. Accessed: Mar. 2, 2025. [Online]. Available: <https://github.com/Genesis-Embodied-AI/Genesis>
- [9] Blender Foundation. blender.org - Home of the Blender project - Free and Open 3D Creation Software. Accessed: Mar. 7, 2025, [Online]. Available: <https://www.blender.org/>
- [10] Autodesk. Autodesk Maya. Accessed: Mar. 7, 2025, [Online]. Available: <https://www.autodesk.com/de/products/maya/overview>
- [11] Lieret M, Kogan V, Hofmann C, Franke J. Automated Exploration, Capture And Photogrammetric Reconstruction Of Interiors Using An Autonomous Unmanned Aircraft. In *2021 IEEE International Conference on Mechatronics and Automation (ICMA)*, Takamatsu, Japan, 2021, pp. 301–306. DOI 10.1109/ICMA52036.2021.9512707
- [12] Choi S, Zhou QY, Koltun V. Robust reconstruction of indoor scenes. In *2015 IEEE Conference on Computer Vision and Pattern Recognition (CVPR 2015)*, Boston, Massachusetts, USA, 7-12 June 2015, Boston, MA, USA, 2015, pp. 5556–5565. DOI 10.1109/CVPR.2015.7299195
- [13] NVIDIA. Domain Randomization for RL. Accessed: Mar. 11, 2024, [Online]. Available: [https://docs.omniverse.nvidia.com/isaacsim/latest/isaac\\_gym\\_tutorials/tutorial\\_gym\\_domain\\_randomization.html](https://docs.omniverse.nvidia.com/isaacsim/latest/isaac_gym_tutorials/tutorial_gym_domain_randomization.html)
- [14] GitHub. Romea/cropcraft: A Procedural World Generator for Robotics Simulation of Agricultural Tasks. Accessed: Mar. 11, 2024, [Online]. Available: <https://github.com/Romea/cropcraft>
- [15] Brewer N. Computerized Dungeons and Randomly Generated Worlds: From Rogue to Minecraft [Scanning Our Past]. *Proc. IEEE*, vol. 105, no. 5, pp. 970–977, 2017. DOI 10.1109/JPROC.2017.2684358.
- [16] Togelius J, Shaker N, Nelson MJ. Introduction. In *Procedural Content Generation in Games (Computational synthesis and creative systems)*, Shaker N, Togelius J, Nelson MJ, Eds., Cham: Springer International Publishing, 2016, pp. 1–15.
- [17] Goodfellow IJ, et al. Generative Adversarial Networks. Jun. 2014. Accessed: Apr. 19, 2024, [Online]. Available: <http://arxiv.org/pdf/1406.2661.pdf>
- [18] Kingma DP, Welling M. Auto-Encoding Variational Bayes. Dec. 2013, Accessed: Apr. 19, 2024 [Online]. Available: <http://arxiv.org/pdf/1312.6114>
- [19] Vaswani A, et al. Attention Is All You Need. Jun. 2017, Accessed: Apr. 19, 2024, [Online]. Available: <http://arxiv.org/pdf/1706.03762>
- [20] Ho J, Jain A, P. Abbeel P. Denoising Diffusion Probabilistic Models. Jun. 2020, [Online]. Available: <http://arxiv.org/pdf/2006.11239>
- [21] Saharia C, et al. Photorealistic Text-to-Image Diffusion Models with Deep Language Understanding. May 2022, Accessed: Apr. 19, 2024, [Online]. Available: <http://arxiv.org/pdf/2205.11487>
- [22] Mildenhall B, Srinivasan PP, Tancik M, Barron JT, Ramamoorthi R, Ng R. NeRF: Representing Scenes as Neural Radiance Fields for View Synthesis. Mar. 2020, Accessed: Apr. 19, 2024, [Online]. Available: <http://arxiv.org/pdf/2003.08934>

- [23] B. Osinski B, et al. Simulation-Based Reinforcement Learning for Real-World Autonomous Driving. In *2020 IEEE International Conference on Robotics and Automation (ICRA)*, Paris, France, 2020, pp. 6411–6418. DOI 10.1109/ICRA40945.2020.9196730
- [24] Zwingel M, May C, Kalenberg M, Franke J. Robotics simulation – A comparison of two state-of-the-art solutions. In *ASIM SST 2022 Proceedings Langbeiträge*, Breitenacker F, Deatcu C, Durak U, Körner A, Pawletta T, Eds., Jul. 2022, pp. 171–178. DOI 10.11128/arep.20.a2033
- [25] Shi Y, Wang P, Ye J, Long M, Li K, Yang X. MVDream: Multi-view Diffusion for 3D Generation. Aug. 2023, Accessed: Apr. 19, 2024, [Online]. Available: <http://arxiv.org/pdf/2308.16512.pdf>
- [26] Lin CH, et al. Magic3D: High-Resolution Text-to-3D Content Creation. In *IEEE Conference on Computer Vision and Pattern Recognition (CVPR)*, 2023.
- [27] Y.-C. Guo YC, et al. threestudio: A unified framework for 3D content generation. Accessed: Mar. 28, 2024, [Online]. Available: <https://github.com/hreestudio-project/threestudio>
- [28] Gilbert DT, Wilson TD. Prospection: experiencing the future. *Science (New York, N.Y.)*, vol. 317, no. 5843, pp. 1351–1354, 2007. DOI 10.1126/science.1144161
- [29] Suddendorf T, Corballis MC. The evolution of foresight: What is mental time travel, and is it unique to humans?. *The Behavioral and brain sciences*, vol. 30, no. 3, 299-313; discussion 313-51, 2007. DOI 10.1017/S0140525X07001975
- [30] Oxford English Dictionary. *imagination, n.* Oxford University Press, 2024.
- [31] *The Oxford Dictionary of Philosophy*. Oxford University Press, 2008.
- [32] Siegwart R, Nourbakhsh IR, Scaramuzza D. *Introduction to autonomous mobile robots*. 2nd ed. Intelligent robotics and autonomous agents. Cambridge, Massachusetts, London, England, MIT Press, 2011.
- [33] S. Liu S et al. Grounding DINO: Marrying DINO with Grounded Pre-Training for Open-Set Object Detection. Mar. 2023, [Online]. Available: <http://arxiv.org/pdf/2303.05499>
- [34] Hofmann C, May C, Ziegler P, Ghotbiravandi I, Franke J, Reitelshöfer S. Automated Individualization of Object Detectors for the Semantic Environment Perception of Mobile Robots. In *Proceedings of the 20th International Joint Conference on Computer Vision, Imaging and Computer Graphics Theory and Applications*, Porto, Portugal, 2025, pp. 851–862. DOI 10.5220/0013162500003912
- [35] Oxford English Dictionary. *anticipation, n.* Oxford University Press, 2024.
- [36] Settles B. Active Learning Literature Survey. Rep. TR1648, 2009, Accessed: Mar. 2, 2025, [Online]. Available: <http://digital.library.wisc.edu/1793/60660>
- [37] Bengio Y, Louradour J, Collobert R, Weston J. Curriculum learning. In *Proceedings of the 26th Annual International Conference on Machine Learning*, Montreal Quebec Canada, Danyluk A, Bottou L, Littman M. Eds., 2009, pp. 41–48. DOI 10.1145/1553374.1553380
- [38] Xiang J, et al. Structured 3D Latents for Scalable and Versatile 3D Generation. Dec. 2024, [Online]. Available: <http://arxiv.org/pdf/2412.01506v1>
- [39] K. Xie K, et al. LATTE3D: Large-scale Amortized Text-To-Enhanced3D Synthesis. Mar. 2024, [Online]. Available: <http://arxiv.org/pdf/2403.15385>



## EUROSIM Data and Quick Info

	Simulation in Production and Logistic - 21 <sup>st</sup> ASIM Expert Conference September 24-26, 2025, Dresden, Germany <a href="http://www.asim-gi.org/spl2025">www.asim-gi.org/spl2025</a>	<b>ASIM SPL</b>
<b>SIMS</b> SIMS 2025	66 <sup>th</sup> Int. Conference of Scandinavian Simulation Society – SIMS 2025 Stavanger, Norway, Sept. 23-24, 2025 <a href="http://www.scansims.org">www.scansims.org</a>	 Winter Simulation Conference 2025 December 7 - 10, 2025 Seattle, WA, USA <a href="http://www.wintersim.org">www.wintersim.org</a>
	I3M 2025 International Multidisciplinary Modeling & Simulation Multiconference Fes, Morocco, September 17-19, 2025 <a href="http://www.msc-les.org/i3m2025">www.msc-les.org/i3m2025</a>	
	EUROSIM Congress 2026 12th Congress of the European Simulation Societies July 2026, Italy <a href="http://www.eurosim.info">www.eurosim.info</a>	 ASIM STS/GMMS/EDU Workshop 2025 April 10-11, 2025, Oberpfaffenhofen, Germany <a href="http://www.asim-gi.org/ws2025">www.asim-gi.org/ws2025</a>



**EUROSIM** – the **Federation of European Simulation Societies** was set up in 1989.

The purpose of EUROSIM is to provide a European forum for simulation societies and groups to promote modelling and simulation in industry, research, and development – by publication and conferences.

[www.eurosim.info](http://www.eurosim.info)

EUROSIM members may be national simulation societies and regional or international societies and groups dealing with modelling and simulation.

Full Members are ASIM, CEA-SMSG, CSSS, DBSS, KASIM, LIOPHANT, LSS, PTSK, NSSM, SIMS, SLOSIM, UKSIM. Observer Members are ALBSIM and ROMSIM. Former Members (societies in re-organisation) are: CROSSIM, FRANCOSIM, HSS, ISCS.

EUROSIM is governed by a **Board** consisting of one representative of each member society, president, past president, and SNE representative.

<b>President</b>	Agostino Bruzzone (LIOPHANT) <a href="mailto:agostino@itim.unige.it">agostino@itim.unige.it</a>
<b>Past President</b>	M. Mujica Mota (DBSS), <a href="mailto:m.mujica.mota@hva.nl">m.mujica.mota@hva.nl</a>
<b>Secretary</b>	Marina Massei (LIOPHANT), <a href="mailto:massei@itim.unige.it">massei@itim.unige.it</a>
<b>Treasurer</b>	Felix Breitenecker (ASIM) <a href="mailto:felix.breitenecker@tuwien.ac.at">felix.breitenecker@tuwien.ac.at</a>
<b>Webmaster</b>	Irmgard Husinsky (ASIM), <a href="mailto:irmgard.husinsky@tuwien.ac.at">irmgard.husinsky@tuwien.ac.at</a>

**SNE** SNE – Simulation Notes Europe is EUROSIM's membership journal with peer reviewed scientific contributions about all areas of modelling and simulation, including new trends as big data, cyber-physical systems, etc.

The EUROSIM societies distribute e-SNE in full version to their members as official membership journal. The basic version of e-SNE is available with open access (Creative Commons license CC BY). Publishers are ASIM, ARGESIM and EUROSI.

[www.sne-journal.org](http://www.sne-journal.org)

[office@sne-journal.org](mailto:office@sne-journal.org)

SNE-Editor: Felix Breitenecker (ASIM)  
[eic@sne-journal.org](mailto:eic@sne-journal.org)

### EUROSIM Congress and Conferences

Each year a major EUROSIM event takes place, as the EUROSIM CONGRESS organised by a member society, SIMS EUROSIM Conference, and MATHMOD Vienna Conference (ASIM).

On occasion of the EUROSIM Congress 2023, the 11<sup>th</sup> EUROSIM Congress in Amsterdam, July, 2023, a new EUROSIM president has been elected: we welcome Agostino Bruzzone, well known simulationist, as new president. His society LIOPHANT will organize the next EUROSIM Congress in 2026 in Italy.

Furthermore, EUROSIM Societies organize local conferences, and EUROSIM co-operates with the organizers of I3M Conference and WinterSim Conference Series.



## EUROSIM Member Societies



### ASIM German Simulation Society Arbeitsgemeinschaft Simulation

ASIM is the association for simulation in the German speaking area, servicing mainly Germany, Switzerland and Austria.

President	Felix Breiteneker, <i>felix.breiteneker@tuwien.ac.at</i>
Vice President	Sigrid Wenzel, <i>s.wenzel@uni-kassel.de</i> Thorsten Pawletta, <i>thorsten.pawletta@hs-wismar.de</i> Andreas Körner, <i>andreas.koerner@tuwien.ac.at</i>

ASIM is organising / co-organising the following international conferences: ASIM SPL Int. Conference 'Simulation in Production and Logistics' (biannual), ASIM SST 'Symposium Simulation Technique' (biannual), MATHMOD Int. Vienna Conference on Mathematical Modelling (triennial). Furthermore, ASIM is co-sponsor of WSC - Winter Simulation Conference and of the *I3M* and conference series.

#### ASIM Working Committees

GMMS: Methods in Modelling and Simulation

U. Durak, *umut.durak@dlr.de*

SUG: Simulation in Environmental Systems

J. Wittmann, *wittmann@informatik.uni-hamburg.de*

STS: Simulation of Technical Systems

W. Commerell, *commerell@hs-uhl.de*

SPL: Simulation in Production and Logistics

S. Wenzel, *s.wenzel@uni-kassel.de*

EDU: Simulation and Education

A. Körner, *andreas.koerner@tuwien.ac.at*

Working Group Big Data: Data-driven Simulation in

Life Sciences, N. Popper, *niki.popper@dwh.at*

Other Working Groups: Simulation in Business Administration, in Traffic Systems, for Standardisation, etc.

#### Contact Information

[www.asim-gi.org](http://www.asim-gi.org)

*info@asim-gi.org, admin@asim-gi.org*

ASIM – Office Germany, Univ. Bundeswehr Munich, Inst. für Technische Informatik, Tobias Uhlig, Werner-Heisenberg Weg 39, 85577 Neubiberg, Germany

ASIM – Office Austria, dwh Simulation Services, F. Breiteneker, N. Popper, Neustiftgasse 57-59, 1070, Wien, Austria

### CEA-SMSG – Spanish Modelling and Simulation Group

CEA is the Spanish Society on Automation and Control. The association is divided into national thematic groups, one of which is centered on Modeling, Simulation and Optimization (CEA-SMSG).

President	José L. Pitarch, <i>jlpitarch@isa.upv.es</i>
Vice President	Juan Ignacio Latorre, <i>juanignacio.latorre@unavarra.es</i>

#### Contact Information

[www.ceautomatica.es/grupos/](http://www.ceautomatica.es/grupos/)

*simulacion@cea-ifac.es*

CEA-SMSG / Emilio Jiménez, Department of Electrical Engineering, University of La Rioja, San José de Calasanz 31, 26004 Logroño (La Rioja), Spain



### CSSS – Czech and Slovak Simulation Society

CSSS is the Simulation Society with members from the two countries: Czech Republic and Slovakia. The CSSS history goes back to 1964.

President	Michal Štepanovský <i>michal.stepanovsky@fit.cvut.cz</i>
Vice President	Mikuláš Alexík, <i>alexik@frtk.fri.utc.sk</i>

#### Contact Information

[cssim.cz](http://cssim.cz)

*michal.stepanovsky@fit.cvut.cz*

CSSS – Český a Slovenský spolek pro simulaci systémů, Novotného lávka 200/5, 11000 Praha 1, Česká republika



### DBSS – Dutch Benelux Simulation Society

The *Dutch Benelux Simulation Society* (DBSS) was founded in July 1986 in order to create an organisation of simulation professionals within the Dutch language area.

President	M. Mujica Mota, <i>m.mujica.mota@hva.nl</i>
Vice President	A. Heemink, <i>a.w.heemink@its.tudelft.nl</i>
Secretary	P. M. Scala, <i>paolo.scala@fedex.com</i>

**Contact Information**[www.DutchBSS.org](http://www.DutchBSS.org)[a.w.heemink@its.tudelft.nl](mailto:a.w.heemink@its.tudelft.nl)

DBSS / A. W. Heemink, Delft University of Technology, ITS – twi, Mekelweg 4, 2628 CD Delft, The Netherlands

**KA-SIM Kosovo Simulation Society**

The Kosova Association for Modeling and Simulation (KA-SIM) is closely connected to the University for Business and Technology (UBT) in Kosovo.

President	Edmond Hajrizi, <a href="mailto:ehajrizi@ubt-uni.net">ehajrizi@ubt-uni.net</a>
Vice President	Muzafer Shala, <a href="mailto:info@ka-sim.com">info@ka-sim.com</a>

**Contact Information**[www.ubt-uni.net](http://www.ubt-uni.net)[ehajrizi@ubt-uni.net](mailto:ehajrizi@ubt-uni.net)

Dr. Edmond Hajrizi  
Univ. for Business and Technology (UBT)  
Lagjja Kalabria p.n., 10000 Prishtina, Kosovo

**LIOPHANT Simulation**

LIOPHANT Simulation is a non-profit association born in order to be a trait-d'union among simulation developers and users; LIOPHANT is devoted to promote and diffuse the simulation techniques and methodologies; the Association promotes exchange of students, sabbatical years, organization of International Conferences, courses and internships focused on M&S applications.

President	A.G. Bruzzone, <a href="mailto:agostino@itim.unige.it">agostino@itim.unige.it</a>
Director	E. Bocca, <a href="mailto:enrico.bocca@liophant.org">enrico.bocca@liophant.org</a>

**Contact Information**[www.liophant.org](http://www.liophant.org)[info@liophant.org](mailto:info@liophant.org)

LIOPHANT Simulation, c/o Agostino G. Bruzzone, DIME, University of Genoa, Savona Campus, via Molinero 1, 17100 Savona (SV), Italy

**LSS – Latvian Simulation Society**

The Latvian Simulation Society (LSS) has been founded in 1990 as the first professional simulation organisation in the field of Modelling and simulation in the post-Soviet area.

President	Artis Teilans, <a href="mailto:Artis.Teilans@rtu.lv">Artis.Teilans@rtu.lv</a>
Vice President	Oksana Kuznecova, <a href="mailto:Oksana.Kuznecova@rtu.lv">Oksana.Kuznecova@rtu.lv</a>

**Contact Information**[www.itl.rtu.lv/imb/](http://www.itl.rtu.lv/imb/)[Artis.Teilans@rtu.lv](mailto:Artis.Teilans@rtu.lv), [Egils.Ginters@rtu.lv](mailto:Egils.Ginters@rtu.lv)

LSS, Dept. of Modelling and Simulation, Riga Technical University, Kalku street 1, Riga, LV-1658, Latvia

**NSSM – National Society for Simulation Modelling (Russia)**

NSSM – The National Society for Simulation Modelling (Национальное Общество Имитационного Моделирования – НОИМ) was officially registered in Russia in 2011.

President	R. M. Yusupov, <a href="mailto:yusupov@iias.spb.su">yusupov@iias.spb.su</a>
Chairman	A. Plotnikov, <a href="mailto:plotnikov@sstc.spb.ru">plotnikov@sstc.spb.ru</a>

**Contact Information**[www.simulation.su](http://www.simulation.su)[yusupov@iias.spb.su](mailto:yusupov@iias.spb.su)

NSSM / R. M. Yusupov, St. Petersburg Institute of Informatics and Automation RAS, 199178, St. Petersburg, 14th line, h. 39

**PTSK – Polish Society for Computer Simulation**

PTSK is a scientific, non-profit association of members from universities, research institutes and industry in Poland with common interests in variety of methods of computer simulations and its applications.

President	Tadeusz Nowicki, <a href="mailto:Tadeusz.Nowicki@wat.edu.pl">Tadeusz.Nowicki@wat.edu.pl</a>
Vice President	Leon Bobrowski, <a href="mailto:leon@ibib.waw.pl">leon@ibib.waw.pl</a>

**Contact Information**[www.ptsk.pl](http://www.ptsk.pl)[leon@ibib.waw.pl](mailto:leon@ibib.waw.pl)

PSCS, 00-908 Warszawa 49, ul. Gen. Witolda Urbanowicza 2, pok. 222



## SIMS – Scandinavian Simulation Society

SIMS is the Scandinavian Simulation Society with members from the five Nordic countries Denmark, Finland, Norway, Sweden and Iceland. The SIMS history goes back to 1959.

President	Tiina Komulainen, <i>tiina.komulainen@oslomet.no</i>
Vice President	Erik Dahlquist, <i>erik.dahlquist@mdh.se</i>

### Contact Information

[www.scansims.org](http://www.scansims.org)

*vadime@wolfram.com*

Vadim Engelson, Wolfram MathCore AB,  
Teknikringen 1E, 58330, Linköping, Sweden



## SLOSIM – Slovenian Society for Simulation and Modelling

The Slovenian Society for Simulation and Modelling was established in 1994. It promotes modelling and simulation approaches to problem solving in industrial and in academic environments by establishing communication and cooperation among corresponding teams.

President	Goran Andonovski, <i>goran.andonovski@fe.uni-lj.si</i>
Vice President	Božidar Šarler, <i>bozidar.sarler@fs.uni-lj.si</i>

### Contact Information

[www.slosim.si](http://www.slosim.si)

*slosim@fe.uni-lj.si, vito.logar@fe.uni-lj.si*

SLOSIM, Fakulteta za elektrotehniko, Tržaška 25,  
SI-1000, Ljubljana, Slovenija

## UKSIM - United Kingdom Simulation Society

The UK Modelling & Simulation Society (UKSim) is the national UK society for all aspects of modelling and simulation, including continuous, discrete event, software and hardware.

President	David Al-Dabass, <i>david.al-dabass@ntu.ac.uk</i>
Secretary	T. Bashford, <i>tim.bashford@uwtsd.ac.uk</i>

### Contact Information

[uksim.info](mailto:uksim.info)

*david.al-dabass@ntu.ac.uk*

- UKSIM / Prof. David Al-Dabass, Computing & Informatics, Nottingham Trent University, Clifton lane, Nottingham, NG11 8NS, United Kingdom

## Observer Members

### ROMSIM – Romanian Modelling and Simulation Society

ROMSIM has been founded in 1990 as a non-profit society, devoted to theoretical and applied aspects of modelling and simulation of systems.

### Contact Information

*florin\_h2004@yahoo.com*

ROMSIM / Florin Hartescu, National Institute for Research in Informatics, Averescu Av. 8 – 10, 011455 Bucharest, Romania

### ALBSIM – Albanian Simulation Society

The Albanian Simulation Society has been initiated at the Department of Statistics and Applied Informatics, Faculty of Economy at the University of Tirana, by Prof. Dr. Kozeta Sevrani.

### Contact Information

*kozeta.sevrani@unitir.edu.al*

Albanian Simulation Goup, attn. Kozeta Sevrani, University of Tirana, Faculty of Economy, rr. Elbasanit, Tirana 355, Albania

## Former Societies / Societies in Re-organisation

- CROSSIM – Croatian Society for Simulation Modelling  
Contact: Tarzan Legović, *Tarzan.Legovic@irb.hr*
- FrancoSim – Société Francophone de Simulation
- HSS – Hungarian Simulation Society  
Contact: A. Gábor, *andrasi.gabor@uni-bge.hu*
- ISCS – Italian Society for Computer Simulation

The following societies have been formally terminated:

- MIMOS – Italian Modeling & Simulation Association; terminated end of 2020.



24. bis 26. Sept.

2025

„Haus der Kirche“

Schlüsselrolle Simulation: Wandel gestalten.  
Herausforderungen meistern.

Dresden

## 21. ASIM Fachtagung „Simulation in Produktion und Logistik“

Als größte europäische Tagung zum Thema Simulation im Bereich Produktion und Logistik gibt die ASIM Fachtagung alle zwei Jahre einen Überblick der zukunftsweisenden Trends, aktuellen Entwicklungen und erfolgreichen Projekte. Präsentiert und diskutiert werden wissenschaftliche Arbeiten sowie interessante Anwendungen aus der Industrie.

Themen der Tagung

### Supply Chain Simulation & Logistik

- Produktionsnetzwerke & -logistik
- Intralogistik; Lieferketten
- Transport & Verkehr
- Innovative Materialflusstechnik
- Produktionsplanung & -steuerung
- Systemresilienz; (Cyber-)Sicherheit

### Simulationsanwendungen in Industrie und Dienstleistung

- Automobilindustrie
- Maschinen- & Anlagenbau
- Halbleiterindustrie
- Simulation as a Service
- Energieeffizienz; Nachhaltigkeit

### Methoden, Werkzeuge & Simulationstechnik

- Virtuelle Inbetriebnahme; Digitaler Zwilling; Digitaler Schatten
- Simulationsbasierte Optimierung
- Verifikation & Validierung
- Data Science; Visual Analytics; Virtual Reality; Augmented Reality
- Künstliche Intelligenz; Maschinelles Lernen
- Ereignisdiskrete Simulation; Agentenbasierte Simulation
- Interoperabilität; verteilte Simulation; Cloud-basierte Simulation

## Tagungsleitung

Prof. Dr.-Ing. habil.  
Thorsten Schmidt

Professur für  
Technische Logistik  
Fak. Maschinenwesen  
TU Dresden

## Tagungsort

„Haus der Kirche“  
Hauptstraße 23  
01097 Dresden

## Anmeldung

Alle Informationen zur  
Anmeldung finden Sie  
auf unserer Website:



[<https://asim-gi.org/spl2025>]

Teilnahme

### Ausstellung

Die begleitende Ausstellung zeigt den aktuellen Stand von Simulationswerkzeugen, verwandter Software und Dienstleistungen im Simulationsumfeld. Falls Sie sich als Aussteller auf der Fachtagung präsentieren möchten, kontaktieren Sie uns bitte.

### Teilnahmegebühr (pro Person, inkl. Mehrwertsteuer)

Im Preis enthalten sind die Teilnahme an Vorträgen, der Ausstellung, Mittagessen, Erfrischungsgetränke mit Pausensnack, ein Get-Together sowie eine Abendveranstaltung. Ein gedruckter Tagungsband kann gegen einen Aufpreis von 50,00 € optional erworben werden.

Grundpreis		1190,00 €
Frühbucherrabatt (bis 01.07.2025)	abzgl.	50,00 €
Mitglieder von ASIM, GI, EUROSIM	abzgl.	140,00 €
Einreichung Beitrag (1 x pro Beitrag und Autor)	abzgl.	170,00 €
ab dem 2. Teilnehmer einer Institution	abzgl.	140,00 €

Hochschulangehörige erhalten 40 % Nachlass auf den Endpreis.





### ASIM STS/GMMS Workshop 2025

April 10-11, 2025, Oberpfaffenhofen, Germany  
[www.asim-gi.org/ws2025](http://www.asim-gi.org/ws2025)



### I3M 2025

International Multidisciplinary Modeling & Simulation Multiconference

September 17-19, 2025, Fes, Morocco  
[www.msc-les.org/i3m2025/](http://www.msc-les.org/i3m2025/)



Scandinavian  
Simulation  
Society

### SIMS 2025

September 23-24, 2025, Stavanger, Norway  
[www.scansims.org](http://www.scansims.org)



### Simulation in Produktion und Logistik 2025

September 24-26, 2025, Dresden, Germany  
[www.asim-gi.org/spl2025](http://www.asim-gi.org/spl2025)



### Winter Simulation Conference 2025

December 7-10, 2025, Seattle, WA, USA  
[meetings.informs.org/wordpress/wsc2025/](http://meetings.informs.org/wordpress/wsc2025/)



### EUROSIM Congress 2026

July 2026, Italy  
[www.eurosim.info](http://www.eurosim.info)

[www.sne-journal.org](http://www.sne-journal.org)  
[www.argesim.org](http://www.argesim.org)

